EXPERIMENTAL AND NUMERICAL INVESTIGATION OF PREMIXED OXY COMBUSTION IN A GAS TURBINE MODEL COMBUSTOR ADAPTING MULTI-HOLE BURNER COMBUSTION TECHNOLOGY

BY

ARAOYE ABDULRAZAQ ADENIYI

A Dissertation Presented to the

FACULTY OF THE COLLEGE OF GRADUATE STUDIES

KING FAHD UNIVERSITY OF PETROLEUM & MINERALS

DHAHRAN, SAUDI ARABIA

In Partial Fulfillment of the
Requirements for the Degree of

DOCTOR OF PHILOSOPHY

In

MECHANICAL ENGINEERING

MAY, 2021

KING FAHD UNIVERSITY OF PETROLEUM & MINERALS

DHAHRAN- 31261, SAUDI ARABIA

DEANSHIP OF GRADUATE STUDIES

This thesis, written by **ARAOYE ABDULRAZAQ ADENIYI** under the direction of his thesis advisor and approved by his thesis committee, has been presented and accepted by the Dean of Graduate Studies, in partial fulfillment of the requirements for the degree of **DOCTOR OF PHILOSOPHY IN MECHANICAL ENGINEERING.**

R. B. Tansour

Dr. Rached Ben-Mansour
(Advisor)

Dr. Khaled S. Al-Athel
Department Chairman

Med Habib

Dr. Mohamed A. Habib
(Co-Advisor)

Dr. Suliman S. Al-Homidan
Dean of Graduate Studies

Mozzhar Hossain

Dr. Mohammad M. Hossain
(Member)

Date

M Antar

Dr. Mohamed A. Antar
(Member)

A. Khalifa

Dr. Atia E. Khalifa
(Member)

Dedicated:

To my parents, Mr AbdulRasheed Araoye and Mrs Risikat Araoye

To my wife and kid, Mrs Rashidat Araoye & Abdurrahman Araoye

To my siblings, Mr Ibrahim Araoye & Rasheedat Araoye

To my beloved country, Nigeria

ACKNOWLEDGMENTS

All praise and adoration are due to Almighty Allah for HIS infinite mercy and guidance over the course of my PhD program. I am grateful to the Kingdom of Saudi Arabia and the management of KFUPM for providing me with the scholarship and privilege to conduct my PhD program and providing adequate funding for my research through the center for carbon capture and sequestration (CCS).

My profound gratitude goes to my dissertation advisor, Dr. Rached Ben-Mansour for his guidance, insightful contributions, support, patience, and encouragement throughout this research work. I would also like to express my sincere gratitude to my co-advisor, Dr. M. A. Habib for his contributions towards idea formulations, executions, supervision, and discussions. Special appreciation goes to Dr. M. M. Hossain, Dr. M. A. Antar and Dr. A. E. Khalifa for the enormous recommendations and corrections to my research work.
I would also like to acknowledge the assistance of Dr. M. A. Nemitallah and Dr. A. Abdelhafez in the design of the experiment and formulation of numerical models. My appreciation also goes to my colleagues in the combustion research group.

My heartfelt gratitude and love go to my family especially my parents Mr. AbdulRasheed & Mrs. Risikat Araoye for their prayers and unbridled support in terms moral, financial, encouragements. Special thanks to my wife Rashidat-Aderemi, my son Abdurrahman and my siblings Ibrahim and Rasheedat Araoye, for their patience and understanding. May Almighty Allah bless and reward them abundantly.

Finally, I would like to show my appreciation to the faculty and staff of Dept. Mechanical Engineering KFUPM and the Nigerian community in KFUPM for their reception and advice during my PhD study.

Thank you all for making my PhD a reality.

TABLE OF CONTENTS

LIST OF TABLES

LIST OF FIGURES

LIST OF ABBREVIATIONS

AFT	Adiabatic Flame Temperature
CFD	Computational fluid dynamics
IEA	International Energy Agency
FGR	Flue gas recirculation
HF	Hydrogen Fraction
LBO	Lean Blowout
MM	Micromixer
OF	Oxygen Fraction
PD	Power Density
SLPM	Standard liter per minute

LIST OF SYMBOLS

3D	Three-dimensional
c	Progress variable
CH_4	Methane
CO	Carbon monoxide
CO_2	Carbon dioxide
c_p	Specific heat capacity (J/kg-K)
D	Tube diameter
Da	Damköhler number
D_f	Diameter of fuel hole
$D_{k,m}$	Mass diffusion coefficient of specie k (m^2/s)
f	Mixture fraction
f’	Mixture fraction variance
H_2	Hydrogen
H_2O	Water vapor
I_m	Mixing Index
J_k	Diffusion flux of specie k

Ka	Karlovitz number
l_t	Integral length scale (m)
L_s	Subgrid scale mixing length (m)
N_2	Nitrogen
NO	Nitrogen oxide
NOx	Combined nitrogen oxides (NO + NO_2)
O_2	Oxygen
r	Radial location within quartz combustor (m)
Re	Reynolds number
Sc	Schmidt number
S_L	Laminar flame speed (m/s)
S_T	Turbulent flame speed (m/s)
T	Temperature (K)
T_{ad}	Adiabatic flame temperature (K)
u’	Root mean square velocity fluctuation (m/s)
U	Uniformity index
y	Mole fraction
x	Mass fraction

Z	Axial location within quartz combustor (m)

Greek Symbols

ρ	density (kg/m^3)
γ	heat release factor
λ	thermal conductivity (W/mK)
υ	kinematic viscosity (m^2/s)
δ	flame thickness (m)
ε	turbulent dissipation rate (m^2/s^3)
Ø	equivalence ratio
μ_t	turbulent viscosity (kg/ms)
Γ_φ	diffusion coefficient (m^2/s)
τ_{ij}	subgrid-scale stress tensor (N/m^2)
Δp	Pressure Drop (Pa)
ρ_{mix}	mixture density
μ_{mix}	mixture viscosity

THESIS ABSTRACT

Full Name	[ARAOYE ABDULRAZAQ ADENIYI]
Thesis Title	[Experimental and Numerical Investigation of Premixed Oxy combustion in a gas turbine model combustor adapting multi-hole burner combustion technology]
Major Field	[Mechanical Engineering]
Date of Degree	[May 2021]

Combustors are designed to conform to certain requirements such as low emissions and high efficiency to meet global efforts towards minimizing CO_2 emissions. The preferred technology for achieving these objectives is oxy-combustion of premixed flames. This technology's drawback is its narrow operability window, which is due to weak flames and combustion instabilities. To solve this limitation, burner technologies and hydrogen enrichment are generally implemented to achieve a wide stability range. Unlike other burners, the micromixer technology can suppress the early occurrence of flashback and operate conveniently at high CO_2-dilution requirements for zero-emission power cycles. Thus, this study investigates experimentally and numerically multi-hole burner stabilized combustors for oxy-combustion of hydrogen-enriched premixed flames.

Firstly, the non-reacting flow and mixing characteristics inside a single tube of a micromixer burner were numerically studied for potential zero-emission premixed oxy-fuel combustion applications, such as gas turbines. The influence of geometrical parameters on the mixing quality of an oxy-fuel reactant mixture consisting of CH_4, O_2, and CO_2 was investigated for design parameters: fuel inlet diameter (from 0.2 to 1.0 mm), number of fuel holes (4 and 6), and tube length (from 5D to 15D). The results showed that mixing quality is not directly dependent on fuel hole size but the main flow ratio to jet flow momenta. Also, micromixers can achieve high mixing quality feasible for premixed combustion at a reasonable burner height.

Secondly, the study investigated experimentally the effects of H_2-enrichment on premixed oxy-methane flames stabilized on a micromixer-like burner for clean energy production in gas turbines. The stable combustion zone was established over ranges of fuel hydrogen fraction (HF: 25-70%) and equivalence ratio (ϕ: 0.1-1) at fixed oxidizer oxygen fraction (OF=30%) and fixed jet velocity (5.2 m/s). Also, the effects of various operating parameters on flame stability and macrostructures were studied. Results showed that the extremely lean blowout limit of ϕ = 0.1 at HF = 70% and no flashback occurrence at ϕ = 1 for HF range 25 – 70% is achievable with the model micromixer-like burner.

Thirdly, a numerical study of combustion and emission characteristics of turbulent premixed oxy-methane flames with hydrogen-enrichment (CH_4-

H_2/O_2-CO_2 flames) was conducted. Combustion chamber condition depicts that of the corrugated premixed flame regime. The premixed turbulent flame was modeled using the reaction progress variable flame front topology approach with the Large Eddy Simulation (LES) technique. The numerical model was validated with temperature data obtained from the premixed micromixer-like burner combustor. The CO emission was significantly reduced with 10% (fuel fraction) hydrogen enrichment but increased with further addition of hydrogen.

ملخص الرسالة

الرئيسي إلى الاسم الكام:عراوأي عبد الرزاق أديني

عنوان الرسالة: التحقيق التجريبي والرقمي لاحتراق الأكسجين المخلوط مسبقًا في جهاز احتراق نموذج التوربينات الغازية يتكيف مع تقنية احتراق الموقد متعدد الفتحات

التخصص: الهندسة المكانيكية

تاريخ الدرجة العلمية: مايو 2021

تم تصميم أجهزة الاحتراق لتتوافق مع متطلبات معينة مثل الانبعاثات المنخفضة والكفاءة العالية لتلبية الجهود العالمية لتقليل انبعاثات ثاني أكسيد الكربون. التكنولوجيا المفضلة لتحقيق هذه الأهداف هي الاحتراق بالأكسجين لهب مختلط مسبقًا. عيب هذه التقنية هو نافذة التشغيل الضيقة ، والتي تنتج عن ضعف اللهب وعدم استقرار الاحتراق. لحل هذا القيد ، يتم تنفيذ تقنيات الموقد وتخصيب الهيدروجين بشكل عام لتحقيق نطاق استقرار واسع. على عكس الشعلات الأخرى ، فإن تقنية micromixer قادرة على قمع التكرار المبكر للارتجاع وكذلك العمل بشكل ملائم في متطلبات تخفيف ثاني أكسيد الكربون العالية لدورات الطاقة بدون انبعاثات. وبالتالي ، تبحث هذه الدراسة في الاحتراق المستقر تجريبيًا وعدديًا متعدد الفتحات للاحتراق بالأكسجين للهب مختلط مسبقًا المخصب بالهيدروجين.

أولاً ، تمت دراسة خصائص التدفق والخلط غير المتفاعلة داخل أنبوب واحد من موقد المزج الدقيق رقميًا من أجل تطبيقات احتراق وقود أوكسي مختلطة بانبعاثات صفرية محتملة ، مثل توربينات الغاز. تم التحقيق في تأثير المعلمات الهندسية على جودة الخلط لخليط متفاعل مع وقود الأكسجين يتكون من CH4 و O2 و CO2 لمعلمات التصميم: قطر مدخل الوقود (من 0.2 إلى 1.0 مم) ، عدد فتحات الوقود (4 و 6) ، وطول الأنبوب (من D5 إلى D15). أظهرت النتائج أن جودة الخلط لا تعتمد بشكل مباشر على حجم ثقب الوقود ولكن على نسبة التدفق عزم التدفق النفاث. أيضًا ، يمكن أن تحقق الخلاطات الدقيقة جودة خلط عالية ممكنة للاحتراق المخلوط مسبقًا على ارتفاع معقول للموقد.

ثانيًا ، بحثت الدراسة بشكل تجريبي في تأثيرات تخصيب H2 على لهب الأكسجين والميثان المخلوط مسبقًا والمثبت على موقد يشبه المزج الدقيق لإنتاج الطاقة النظيفة في توربينات الغاز. تم إنشاء منطقة الاحتراق المستقرة على نطاقات جزء الهيدروجين للوقود (٪70-25 :HF) ونسبة التكافؤ (1-0.1 :ϕ) عند جزء أكسجين مؤكسد ثابت (٪30 = OF) وسرعة نفاثة ثابتة (5.2 م / ث). كما تم دراسة تأثير عوامل التشغيل المختلفة على ثبات اللهب والبنى الكلية. أظهرت النتائج أن حد الانفجار الخفيف للغاية عند of = 0.1 عند ٪70 = HF ولا يوجد حدوث ارتجاع عند ϕ = 1 لمدى ٪70 - 25 HF يمكن تحقيقه باستخدام الموقد الشبيه بالميكروكسير.

ثالثًا ، تم إجراء دراسة عددية لخصائص الاحتراق والانبعاثات لهب أوكسي ميثان المضطرب مع تخصيب الهيدروجين (لهب CH4-H2 / O2-CO2). حالة غرفة الاحتراق تصور حالة نظام اللهب المموج المموج. لذلك ، تم نمذجة اللهب المضطرب الممزوج مسبقًا باستخدام نهج طوبولوجيا مقدمة اللهب المتغير لتقدم التفاعل باستخدام تقنية محاكاة إيدي الكبيرة (LES). تم التحقق من صحة النموذج العددي من خلال بيانات درجة الحرارة التي تم الحصول عليها من جهاز الاحتراق الذي يشبه المزج الدقيق المسبق. تم العثور على انبعاث ثاني أكسيد الكربون يقلل بشكل كبير مع ٪10 (جزء الوقود) تخصيب الهيدروجين ولكنه يزداد مع إضافة المزيد من الهيدروجين.

CHAPTER 1

INTRODUCTION

1.1 Research Background

Recent rapid development in the global economy, technological advancement, and the increasing human population has led to an enormous increase in energy demand. Electricity demand is estimated to rise by more than 50% over two decades up to 2040 [1], indicating a continuous rise in energy production. Unfortunately, the rising energy demand is accompanied by an increase in carbon dioxide (CO_2) emission (as shown in Figure 1.1) because energy production accounts for 72% of total CO_2 emission [2]. According to the International Energy Agency (IEA) report on the world's electricity production in 2017, 66.3% was sourced from fossil fuels [3]. Also, fossil fuel energy source is projected to constitute four-fifth of the total energy source by 2035 [4–6]. However, fossil-fuel combustion contributes to the threat of global warming, as it is a primary source of CO_2 emission. Figure 1.2 shows that CO_2 constitutes 81% of the total greenhouse gases in 2018 [7].

Several industry regulatory standards and frameworks are set towards emission controls to achieve low greenhouse gas emissions and mitigate global warming's adverse effects [8]. Carbon capture technology has proven effective in reducing CO_2 emissions from fossil-based fuels, and it is projected to cut global CO_2 emissions by an average of 35% by 2050 [9].

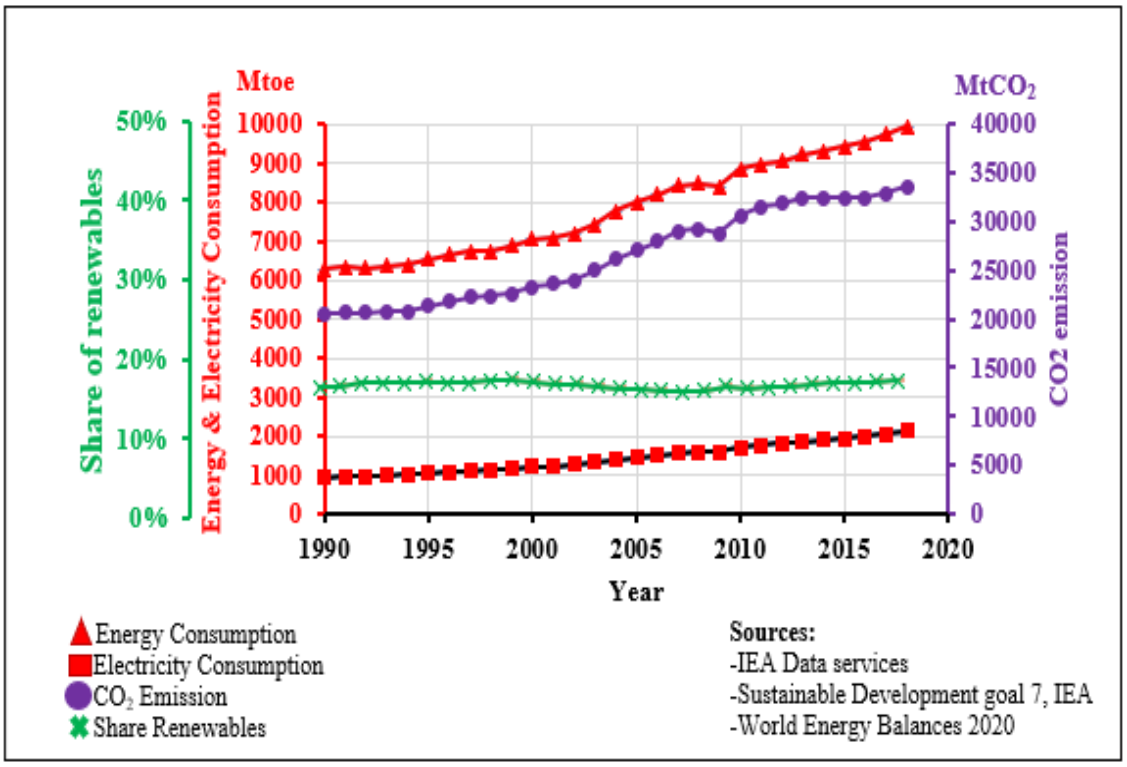

Figure 1.1 Total final consumption (TFC) by source, Electricity consumption, CO2 emission, and Renewable share in final consumption (SDG 7.2); World 1990-2018 (Adapted from IEA [3]).

The other available practical way of reducing CO_2 emission is the use of carbon-free fueled energy technologies. Despite the considerable progress recorded in recent years in the utilization of low-carbon energy sources like hydro, solar, wind, geothermal, tidal, and nuclear energies, they widely fall short of meeting energy consumption rates if solely relied upon. As shown in Figure 1.2, while the total energy consumed has increased by 67% over the period 1990-2018, renewable energy contributed averagely 17.5% over the same period. Hence, an extensive study on carbon capture technology is still of utmost importance. It provides the most feasible option of meeting energy demands while fulfilling the regulations on greenhouse emissions.

Oxy-fuel combustion technology is the most promising carbon capture technology compared to pre and post-carbon capture technologies. This merit is primarily due to advantages such as online CO_2 capture [10], easy retrofitting to existing power plants [11], and reduction in flue-gas treatment plant size [12]. The Oxy-fuel combustion technology involves burning fuel in pure oxygen (O_2), instead of air, to produce CO_2 and water vapor (H_2O), where the CO_2 is separated by condensing the H_2O as seen in Figure 1.3 showing the supercritical-CO_2 Allam cycle for power production [13]. This methodology indirectly eliminates NOx production, which is prevalent in conventional air-fuel combustion systems.

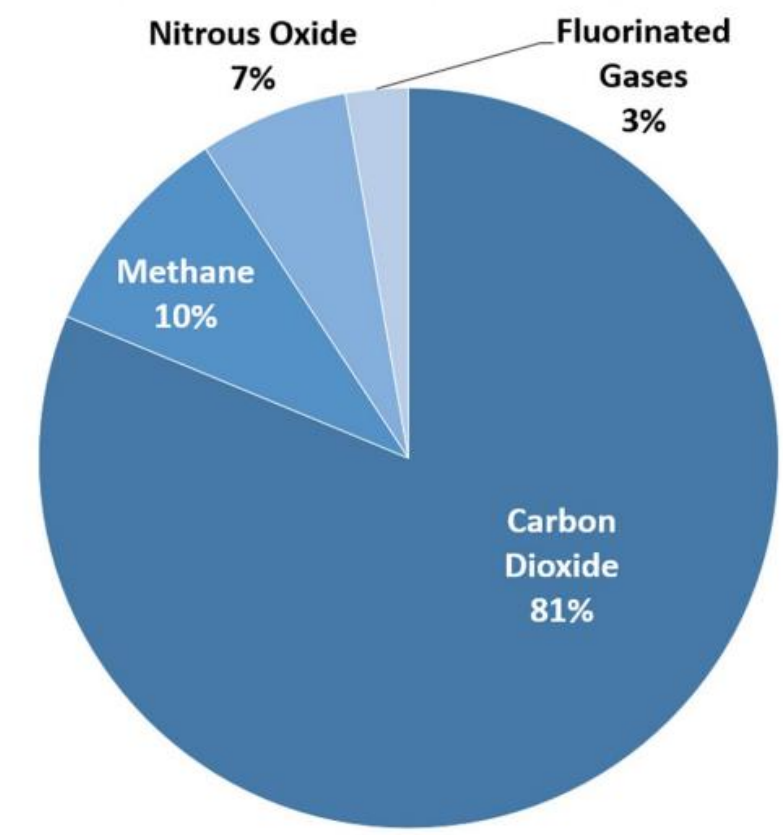

U.S. Environmental Protection Agency (2020). Inventory of U.S. Greenhouse Gas Emissions and Sinks: 1990-2018

Figure 1.2 Summary of Greenhouse gas emission in 2018 [7].

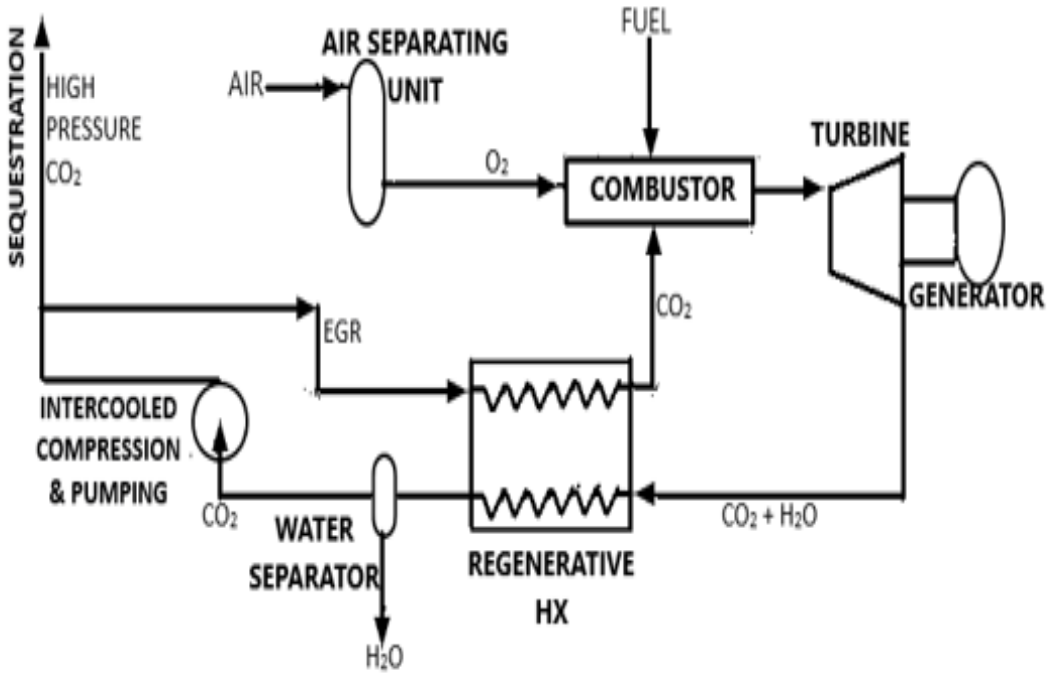

Figure 1.3 Supercritical-CO2 Allam zero-emission cycle [Adapted from [13]]

Using pure oxygen, however, results in high flame temperatures, which is detrimental to the hardware. To overcome this issue, part of the effluent CO_2 is recirculated to dilute the O_2 at the combustor inlet, termed flue-gas recirculation (FGR). Oxy-fuel combustion is preferably operated near stoichiometry to ensure effective utilization of O_2 [14] since its separation from the air is energy-consuming and poses an economic penalty [15]. The introduction of CO_2 as diluent causes unwanted flame instabilities and different combustion behavior compared with an air combustion. These can be attributed to the significant difference between the physical and chemical attributes of CO_2 and N_2 [16]. Oxy-fuel combustors are characterized by lower flame speeds [17], longer and weaker flames [18,19], and narrower operability windows, induced by slower chemical kinetics and flame instability [20,21]. These are evident in all flame types, non-premixed [22], premixed [23], and partially-premixed flames [24]. Hence, oxy-combustion requires oxygen fraction (OF) in the oxidizer mixture (O_2 plus CO_2) to be more than the typical 21% of oxygen in the air to produce similar flame characteristics and stability at the same stoichiometric ratio [21].

Lean premixed combustion is widely used in energy-conversion devices because of its advantages, such as high efficiency and low pollutant emission over non-premixed combustion. Such practical applications are found in spark-ignition automotive engines, power generation gas turbines, supersonic aircraft reheat systems, and glass manufacturing furnaces. Premixed combustion involves the mixing of reactants before introduction into the combustor.

It requires high mixing quality [25] and velocity uniformity [26,27] to ensure effective control of combustion stoichiometry, which promotes complete combustion and reduces pollutants emissions. However, premixed flames are more prone to instabilities, static stability limit on the lean side, which is associated with flame blow off, and thermoacoustic instability on the rich side, which may lead to flashback, structural vibration, noise, or damage. The stability ranges are usually expanded using flame holders/stabilizers, such as bluff bodies [25] and perforated plates [26]. Bluff-bodies and swirl vanes are primarily applied in turbulent combustion systems, such as gas turbines. They achieve flame stabilization by creating an internal recirculation zone of low local velocity inside the flame through abrupt divergence of flow [27].

Nevertheless, the inferior stability of oxy-combustion may aggravate other instabilities when operated in the premixed mode, as this mode is already naturally prone to instabilities. Premixed oxy-combustion characteristics can be significantly improved by hydrogen enrichment [28,29].Hydrogen addition typically affects flame characteristics positively due to the better burning properties of hydrogen in terms of faster reaction rate, higher laminar burning velocity, and higher diffusivity [30]. Hydrogen, as pure fuel, is considered a clean energy source, as its combustion product is only water vapor. The demand for hydrogen for oil refining usage, ammonia production, and others has increased by over 300% from 1975 to 2018, as shown in Figure 1.4.

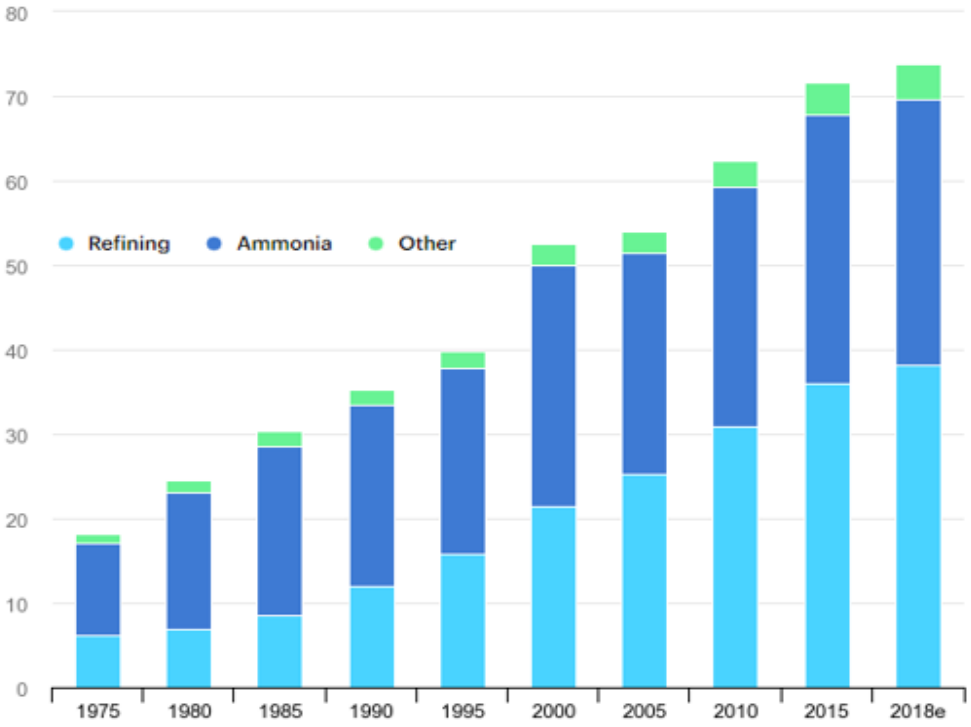

Figure 1.4 Global demand for pure hydrogen, 1975-2018 [31]

However, the growth in demand is accompanied by numerous CO_2 emissions as a significant portion of hydrogen produced is sourced from hydrocarbons (2% and 6% of global coal and natural gas, respectively) [31]. Also, hydrogen usage for power generation is still limited by higher production costs, cumbersome storage and transport, and safety issues with its high flammability. While low carbon hydrocarbons such as methane (CH_4) are widely used as sources of recent because of low CO2 emission and low production cost compared to other fossil fuels and hydrogen, respectively, CH_4 flames are prone to blow off under lean conditions [32]. Studies have shown that the proactive use of hydrogen as a fuel blend with conventional fuels helps widen static flammability limits and diminish combustion instability under both air and O_2/CO_2 conditions[33,34] [35,36]. Also, the addition of H_2 reduces the emissions of CO_2, NOx, and soot [33,37–39].

These advantages are mainly attributed to hydrogen properties such as lower ignition temperature, higher diffusivity, higher burning velocity, and faster reaction rates. Hydrogen enrichment can widen the combustor operability down to ultra-lean conditions; however, the combustor should be flexible enough to handle different enrichment levels to avoid flame flashback. With this requirement, micromixer (MM) combustion technology seems to be an excellent choice with a very low possibility for a flame flashback. In MM combustors, fuel is premixed with the oxidizer at the micro-scale level inside a multi-hole combustor headend, and subsequent burning produces several small flamelets, thereby reducing the possibility of flame extinction.

Micromixer combustors have been implemented successfully in utility gas turbines by different gas-turbine manufacturers, such as General Electric, Honeywell Garrett, and Mitsubishi Hitachi Power Systems [40–42]. Other benefits of using micromixers are compactness, easy scalability [43], and low NOx at lean conditions [44]. While most industrial applications of micromixers are operated on H_2-air combustion, it will be interesting to study the viability of operating hydrogen-methane fuel blends with oxy-combustion technology in a micromixer gas turbine combustor.

Achieving the goal of developing combustors with low pollutant emission, high combustion efficiency, and stability over extended operating conditions lies with understanding the fundamental mechanism of combustion dynamics and stability. Experimental investigation offers the benefits of direct measurements of temperatures, velocity, and exhaust gases using laser diagnostic equipment and gas analyzers.

However, the repetition of experiments for parametric studies, especially design modifications, is usually tedious and expensive. A relatively less demanding and less costly alternative is the Computational Fluid Dynamics (CFD) method, widely accepted in design processes, investigations of parameter variations, and scientific research in combustion systems. Recent developments in CFD tools have considerably narrowed the disparity between computational and experimental results, reinforcing the confidence and assurance in CFD calculations.

1.2 Research Objectives

The current research work is focused on experimental investigation and numerical simulation of oxy-combustion characteristics of lean premixed hydrogen-enriched methane flame in a small-scale gas turbine combustor using a novel multi-hole/micromixer burner design. Validation of the numerical models was carried out against experimental data obtained from the conducted experiments. The specific objectives are:

1. To investigate cold flow (non-reacting) mixing of gases in a micro-mixing burner using computational Fluid dynamic (CFD) modeling tools.
2. To experimentally investigate the stability and characteristics of premixed hydrogen-enriched oxy-methane flame under varying operating conditions of hydrogen fraction (HF), adiabatic flame temperature (AFT), and equivalence ratio (ϕ).
3. To develop a computational Fluid dynamic (CFD) model to investigate the combustion and emission characteristics of premixed H_2-enriched oxy-methane flames.

1.3 Dissertation Methodology

The objectives of this dissertation were achieved through the procedures outlined below:

- Numerical simulation of mixing quality and characteristics in a single tube of the micromixer was performed using laminar, species transport model with kinetic theory method of estimating mass diffusivity on ANSYS FLUENT 19. The numerical model was validated with experimental results and was used to conduct parametric studies on the effects of fuel hole size, tube length, and number of fuel holes on mixing quality.
- Experiments were conducted in a vertically oriented upward-fired micromixer-fitted premixed combustor with power density range (3.5 – 20 MW/m^3bar) at different equivalence ratios (0.1 - 1) and hydrogen fraction (0 – 70%) of CH_4/H_2 fuel mixture in CO_2/O_2 environment at atmospheric condition. At every hydrogen fraction (HF) (step of 5%), the equivalence ratio was swept in steps of 0.05 to determine the both the flashback and blowout stability limits. Images of some flames within the stable flame zone were captured and temperature distributions along axial and radial directions were measured.
- The stability map for the micromixer combustor was plotted on an equivalence ratio vs hydrogen fraction axes and delineated by blowout and flashback limits.

The stability map was superimposed on the numerically generated contours of adiabatic flame temperature (AFT), power density (PD), headend pressure drop (Δp) and Reaynolds number (Re) to investigate the effects of these parameters on the stability limit.

- Numerical simulation of flame and emission characteristics of selected stable flame points were conducted using ANSYS FLUENT 19. The numerical model was validated with experimental results and was used to conduct parametric studies of the effects of hydrogen enrichment on combustion characteristics.

1.4 Organization of Dissertation

This dissertation is made up of seven chapters.

Chapter 1 covers the concept of global warming as related to CO_2 emissions, carbon capture technologies, combustion techniques and methods of flame stabilization

Chapter 2 entails the literature review covering flame types, implementation of oxycombustion technology, effects of hydrogen enrichments on combustion process, flame stabilization with flameholders, computational models for premixed combustion.

Chapter 3 describes the experimental set up for the micromixer-stabilized oxycombustion, numerical models implemented in solving mixing and combustion problems, uncertainty analysis in temperature and flow rates.

Chapter 4 focuses on the numerical solution of the mixing problem for reactants of oxycombustion of methane in a single tube of the micromixer. The validation of the model through comparison with experimental results is presented.

Chapter 5 shows the stability map, flame images and temperature measurements of oxycombustion of hydrogen-enriched methane in a laboratory scale combustor under atmospheric conditions.

Chapter 6 presents the CFD modeling of selected flame points in the stability zone identified in the previous chapter. Grid independence of the cylindrical combustor has been investigated and presented. Numerical results are compared with the experimental results obtained. Effects of hydrogen enrichment on flame and emission characteristics are presented.

Chapter 7 comprises of the conclusion which highlights the main findings of this thesis and recommendations for future research.

CHAPTER 2

LITERATURE REVIEW

2.1 Combustion Techniques

Generally, combustion techniques are classified by the manner of injecting reactants into the combustion chamber. Hence, we have (i) a non-premixed combustion technique that involves the separate introduction of reactants into the combustor and produces diffusion flame. This technique is less cumbersome in design (absence of premixing chamber), produces flame with wide stability limit, but has a drawback of low efficiency (ii) premixed combustion technique in which the reactants are mixed before injection into the combustor and produces a premixed flame. This technique has high combustion efficiency and low NOx emission. Premixed flames are short and intense but highly susceptible to instability at low equivalence ratio (iii) partially-premixed mode involves burning non-uniformly mixed reactants that produce a flame with both diffusion and premixed characteristics flames.

Fossil fuel usage is still attractive due to its abundance, high energy content, cheap cost, and well-established combustion technology as found in power plants. However, the main drawback of fossil fuel energy sources is that their burning is linked to greenhouse gas emissions such as CO_2, H_2O, and others like CO and NOx, which are drivers of adverse climatic changes.

Fossil fuel combustion, therefore, has been one of the largest contributors to global warming. Established technologies for carbon capture in the utilization of fossil fuels for greenhouse (CO_2) emission control, as shown in Figure 2.1, are;

(i) pre-combustion capture involves removal of carbon from the fuel before combustion through processes such as steam reforming, shift reaction, and CO_2 separation,

(ii) post-combustion capture entails removal of CO_2 from combustion products by absorption or adsorption using amine solvents or Metal-Organic Frameworks respectively,

*(iii)*oxy-fuel combustion technology of burning fuel in oxygen.

Oxy-combustion of fuel is the most promising of the carbon capture/sequestration techniques primarily because of advantages such as in-process CO_2 capture, complete elimination of thermal NOx emission and low-cost incorporation into existing combustion systems [10].

2.2 Oxy-fuel combustion

Oxy-fuel combustion involves burning fuel with pure oxygen, resulting in CO_2 and H_2O as the main combustion products. This ensures the eradication or significant reduction of oxides of nitrogen in the products based on small percentage of N_2 that may exist in the fuel. However, combustion with ordinary oxygen results in extreme combustion temperatures that are harmful to combustor liners.

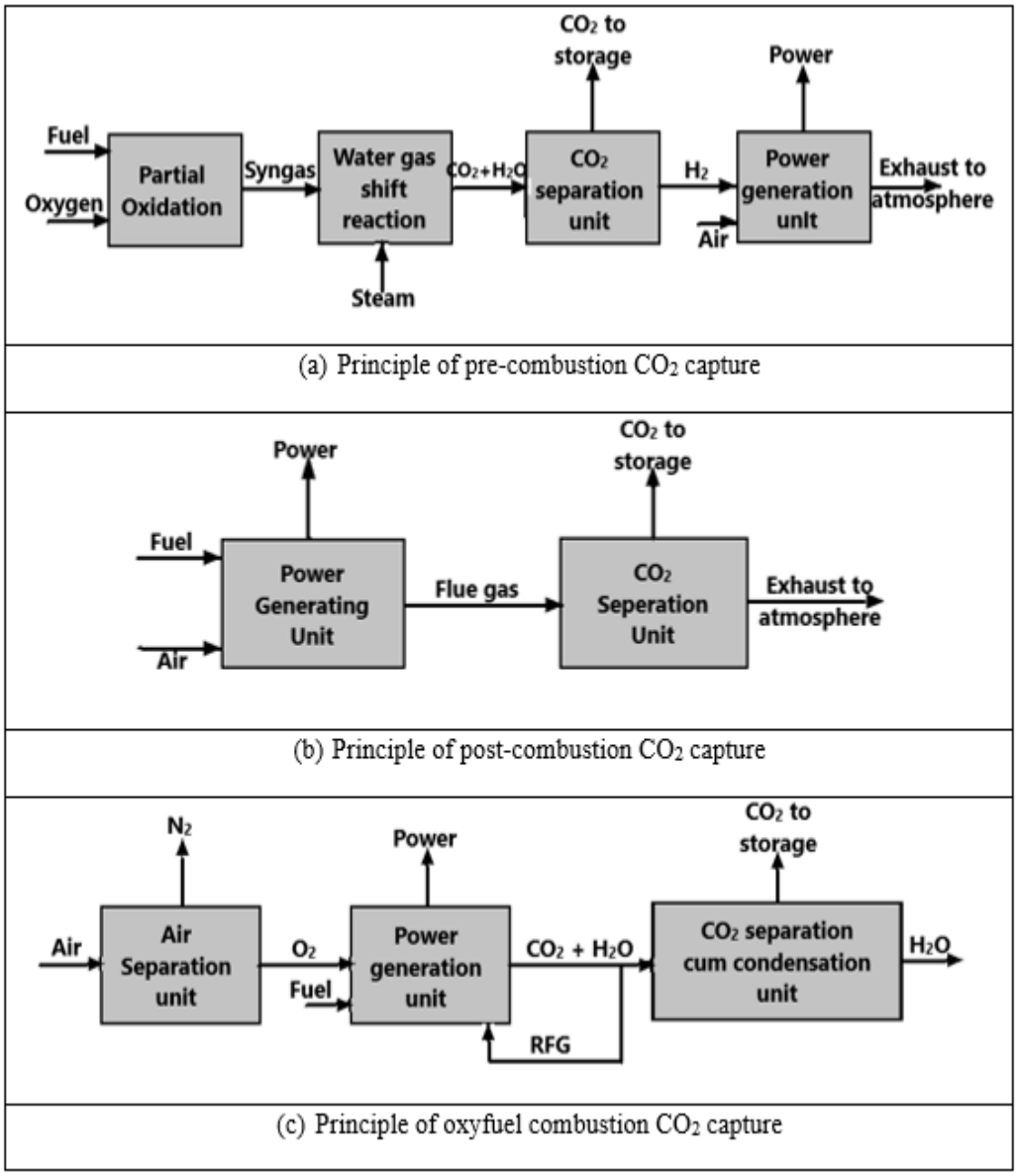

Figure 2.1 Carbon capture combustion technologies

Hence, a specified quantity of the gas is recycled to reduce the combustion temperature while CO_2 is separated from the remaining flue gas by condensing H_2O [45]. The characteristics of oxy-fuel combustion differ significantly from conventional air combustion due to disparity in the chemical kinetics and thermophysical and radiative properties of the diluents (i.e., CO_2 vs. N_2) [21,46,47]. The considerable difference in mixture density, volumetric heat capacity, mass diffusivity, absorption coefficient, and kinematic interactions have adverse effects on flame characteristics (flame shape, flame speed, and flame stability), pressure drop, radiative heat transfer, and chemical kinetic rate [21,48,49].

Carbon dioxide has a higher density and volumetric heat capacity at equal oxygen fraction values and temperature than N_2. The higher density affects the flame shape and pressure drop, while the higher volumetric heat capacity lowers the temperature, thereby reducing the flame speed and flame stability limit. The flame speed is also affected by the slow diffusion rate of O_2 in CO_2, reducing the burning velocity. Summarily, replacing N_2 with CO_2 in the oxidizer produces low flame speed, longer and weaker flames [50,51]. As a result, an oxygen fraction greater than 0.21 is required for oxy-combustion to produce matching flame properties as air–combustion at equal equivalent ratios [21]. This was observed by Liu et al. [52] for oxy-coal combustion in a down-fired furnace, where the OF had to be increased from 21% to 30% to achieve a temperature profile comparable to that of air-combustion.

Andersson et al. [53] also reported unstable oxy-coal combustion for OF less than 25%. Song et al. [54] reported the need for OF of 36% in oxy-methane flames to achieve a temperature profile comparable to that of air-methane flames. Rashwan et al. [48] reported stable oxy-combustion within the OF range of 29-38% for partially-premixed natural gas flames on perforated plate burners. Other studies reported matching flame features for oxy-flames of 30% OF and air-flames [15,55,56].

2.3 Hydrogen enrichment

Strict emission regulations and the ever-increasing energy demand have necessitated using low-carbon fuels such as methane (CH_4) or carbon-free fuels such as hydrogen (H_2). Asides from producing lower amounts of CO_2, CH_4 is widely used fuel to power engines and turbines because of its low production cost. However, CH_4 flames are more likely to blow out at very lean conditions due to the low burning velocity and high ignition temperature [57]. H_2 is synonymous to clean combustion, but it is costly to produce. The economical use of H_2 is thus achieved by blending it with less costly fuels such as CH_4. Studies of CO_2-diluted oxy-fuel combustion show that CO_2 addition reduces laminar flame speed and slows chemical kinetics [58,59]. Such adverse effects can be overcome through hydrogen enrichment. Hence, hydrogen-enriched fuels are considered a viable alternative to natural gases due to better combustion performance [60,61].

Studies have shown that hydrogen addition increases the laminar flame speed (S_L) [34], the turbulent flame speed (S_T) [62], and the adiabatic flame temperature (T_{ad}) [63]. A linear correlation exists between the hydrogen fraction (HF) of the fuel blend and the laminar flame speed [64,65]. Tang et al. [66] reported with the increase of HF that the unstretched S_L increases, and the laminar flame thickness reduces. The increased S_L in hydrogen-enriched fuel combustion can be attributed to the increased molecular diffusivity of hydrogen and enhanced rate of formation of radicals (OH, H, O) [67] due to faster reaction rates and high laminar burning velocity of hydrogen [68]. Zhang et al. [69] reported that hydrogen enrichment causes a monotonic increase in S_T under lean combustion. Daniele et al. [70] explained that S_T increases with hydrogen addition due to enhanced flame wrinkling by small scales caused by a marginal increase in flame-front curvature. Zhang et al. [69] studied the effects of H_2-enrichment and CO_2-dilution on methane-air flames and reported that S_T/S_L increases/decreases with H_2-enrichment/CO_2-dilution, respectively.

Hawkes and Chen [71] performed a Direct numerical simulation (DNS) of lean premixed methane-air flame using reduced chemical kinetics to study the effect of hydrogen addition on flame stability. They measured flame stability through turbulent flame speed and showed that hydrogen addition causes higher turbulent burning velocity in coherence with an extended stability limit. The high burning rate of hydrogen enhances chemical reaction, increases the reaction zone's temperature, and reduces gas recirculation into the reaction zone [33].

Hydrogen addition also influences flame behavior because of its high burning rate [72]. Subash et al. [30] investigated the effects of varying hydrogen concentration, 0-50% by volume, on methane-air flames experimentally stabilized on a 4th generation dry low emission (DLE) burner made of a three-concentric premixing section. They reported that hydrogen enrichment at a constant global equivalence ratio reduces total flame extension due to the higher laminar flame speed of hydrogen. Guo et al. [73] reported enhanced flame anchoring with increased hydrogen addition for a lean-premixed hydrogen-enriched methane-air flame.

Emadi et al. [74] studied the effects of hydrogen addition on the maximum flame surface densities of lean premixed methane-air flame on a low swirl burner. They reported increased flame surface densities due to increased flame wrinkling caused by hydrogen enrichment. Similar results were reported by Hallter et al. [37] for a bunsen burner. Hydrogen addition increases flame wrinkling and flame area due to its preferential diffusive nature, which reduces the Lewis number by making mass diffusion dominant in the transport equation. Cammarota et al. [75] showed the significant effect of 10% molar concentration of hydrogen in fuel on the stability of methane-air flame by increasing Markstein length, indicating the modification of flame sensitivity and stretch rate the addition of hydrogen. Schefer et al. [76] reported that hydrogen enrichment of a swirl stabilized lean premixed methane-air flame increases OH concentration and strain resistance and modifies the flame structure to be shorter and more robust.

The results showed that hydrogen addition extends the lean flammability limit of premixed methane-air flame due to the higher strain resistance before extinction and higher concentration of OH, O, and H radicals. The extended lean flame stability limit of hydrogen-enriched flame can be attributed to the high flame speed of hydrogen [77]. For the effect of hydrogen enrichment on emissions, Schefer et al. [76] reported a substantial decrease in CO emission and a negligible impact on NO emission for lean premixed combustion of methane-air in a swirl combustor. Adding hydrogen to lean and rich premixed methane-air flames resulted in negligible and significant effects on NO emission, respectively [78]. Significant reduction in CO emission due to hydrogen addition was reported for lean premixed combustion of methane-air mixture for swirler fitted Colorless Distributed Combustor (CDC) [79] and CDC reversed flow configuration as well [80].

The literature is rich with studies on the influence of hydrogen blending on the stability of air flames in the lean zone, and the hydrogen fraction (HF) was identified as the main factor. Very few studies have, however, investigated H_2-enrichment in oxy-fuel combustion under premixed conditions. Abdelwahid et al. [34] experimentally studied the effects of HF (0 – 90%), OF (0 – 50%), and inlet bulk velocity (4.4, 5.2, and 6.0 m/s) on the static stability characteristics of premixed H_2-CH_4 flames in a swirl combustor. Stability maps showing the stable flame regions, delineated by blowout and flashback zones, were created within the OF-HF space against the contours of mixture Reynolds number (Re), combustor power density (PD), and adiabatic flame temperature (AFT).

Results showed that stable flame was achieved in the range of HF of 0–90% and OF of 16–44% and that H_2-addition limits the range of Re and OF for stable flame operation. A similar study conducted by Imteyaz et al. [28], in which the stability map was created within the HF-ϕ space at fixed OF=30% for HF range of 0-75%, showed that the most effective range of H_2-enrichment on flame stability is 20-50%. Increasing HF was generally found to enhance the reaction kinetics in the combustion zone, resulting in shorter and more compact flames. The flame stability limits were found to be independent of AFT. Asif et al. [84] reported shorter and more robust flame with hydrogen addition indicating enhanced chemical reaction rates on the same combustor. A numerical and experimental investigation was conducted by Nemitallah et al. [81] to study the effects of hydrogen fraction and inlet velocity on the combustion characteristics of swirl-stabilized premixed $H_2/CH_4/O_2/CO_2$ flame at fixed oxygen fraction (OF) and at stoichiometric condition. They reported high Damköhler number values indicating that the reaction rates mainly dominate the flame structure with negligible influence by swirl-generated turbulence. It was also shown that hydrogen addition causes enhanced heat release rate and wider operability limits.

2.4 Flame-holders/Burners

Premixed combustion is more efficient, in terms of lowered emissions rates, when operated at lean conditions. However, premixed flames are more susceptible to combustion instabilities in flame blow-off mode under this condition. Thus, making flame stabilization a critical factor in the design of burners.

Flame stabilization is achieved in most gas turbines by incorporating bluff bodies such as swirl vanes and multi-holes in burner heads.

2.4.1 Swirlers

Swirl stabilized flames are widely utilized in technical and industrial applications such as combustors for gas turbines. The flames can be sustained over a broad operational range even at low equivalence ratios, which is of great importance in lean premixed combustion systems. They offer a non-intrusive way of creating disturbances in flow fields and flame temperature control to minimize thermal NOx emissions [82]. Swirl vanes as shown in Figure 2.2a induce swirling on reactant mixtures before introduction into the combustor. The swirl vanes impact centrifugal force, which causes the flow to spread right from the combustor entrance and create a low-pressure region at the combustor centerline [83], which eventually causes vortex breakdown as the centrifugal force decays gradually downstream due to viscous effects [84].

The swirled flow has two velocity components; axial and swirl. The swirling effect reduces the magnitude of the axial velocity flow component, and this wanes the strength by which flame is convected downstream, thereby enhancing flame anchoring [85]. The swirl velocity component creates an inner (central) recirculation zone (IRZ) and outer (corner) recirculation zone (ORZ) close to the wall at the combustor inlet as shown in Figure 2.2b. The IRZ ensures flow entrainment and mix of burnt and upstream fresh unburnt mixtures, which sustain continuous and stable combustion [86].

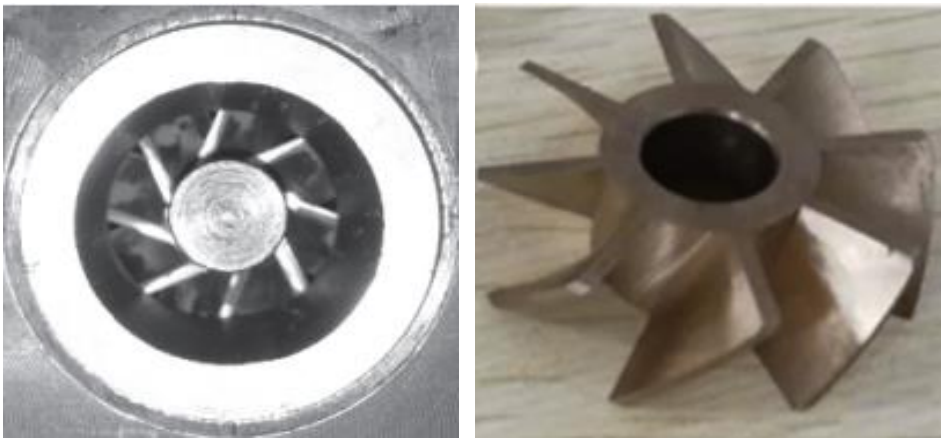

(a)

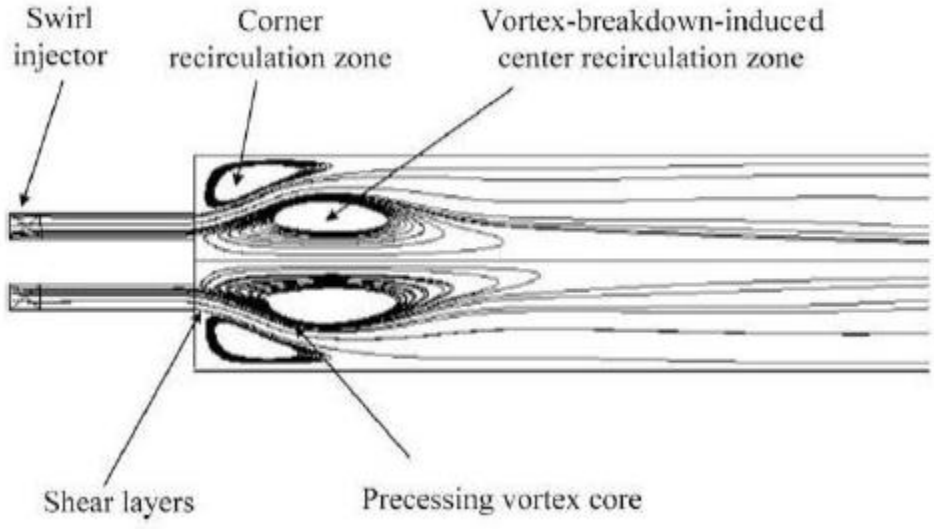

(b)

Figure 2.2 Diagrams of (a) swirl vanes [73,89] (b) typical flow field in a swirled combustor [90].

Although similar mixing occurs in the ORZ, flame stabilization is not supported by the outer shear layer because of low heat release and significantly reduced reaction as detected by OH^* chemiluminescence measurements [87]. Also, flame stabilization in the outer shear layer is limited by the combined effects of heat losses and strain [88].

2.4.2 Micromixers/multi-hole/perforated plate burners

Recently, micromixers/multi-hole burners as shown in Figure 2.3 have found applications in small-scale gas turbines and condensing boilers because of benefits such as compactness, low pollutant emission, and well-distributed flames. Multi-hole burners are more efficient in fuel economy and heat generation in lean combustion mode due to how the flames are attached to the burner [91]. The burners are solid bodies with patterned holes (either circular or rectangular), which anchor a set of miniature conical or bell-shaped flames downstream. The geometry is carefully designed to achieve operability and emission control with respect to the number of holes and pitch distances [92].

The operating conditions, such as pressure difference across the plates and equivalence ratio, are meticulously selected to avert flashback [93]. They produce miniature flames, which are more stable than a single large flame. The micromixer flame is characterized by several conical flames' collective effect, making the flame dynamics different from a single conical flame [94]. The closeness of multiple conical bases restricts the lateral motion of micromixer flames.

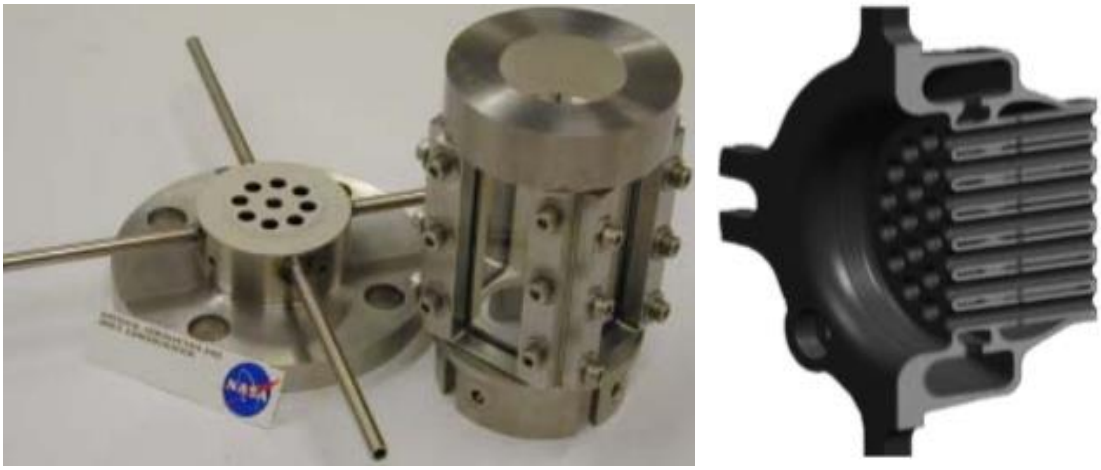

Figure 2.3 Multi-hole or micromixer burners [96,97].

The flames are connected and stabilized by U-shaped zones situated near the stagnation point and characterized by combined heat loss and flame stretch [95]. Kedia and Ghoneim [95] reported that the stabilization point is reached when flame displacement speed equals flow speed and flame displacement speed gradient supersedes flow speed gradient.

One of the main advantages of using multi-hole burners is the low NOx emission. Multi-hole burners induce shorter residence time on reactants to produce miniature flames with low NOx emission [98]. Other parameters available for optimizing low NOx are the control of reaction rate (adjusting combustor temperature and pressure) and premixing [85]. However, they are associated with reduced turbine efficiency and instability as drawbacks, respectively. Emission produced by perfectly-premixed combustion of natural gas/air with a perforated plate burner under real-time industrial gas turbine cycle operating conditions was experimentally and numerically investigated by Elkady et al. [99]. They studied the effects of pressure (6.8 – 16.3 atm) and combustion residence time (10 – 20 ms) on NOx production and reported that increasing these parameters increases NOx emission at elevated temperature. They suggested that the relationship P^n = NOx emission has n as the temperature-dependent variable.

Supplying uniformly mixed reactant mixture to multi-hole burners ensures low NOx emissions at a low equivalence ratio [100]. A sub 10ppm NOx emission was achieved in another study by an N_2-diluted hydrogen multi-tube heavy-duty gas turbine combustor under practical turbine conditions [43].

AlAdawy et al. [101] experimentally studied the effect of turbulence on NO_x emission in lean perfectly premixed CH_4-air combustion by varying the multi-hole burner channel height to vary the turbulence level. They reported that turbulence level has a negligible effect on overall NO_x emission of the post-flame zone.

Multi-hole burners are inherently fueled flexible, as reported in the literature. Aside from methane-air combustion cited above, some other studies also utilized high carbon fuels (ethane-butane) and syngas. Edacheri Veetil et al. [102,103] numerically studied the effects of operating parameters on stabilizing premixed propane-air and premixed syngas flames, respectively, using perforated plates of similar geometrical design. Also, Jatoliya et al. [104] studied the propane-air mixture's premixed flame characteristic using a multi-hole matrix burner. Kim et al. [105] experimentally and numerically investigated non-premixed flame characteristics of LPG (98% propane) and pure oxygen mixture using a multi-jet burner by studying the mixing characteristics using the scalar dissipation rate. York et al. [43] designed and tested single and full can micromixer for air combustion of carbon-free syngas (60% H_2-40% N_2) at actual turbine conditions.

Some studies on multi-hole burners revolve around the effects of geometric designs, material properties, and operating conditions on premixed flame stability.

An analytical model for predicting temperature and flame standoff distance for methane-air combustion on a perforated plate was proposed by [106].

Kedia and Ghoneim [95] conducted a numerical investigation of flame stabilization and blow-off of lean premixed CH_4-air flame anchored by a perforated plate. They reported that blow-off, which is affected by heat loss, sets in when flame displacement speed gradient equals flow speed gradient. Flame displacement speed was said to be non-monotonically dependent on the mean inlet velocity of the reactants. Decreasing the width of perforated burners reduces flame stability which eventually leads to blow-off [107]. Altay et al. [108] reported that increasing thermal conductivity reduces flame–wall heat transfer while hole-pitch defines the flame base curvature. Also, increasing operating parameters such as the mean inlet velocity and mixture equivalence ratio increases flame height and lift-off [102]. Lee & Hwang [44] observed that flame stability and blow-off depend on flow distribution and equivalence ratio. As the equivalence ratio decreases, flame color changes from green to yellow to blue (most stable flame), after which blow-off occurs.

Dodo et al. [109] conducted a flame-stability and NOx-emission test on a prototype MM-fitted low-NOx combustor for air-combustion of H_2-rich syngas (40-65% hydrogen). They reported stable combustion with very low NOx emissions for the fuel blends considered, thereby overcoming the challenge of flashback inherent in premixed combustion of high H_2-content syngas with conventional low-NOx combustor technologies.

Asai et al. [110] discovered that MM with a convex-shaped perforated plate could suppress combustion oscillation to achieve stable combustion and stable sub-10-ppm NOx emission for the air-combustion of H_2-rich syngas over a wide range of H_2 content. Hollon et al. [93] developed and tested a full-scale MM injector for lean premixed combustion of H_2-rich fuels with air as an oxidizer. Flashback-free stable combustion was observed with extremely low NOx emission. Rodrigues and Fernandes [111] conducted an experimental study to investigate the effects of hole quantity, hole size, and inter-hole spacing of a perforated plate on premixed flame stability for both methane-air and propane-air mixtures. Similar results were obtained for both fuels. They reported that flame stability degrades with increasing inter-hole spacing, while the hole size and number of holes have negligible effects on stability. Zhou et al. [112] reported that hole size affects flame front propagation and pressure oscillations of premixed H_2/air flames. Perforated plates with smaller hole sizes are more effective in stabilizing combustion-induced oscillations, according to Oh et al. [113]. Some methods of enhancing uniformly distributed stable flames include incorporating baffle plates to adjoin the burner and creating retention holes at the periphery of the plates [24]. Raghvan et al. [114] experimentally investigated flame stability's dependence on retention holes of a rectangular multi-hole burner utilizing methane as fuel. They observed that inclusion of retention holes aided flame stability at low equivalence ratios. The above studies were carried out with air as an oxidizer.

So far, few studies have explored the oxy-fuel combustion characteristics in premixed multi-hole/micromixer burners. Rashwan et al. [115] conducted an experimental investigation on oxy-combustion characteristics of perforated plate stabilized CNG premixed flame to study the influence of oxygen fraction on flammability limits and reported oxygen fraction of 29% as lower flammability limit due to blow-off and 42% oxygen fraction as upper flammability limit due to flashback. Ibrahim et al. [116] experimentally investigated the effects of HF, OF, and equivalence ratio on the combustion characteristics of partially-premixed H_2/CNG/O_2/CO_2 flame supported on a perforated plate burner. Hussain et al. [117] carried out experiments to quantify the stability limits of a premixed oxy-combustion gas turbine micromixer over ranges of HF and OF. They reported the burner's ability to sustain stable flames down to OF=21% without hydrogen enrichment and OF=13% at 65% HF. The focus of this work is to experimentally and numerically investigate the combustor operability limits and combustion and emission features of hydrogen-enriched oxy-methane flames in a premixed micromixer-adapted model combustor for gas turbine clean combustion applications. Aliyu et al. [118] experimentally studied the combustion characteristics of lean-premixed CO_2-diluted oxy-methane flames in a micromixer supported gas turbine burner. They mapped the stability limits over equivalence ratio - oxygen fraction (OF) space. They observed that the combustor stability limits are strongly controlled by the adiabatic flame temperature (T_{ad}), while the combustor temperature distribution is strongly dependent on the equivalence ratio.

2.5 Mixing

In many applications, fluid mixing is usually achieved through mixers, either conventional industrial mixers or micromixers. Micromixers differ from the conventional macro-scale types in the fact that they are smaller with more efficient mixing. High quality and rapid mixing of fluids are essential in microfluidic systems, applicable in devices like heat exchangers and micro-reactors, and applications such as synthesis and analysis of organic chemicals. As the mixer's size decreases, fluid patterns become more laminar, tending towards creeping flow in extreme cases of micromixers with sizes in tens of microns. A steady laminar flow is characterized by parallel streamlines, depicting the lack of radial convection mixing and lack of spatial homogeneity. Therefore, mixing is governed by molecular diffusion. Enhanced molecular diffusion and shorter mixing length can be achieved through flow manipulation to profoundly increase the interphase surface area between the fluids and reduce diffusion paths [119]. Several mechanisms have been proposed to achieve enhanced mixing, of which chaotic advection and split and rejoin are the most popular mechanisms.

Mixers are classified as active and passive mixers. The main principle behind these mixers is to reduce the mixing path of molecules to enhance mixing. Active mixers are primarily based on the chaotic advection mechanism and require external energy, such as pressure perturbation [120] and periodic perturbation [121], to divide the flow into tiny filaments to improve contacts between fluids and reduce the mixing path. Their downsides are difficulty in fabrication and maintenance.

These shortcomings are overcome in passive mixers, enhancing surface contacts between fluids to reduce the mixing path without external energy. Some techniques applied in the design of passive mixers are hydrodynamic focusing [122], multi-lamination [123], T-shaped junction [124], splitting and rejoining [125], and bend-induced stirring [126].

Fluid mixing is widely applied in numerous applications. For premixed combustion, in which the reactants must be mixed before introduction into the combustor, the mixing quality [127] and velocity uniformity [128,129] promote complete combustion and reduce pollutants emissions. The nature of mixing concerning the shortest gas mixture residence time significantly affects achieving extended combustion range and high combustion efficiency in micro-combustors used for powering micro-devices [130]. In some processes, the reaction rate is even limited by mixing. Synthesizing gases such as the syngas fuel from natural gas, either by partial oxidation or catalytic auto-thermal reforming, depends on mixing processes in determining the reaction progress [131].

High mixedness can be attained with conventional macro-scale premixing chambers but at the expense of extended length requirements, which are not suitable for small-scale combustion applications. Some premixing techniques that are suitable for small-scale combustion have been explored.

In the study by AlAdawy et al. [101] on the effects of turbulence on NOx emissions using perforated burners, a perfectly premixed methane-air mixture was achieved by radially injecting methane through a 6.35-mm hole into a stream of preheated air and passing the mixture through a coiled tube of length-to-diameter ratio of 280.

Another compact air-fuel mixer, which operates on entrainment of gases by fans rotating at high speed to achieve thorough mixing at low-pressure drop, was employed by Lee et al. [132] to supply premixed liquefied natural gas (LNG)-air to a perforated burner. However, a short manifold was placed between the mixer and the burner plate to straighten the flow. Micromixer burner usually operates in premixed mode as a passive mixer, where the reactants are adequately mixed before injecting them into the combustor. Premixing ensures the homogeneity of the reactant mixture, limiting the occurrence of varying equivalence ratio, which is more likely to occur in non-premixed combustion systems. Haj Ayed et al. [133] studied the influence of burner geometry on flow and flame characteristics and NOx emissions in an industrial gas turbine implementing dry-low-NOx (DLN) hydrogen-air combustion with a prototype micromixer hydrogen combustor that has 1600 tiny fuel injectors. Intense mixing was achieved in each injector by perpendicular injection of hydrogen from a 0.3-mm diameter hole into crossflow of air in a small chamber adjoining the burner head. A previous study by the same group used a 1.0-mm hydrogen injector for a high-density burner to investigate similar factors [134].

Lee et al. [135] experimentally and numerically investigated radial and axial micromixing of fuel and air and concluded that the micromixer technology could reduce the emissions and flashback risk. Funke et al. [136] tested the effect of fuel-to-air momentum-flux ratio on stabilizing H_2/air flames in a micromixer combustor. They reported that this technology allows for secure and low-NOx combustion of hydrogen in air.

2.6 Numerical combustion model

Turbulent combustion of gaseous fuels involves the interaction of complex physical phenomena like turbulence, chemical reaction, and heat transfer, which are diverse and possess a broad range of temporal and spatial scales [137,138]. While the comprehensive modeling of each phenomenon is yet to be fully resolved, combustion modeling is even more challenging due to complex interactions such as turbulence-chemistry interaction, turbulence-temperature-density coupling, chemical kinetics, and radiation effects [139]. For decades, the combination of RANS and simple combustion models have been successfully applied to simulate combustion problems, especially for stable flames in simple geometry. The time-averaging approach is limited in capturing transient effects, adequately captured in the large eddy simulation (LES) approach. The recent rapid upgrade in computational power has made LES more common as a research tool for simulating engineering problems. LES approach has been proven to be more accurate in handling complex turbulent chemical reacting flows [140,141].

Furthermore, LES is a reliable method for unsteady flows because it provides an unsteady solution that can predict flame stability from unsteady behaviors like vortex breakdown, predict pollutant emission from the mixing fields and define operability of an engine from the transient characteristics of flames [141]. The LES approach is a filtering technique that resolves and computes the large eddies directly and models the small, turbulent scales. The large eddies are unsteady, transport the bulk of turbulent kinetic energy and Reynold stresses in the flow, and depends on the boundary and initial condition. In contrast, the small eddies are mostly isotropic in nature, homogeneous in characteristics, dissipates turbulent kinetic energy, and supplies little Reynolds stress to the flow [142,143]. In addition to modeling unresolved scales, LES modeling of chemical reactive flows also requires modeling small scales of chemical reaction and molecular mixing smaller than the LES grid, i.e., reaction rates (rate controlling process) small-scale regime [144]. Except for the linear eddy model, other LES combustion models are variants of the earlier existing RANS-based models [145].

RANS and LES-based combustion models for numerical investigation of flame characteristics are based on theoretical, experimental, and DNS studies. Several combustion models have been developed for different flame types and applied to a wide range of applications such as jet flame, swirl flames, IC engines, etc. The premixed turbulent combustion model's primary challenge is developing an adequate closure model for the mean reaction rates. This forms the basis for the existence of various types of models.

Although there is no distinct classification of combustion models for premixed flames, they can be classified into either assumption-based and non-assumption-based models.

- Assumption-based combustion models: These models simplify the turbulence-chemistry interaction or reaction rate closure with assumptions such as reaction limited, mixing limited, and thin flame assumptions. They are easy to implement, less computationally expensive, and proven to adequately quantify fundamental quantities like flame temperature, flame length, etc. However, their application is limited to specific premixed regimes. It is primarily inaccurate in predicting pollutant emissions, complex fuel flame characteristics, pre-vaporized spray combustion, stability limits, and real combustor conditions [141]. Examples of these models are; chemical reactor model, mixing limited model, flamelet model [146].
- Non-assumption-based combustion models: the models solve each reacting scalar's transport equations and captures the turbulence-chemistry interaction through the simultaneous online solution of reaction kinetics and flow convection/diffusion. They can predict local extinction, pollutant emission, reaction zone length, and position. Although their application is not limited to any regime of the premixed flame, they are computationally expensive to implement. Examples of these models are; transport probability density function (T-PDF) model [147], conditional moment closure (CMC) [148], eddy dissipation concept [149].

2.6.1 Models for Premixed Combustion

There are various models for simulating premixed flames available on commercial software. For cases where the finite rate chemical kinetics are important, reaction-based models which involves solving transport equation for each specie involved in the reaction such as;

- Laminar finite rate model: this model ignores the turbulence fluctuations while the reaction rates are modeled by Arrhenius kinetic expressions. The model is accurate for laminar flames but not suitable for turbulent flames except supersonic flames with slow turbulence-chemistry interaction and relatively slow chemistry.
- Eddy-dissipation-concept model: detailed chemical kinetics are embedded in turbulent flows. The model assumes reaction occurs in fine-scale turbulence structures. It models the reaction rate source term in terms of length fraction of fine scales, time scale, and fine-scale mass fraction. It is computationally expensive.
- Composition PDF Transport model: highly non-linear reaction rate chemical sources are closed without modeling, making it more accurate than others.

Other available models such as c-equation and G-equation are based on the flame front tracking approach. The flame front serves as the combustion zone, which separates the downstream burnt region from the upstream unburnt region.

2.6.2 Flame-front tracking model - c-equation model

This model requires solving transport equations for a scalar variable c, termed reaction progress, compared to solving transport equations for every reacting species found in reaction-based models. The reaction progress c is an accepted variable for describing thermochemistry in premixed turbulent combustion. It varies within the bounded values of 0-1, representing unburnt reactants to burnt products, respectively. Defining thermochemistry in terms of c only is suitable for Lewis number close to 1 defined by low Mach number and adiabatic process. Flow properties such as mass fraction, density, and temperature are computed from the suitable definition of reaction progress which can be in terms of scaled mass fraction of products, fuel mass fraction, or temperature is given as;

$$c = \frac{Y_P}{Y_{P\infty}},\ c = \frac{Y_F - Y_{F0}}{Y_{F\infty} - Y_{F0}},\qquad c = \frac{T - T_0}{T_\infty - T_0} \quad \text{respectively} \qquad (2)$$

where Y_P = product species, $Y_{P\infty}$ = value Y_P in the fully-burned or equilibrium products, Y_F= instantaneous mass fraction of fuel, Y_{F0} = mass fraction of fuel in the fresh reactant, $Y_{F\infty}$ = value of Y_F in the products, T_0 = limiting temperatures in the reactants and T_∞ = limiting temperatures in the products.

Reaction progress defined in terms of temperature is not widely accepted because of its limitation to Lewis number =1, making it invalid whenever the temperature is affected by external factors like heat loss or acoustics. The condition for using reaction progress c is that it must be bounded between 0 and 1, monotonic, and capable of describing the thickness and location of flame structures.

For turbulent flames, the combined effects of turbulence and thermal expansion increase density fluctuation, which introduces additional term to transport equation quantities. An accepted technique for avoiding additional density correlation terms is the Favre density-weighted averaging. The averaging concept is similar to RANS or LES as it filters length and time scales related to turbulence nature. For quantity Q, the Favre decomposition is expressed as, $Q = \tilde{Q} + Q^{"}$ where the mean component $\tilde{Q}$, is defined as $\tilde{Q} = \overline{\rho Q}/\bar{\rho}$ and the fluctuation component $Q^{"}$ behaves as $\overline{Q^{"}} \neq 0$ but $\overline{\rho Q^{"}} = 0$.

2.6.3 Other Premixed Turbulent Flame Modelling

Defining closures for the reaction rates gives rise to various classes of models. Similar reaction rate models are available on RANS and LES platforms. Simple models are based on Eddy Break Up (EBU) approach [150], in which the mean reaction rate is determined by turbulent mixing. The advantages of these models are simplicity and less computational cost but, their shortcoming is insensitivity to reaction chemistry. Dupoirieux et al. [151] conducted an experimental and numerical study of premixed methane-air flame stabilization by hot gases recirculation behind a rearward-facing step. The numerical simulation was carried out with the RANS k-ε turbulence model and EBU combustion model using CHARME solver. Some models, such as the flame surface density model, are based on flamelet concepts. The flamelet concept defines the flamelet as a sheet-like reaction zone within the premixed flame, and it is highly resistant to disruption by turbulent eddies.

Hence, flamelet structure is prevalent in premixed combustion over a broad range of turbulent velocity fluctuation magnitudes and turbulent eddy length scales. Flamelets are robust reaction surfaces which are ensembles of thin, highly-stretched reaction surfaces responsible for most combustion reaction in premixed turbulent flames. The flamelet approach to modeling turbulent premixed flames cannot be applied to all flame types. Its application is limited to premixed regimes with low Karlovitz number (Ka = characteristic chemical time scale/Kolmogorov time scale) cases of corrugated and wrinkled flamelet zones. Defining flame structures in flames approaching flammability limits or extinction due to turbulent straining effects becomes more difficult because of the weakening balance between reaction and diffusion.

Resolving the flame front structure is no more fashionable, and modeling unresolved terms such as turbulence fluctuations can be achieved by more general approaches such as the Premixed Conditional Moment Closure (P/CMC) approach. The model uses the reaction progress variable c and specifies a term called scalar dissipation (also known as micro-mixing or small-scale mixing) to represent small-scale turbulence and characterize turbulent time scale. Reaction rates characterize the chemistry time scale. The P/CMC approach models how a combustion process is influenced by relative sizes of turbulence and chemistry time scales. One advantage of the P/CMC model is how to solve reacting flows with complex chemistry and fluid dynamics at a moderate computational cost.

Broben-diaz et al. [152] implemented Tabulated PCMC in CFD code on OpenFOAM to incorporate thermochemistry in the flow dynamics in their combustion study of fuel surrogate (n-dodecane) in a backward-facing step combustor geometry. P/CMC model is solved along with a steady RANS flow formulation with RNG k-ε turbulence model. Despite the promising results obtained with steady RANS, it is not suitable for predicting the transient nature of flames classified as distributed or well-stirred due to their high turbulent nature [146].

2.6.4 Presumed-PDF model

Most premixed combustion models assume that the fuel-oxidizer mixtures are perfectly mixed based on the equivalence ratio before introducing the combustor. For cases where this assumption does not hold, a form of premixed flame model known as partially premixed combustion model is suitable for the combustion of non-uniform reactant mixtures [153]. The model is a combination of reaction progress variables and PDF concepts. The model determines reaction progress variable c by solving C-equation along with chemical equilibrium model using PDF [21] and Zimont model to determine turbulent flame speed [18-20]. Quali et al. [82] numerically investigated how low swirl stabilized premixed flames behavior such as flow and thermal field, methane distribution, and thermal NOx are affected by methane-air equivalence ratio using partially premixed combustion model coupled with RANS Standard k-ε turbulence model on ANSYS FLUENT 14.

With the same CFD package, Sudarma et al. [154] implemented the partially premixed combustion model in studying the effect of turbulence model on lean premixed methane-air flame in a bluff body stabilized combustor. Their results showed that the two turbulence models investigated (Standard k-ε and Reynolds Stress Model (RSM)) correctly predict combustion features (velocity, temperature, and species distribution) in the recirculation region near the burner. Still, either over-predicts or under-predicts the combustion features downstream the recirculation zones. Although additional scalar variance and covariance transport equations are solved, the presumed PDF model is more suited for turbulence complex reaction mechanisms. It executes a multidimensional PDF for gas temperature and species concentration for efficient computation time. A swirl-stabilized methane-air partially premixed jet flame was simulated using the presumed joint PDF model for temperature and RSM turbulence model for turbulence closure [155]. The presumed PDF includes unresolved turbulent structures in the modeling.

Based on the above literature review, the micromixing concept has been recently developed and implemented successfully for stable lean-premixed ultra-low-emission air-fuel combustion. However, the literature lacks similar studies on using this concept to develop an efficient oxy-fuel micromixer/flame-holder for implementation in zero-emission combustion applications.

The current study thus aims to bridge this gap by proposing a micromixer design that can function as both mixer and oxy-fuel flame-holder and is suitable for small-scale premixed combustors and industrial ones. Part of this work's focus is achieving a high degree of mixing by varying the geometrical and injection features of a single tube of the micromixer. This entails numerical investigation of the effects of fuel inlet diameter, mixing length, and number and circumferential distribution of fuel inlets on the degree of mixing of oxy-fuel reactants, comprising methane, oxygen, and carbon dioxide. The other part of this work investigates experimentally and numerically the effect of H_2-enrichment on the blowout limit of a model gas-turbine combustor stabilizing premixed oxy-methane flames on a micromixer-like multi-hole burner. The micromixer design used in the first part of the work (mixing quality study) is simplified into multi-hole burner and a mixing plenum long enough to ensure perfect mixing of reactants at the inlet of the multi-hole burner, hence the term micro-mixer-like multi-hole burner. All tests were carried out at a fixed jet velocity of 5.2 m/s and fixed OF = 30% (by vol.), analogous to the 21% of air-fuel combustion, as reviewed earlier. Combustor operability limits were depicted in terms of stability maps and flame shapes. The stability maps were obtained over ranges of ϕ (0.1-1) and HF (25-70%) to define the static stability limits, while the flame shapes close to these limits were explored to explain the flame extinction mechanism.

CHAPTER 3

METHODOLOGY

3.1 Introduction

This chapter describes the procedures followed in achieving the objectives of this study. It is divided into three sections, namely:

- methodology for the experimental investigation of the effects of hydrogen on micromixer stabilized premixed oxy-combustion methane flame's stability and flame characteristics.
- numerical modeling of cold flow (no combustion) mixing in a micromixer burner tube.
- numerical modeling of turbulent premixed $H_2/CH_4/O_2/CO_2$ flame in a micromixer fitted model combustor for gas turbine applications.

3.2 Experimental setup

3.2.1 Gas turbine model Combustor

The schematic diagram of the model combustor is shown in Fig. 3.1 shows schematics of the test rig for the multi-hole combustor. The vertical test rig comprises three main sections: mixing chamber, multi-hole burner, and combustor chamber. The mixing chamber and the multi-hole burner are used to simplify real micromixers and perform the mixing and flame holder functions, respectively.

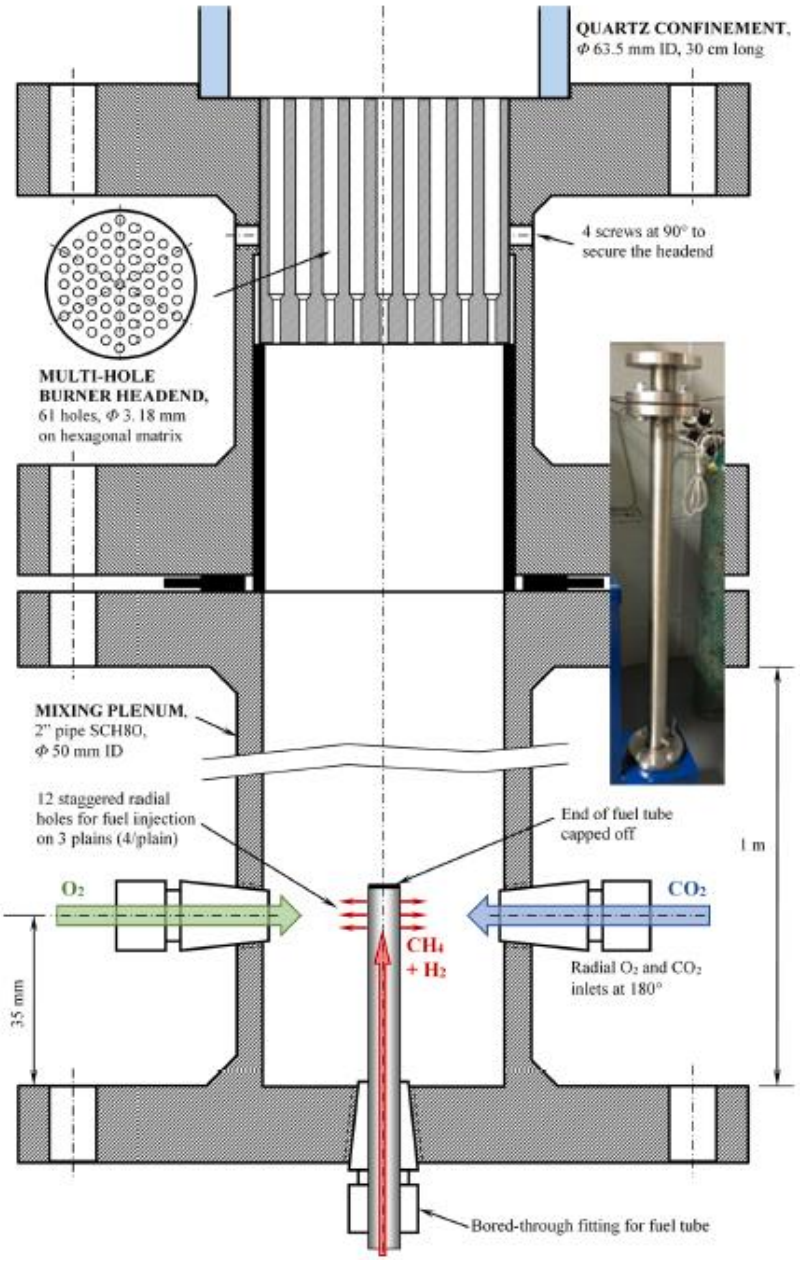

Figure 3.1 Schematics of premixed model gas turbine oxy-combustion set-up.

This ensured a uniform equivalence ratio for all jets to neutralize the effect of jet-to-jet variation in the equivalence ratio. Premixing of reactants and diluents occurs in the cylindrical mixing chamber of height 1.07 m and diameter 50.8 mm, extending from the rig base to the bottom (inlet) of the multi-hole burner. The CO_2-diluent and O_2-oxidizer gases are supplied as cross-flow through wall-fitted 6.7 mm diameter nozzles located at 35 mm height from the base. A premixed mixture of hydrogen and methane is supplied to the mixing chamber through twelve 1mm diameter holes at the tip of a 6.35 mm diameter centralized tube. The holes are circumferentially arranged on three planes around the tube. The fuel mixture is injected at the plane of oxidizer and diluent injection to enhance mixing.

Moreover, the height of the mixing chamber ensures the supply of a homogeneous mixture to the combustor. Upstream the combustor is the multi-hole burner head that serves as a bluff body to stabilize the flames. The multi-hole burner is cylindrical stainless steel with dimensions 50.8mm-diameter and height 50.0mm, consisting of 61 hexagonally patterned holes at 5.5mm pitch distance as depicted in the plan view of Figure 3.2. The holes are designed to serve as flame arrestors in the advent of flashback, which is the main problem of premixed flames. Each hole has a varying cross-section consisting of 1.588 mm (1/16 in) diameter sub-hole of height 8 mm and 3.175 mm (1/8 in) diameter main-hole of height 40 mm adjoining the mixing chamber and combustor, respectively. The combustion chamber is optically accessible made of 63.5 mm internal diameter, 6 mm thick, and 30cm long quartz glass. The combustor exit is open to the atmosphere.

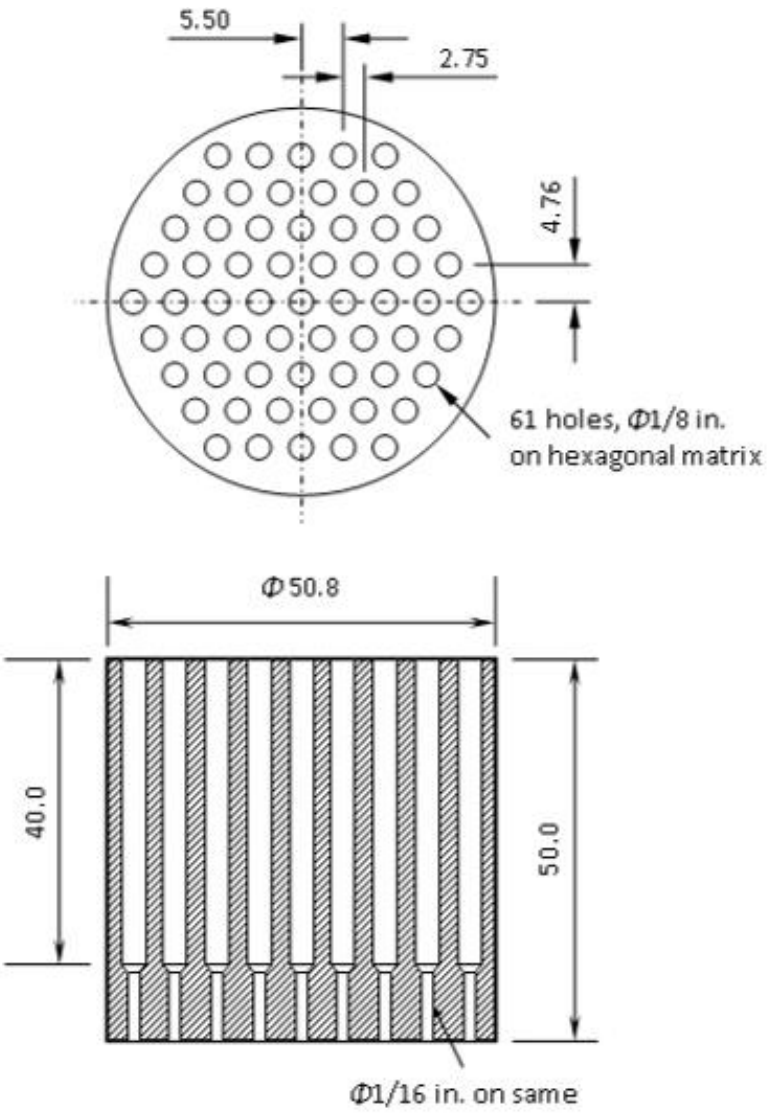

Figure 3.2 Plan and cross-sectional view of the multi-hole burner

3.2.2 Experimental facility

The combustion test rig is connected to the gas supply facility, as shown in Fig. 3.3. The gases (CH_4, H_2, O_2, CO_2) are sourced from compressed gas cylinders. Each gas line is fitted with valves and pressure regulators to control the flow and flow rotameter to control mass flow rates.

The flow is controlled with vales and pressure regulators. All gases are metered using Bronkhorst High-Tech and Aalborg Inc. mass flow controllers with an uncertainty of $\pm$0.5% of full-scale. CH4 and H2 are premixed by passing both gases through a T junction (choke) and the fuel mixer to create turbulence and enhance homogeneous mixing of the fuel mixture before supplying to the combustion rig through the fuel tube. Combustor and flame temperatures were taken using an R-type thermocouple (Pt Rh-13% / Pt) with a maximum reading of 1500 ^{0}C inserted from the combustor's top. The thermocouple is connected to the data logger and computer for data acquisition at one end and fixed to a transverse mechanism that ensures probe movement in axial and radial directions in the combustor. Each of its wires is enclosed in a ceramic tube as a shield from high flame temperatures. Temperature data are corrected for radiation heat transfer to the surroundings using the equation of Brohez et al. [156]. Selected flame images were captured with a 50 frames/sec digital camera set at 5.6 f-stops, 1/60 shutter speed, and 3200 ISO sensitivity to study the effects of various parameters such as adiabatic flame temperature, equivalence ratio, and pressure difference across the burner head on the flame macrostructure.

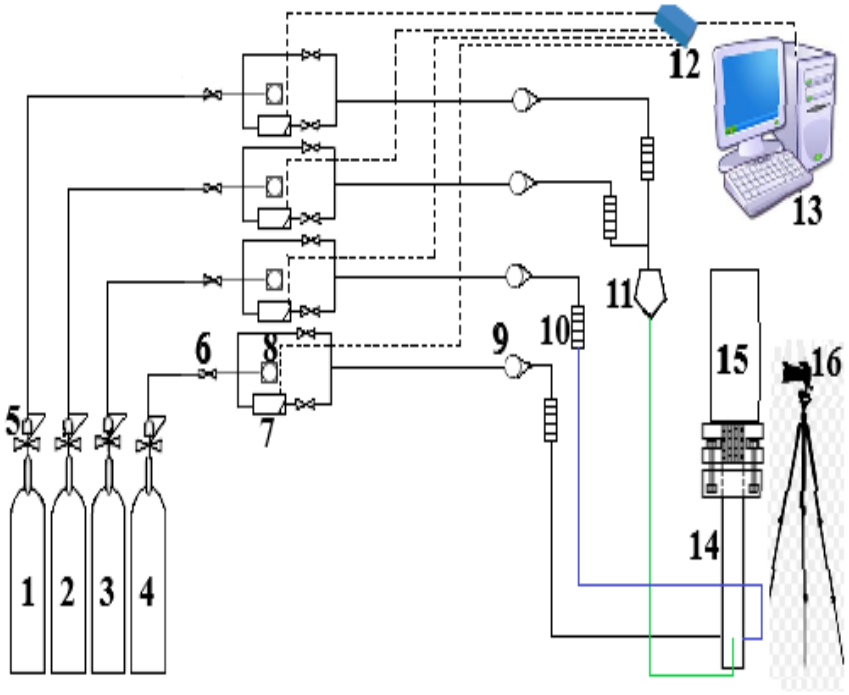

1	Hydrogen cylinder	7	Mass flow controller	13	Computer set-up
2	Methane cylinder	8	Pressure gauge	14	Combustor test rig
3	Oxygen cylinder	9	One way valve	15	Combustion chamber
4	Carbon dioxide cylinder	10	Flow meter	16	Digital camera setup
5	Pressure controller	11	Fuel mixer		
6	Valve	12	MFC interface		

Figure 3.3 Schematics of the experimental test rig of premixed gas turbine model combustor for this study.

3.2.3 Operating conditions

Experiments were conducted to determine the stability for equivalence ratio ranging 0.1 - 1 and different hydrogen concentration in the fuel mixture (HF) ranging from 25% H_2 (75% CH_4) to 70% H_2 (30% CH_4) at constant mixture oxygen concentration in the oxidizer/diluent mixture (OF) of 30% (70% CO_2).

All flames in this study had a fixed jet velocity v=5.2 m/s to maintain similar flow conditions and turbulence intensities for all isothermal flow fields. Keeping the inlet velocity constant also neutralizes its effect on flame stability, as the inlet velocity was proven to be a more relevant parameter controlling flame stability than inlet Reynolds number [157,158].

To maintain the jet velocity constant, the flow rates of CH_4, H_2, O_2, and CO_2 were calculated for each flame at its HF and ϕ. The equivalence ratio is varied in steps of 0.5, while the HF is varied in steps of 5%. Stability limits were determined by varying equivalence ratios between 0.1 -1 at every 5% step of HF until a blow-out occurs or strong acoustic noise is experienced to locate the static stability limit or dynamic stability limit. Then, the flame shape and size are captured with the high-speed camera for studying the flame macrostructure. All gases are supplied at 25^0C, and experiments are conducted at 1 atm.

The stoichiometric combustion equation of hydrogen-enriched oxy-methane combustion is expressed as:

$$CH_4 + \gamma H_2 + \left(2 + \frac{\gamma}{2}\right)\left[O_2 + \left(\frac{1}{OF} - 1\right)CO_2\right] \rightarrow \left[1 + \left(\frac{1}{OF} - 1\right)\left(2 + \frac{\gamma}{2}\right)\right]CO_2 + (2 + \gamma)H_2O \quad (3.1)$$

Where $\gamma = [HF / (1 – HF)]$.

For OF = 30%, the non-stoichiometric equation can be expressed as:

$$CH_4 + \gamma H_2 + \frac{1}{\phi}\left(2 + \frac{\gamma}{2}\right)\left\{O_2 + \frac{7}{3}CO_2\right\} \rightarrow \left[1 + \frac{7}{3\phi}\left(2 + \frac{\gamma}{2}\right)\right]CO_2 + (2 + \gamma)H_2O + \left(\frac{1}{\phi} - 1\right)\left(2 + \frac{\gamma}{2}\right)O_2 \quad (3.2)$$

Equation 3.2 was analyzed thermodynamically to estimate the combustion products' AFT for a given combination of HF and ϕ.

This estimation is based on the negligible effect of CO2 dissociation and the complete combustion of the fuel. This assumption is based on the comparison of estimated peak stoichiometric combustion of the fuel mixture at temperature of 2000 K and onset of CO_2 dissociation at temperature of 2400 K [159]. Such assumptions should result in an insignificant error (~100 K) in calculating the AFT [160–162]. All flames in this study were non-preheated, i.e., the inlet temperature was 300 K.

The power density (PD) of the reactor, which quantifies the amount of energy stored in a given system in $MW/m^3/bar$, is determined from:

$$PD = \frac{\dot{m}_{CH_4} \times CV_{CH_4} + \dot{m}_{H_2} \times CV_{H_2}}{\text{Combustor volume} \times \text{Combustor pressure}} \quad (3.3)$$

Where $\dot{m}$ represents mass flow rate, and CV represents standard tabulated calorific value for simplicity.

The Reynolds number (Re) of the $CH_4/H_2/O_2/CO_2$ mixture, calculated based on each hole of the multi-hole burner, is defined as:

$$Re_{mix} = \frac{v\,\rho_{mix}\,D_h}{\mu_{mix}} \quad (3.4)$$

Where v is the jet velocity (5.2 m/s) and D_h is the hole diameter (3.175 mm).

The mixture density ρ_{mix} is defined as;

$$\rho_{mix} = \frac{P}{R_u T}\sum y_i M_i \quad (3.5)$$

The mixture viscosity μ_{mix} was determined from [163] as;

$$\mu_{mix} = \frac{\sum y_i \mu_i \sqrt{M_i}}{\sum \mu_i \sqrt{M_i}} \quad (3.6)$$

Where y represents mole fraction, M represents molar mass, and i represents each mixture component.

The pressure drops across burner headend, Δp, is approximated as:

$$\Delta p = \frac{1}{2}\rho_{mix} v^2 \quad (3.7)$$

3.3 Computational modeling and formulations for cold flow (tube mixing)

3.3.1 CFD modeling

Two numerical approaches to studying gas mixing have been reported in the literature. The first approach is the well-known method of solving continuity and Navier-Stokes equation for the mixture and mass conservation equation for k-1species, where k is the total number of species. The second approach, known as the two-fluid model, implemented by Zahmatkesh et al. [164] to parallel mixing flow is based on the gas kinetic theory model. It requires solving macroscopic balance equations (continuity, momentum, and energy) for each specific component of the mixture and equation sets (continuity, momentum, and energy) for the mixture average. This eliminates the use of diffusion coefficients for describing the diffusion processes. The first approach was implemented in this study to investigate mixing in a single tube of a micromixer burner fed with CH_4, O_2, and CO_2.

The computational domain of the micromixer tube is shown in Fig.3.4. It has a diameter (D) of 3.2 mm and evenly spaced fuel-injection holes at a height equal to one tube diameter (3.2 mm) from the base. CH_4 fuel is supplied through the holes as jet flow, while the main flow inside the micromixer tube is a mixture of O_2 and CO_2 flowing from bottom to top. A 3-D model of the tube domain was created and discretized using ANSYS DesignModeler and Meshing, respectively, and FLUENT 19.2 was used as the Computational Fluid Dynamics (CFD) solver.

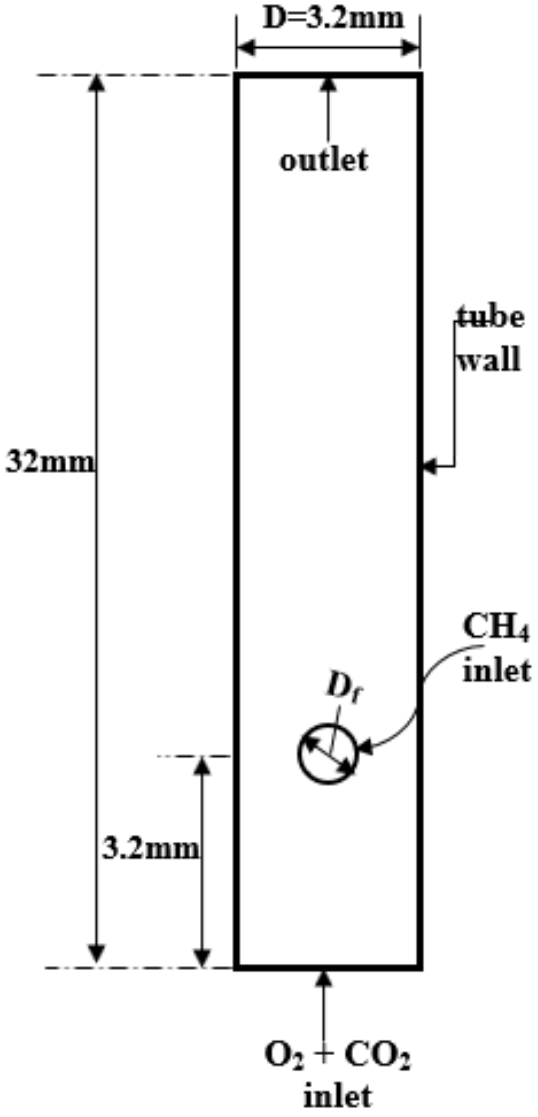

Figure 3.4 Schematic diagram of flow domain.

Laminar flow solution was implemented based on the values of Reynolds number calculated at three different locations: i) at fuel inlet, Re_f = 42.45, ii) at oxidizer inlet, Re_o = 952.9, and iii) at tube mid-length, Re_D = 1078.1.

The gravitational force was also considered due to the vertical orientation. Based on these assumptions, the following general governing equations comprising mass, momentum, and species transport were solved:

- Continuity:

$$\frac{\partial}{\partial x_i}(\rho u_i) = 0 \tag{3.8}$$

- momentum

$$\frac{\partial}{\partial x_i}(\rho u_i u_j) = \frac{\partial \sigma_{ij}}{\partial x_i} - \frac{\partial p}{\partial x_j} - \rho g_i \tag{3.9}$$

The stress tensor can be expressed in terms of strain as:

$$\sigma_{ij} \equiv \left[\mu\left(\frac{\partial u_i}{\partial x_j} + \frac{\partial u_j}{\partial x_i}\right)\right] - \frac{2}{3}\mu\frac{\partial u_l}{\partial x_l}\delta_{ij} \tag{3.10}$$

- Species transport

$$\frac{\partial}{\partial x_i}(\rho u_i Y_k) = -\frac{\partial}{\partial x_i}J_k + R_k \tag{3.11}$$

Where, μ is the molecular viscosity, I is the unit tensor, Y_k is the species mass fraction, and $\vec{J}_k$ is the diffusion flux of species *k*. According to Fick's law, diffusion flux is directly proportional to species concentration gradient:

$$J_k = -\rho D_{k,m}\frac{\partial Y_k}{\partial x_i} \tag{3.12}$$

Where, $D_{k,m}$ is the mass diffusion coefficient of specie k in the mixture.

Out of the various available methods for calculating $D_{k,m}$, the multicomponent method that entails defining diffusion coefficient using kinetic theory was adopted as it is the most suitable for diffusion-dominated laminar flows involving ideal gas mixtures.

It involves specifying the Lennard-Jones parameters for each specie, which will be used to compute the binary diffusion coefficient D_{kl} using the Chapman-Enskog formula [165] in equation (3.13), then, the D_{kl} is related to $D_{k,m}$ through the relation by Wilke [166] in equation (3.14) as follows:

$$\mathrm{D_{kl}} = 0.00188 \frac{\left[\mathrm{T^3}\left(\frac{1}{\mathrm{M_{w,k}}} + \frac{1}{\mathrm{M_{w,l}}}\right)\right]^{1/2}}{\mathrm{p_{abs}}\sigma_{\mathrm{kl}}^2 \Omega_{\mathrm{D}}} \tag{3.13}$$

$$\mathrm{D_{k,m}} = \frac{1 - X_{\mathrm{k}}}{\sum_{\mathrm{l,l\neq i}}(X_{\mathrm{l}}/\mathrm{D_{kl}})} \tag{3.14}$$

Where, D_{kl} is the mass diffusion coefficient of specie k in specie l, T is the temperature, M_w is the molecular weight of species, p_{abs} is the absolute pressure, σ_{kl} is the Lennard-Jones characteristic length, Ω_D is the diffusion collision integral, and X_k is the mole fraction of specie k. The parameter, Ω_D, is a function of T^*, which is related to the Lennard-Jones energy parameter, $(\epsilon/k_B)_{ij}$ by $T^* = \frac{T}{(\epsilon/k_B)_{ij}}$.

3.4 Numerical modeling of the model gas turbine combustor

As one of the objectives of this work, three-dimensional numerical modeling of the micromixer-like combustor was carried out to investigate oxy-combustion characteristics for varying hydrogen concentrations. Large-Eddy Simulation (LES) of the turbulent premixed flame was carried out using the commercial software ANSYS-Fluent 19.2. Three-dimensional conservation equations for mass, momentum, species, and energy were solved simultaneously to predict the flow field, flame features, and emission characteristics of premixed $H_2/CH_4/O_2/CO_2$ flames.

The set of governing equations comprising continuity, momentum, progress variable, mixture fraction, and enthalpy equations can be generally expressed in the form [167,168]:

$$\frac{\partial}{\partial t}(\rho\Phi) + \frac{\partial}{\partial x_i}(\rho u_i) = \frac{\partial}{\partial x_i}\left[\Gamma_\Phi \frac{\delta\Phi}{\delta x_i}\right] + S_\Phi \tag{3.15}$$

Where Φ corresponds to any scalar variable, u_j represents the velocity in j direction, Γ_φ denotes the diffusion coefficient, and S_Φ is the source term.

3.4.1 Turbulence model

The flow turbulence is solved using the LES model, which resolves the large eddies and models the small (sub-grid) ones. It involves applying a filtering process to filter out the small eddies. A low-pass filtering operator was applied as:

$$\bar{\Omega}(x,t) = \int G(r,x)\,\Omega(x-r,t)\,dr \tag{3.16}$$

Where *G* denotes the filter function that determines the large-scale eddies, and the equation is integrated over the whole domain. The Favre-averaged filtered forms of the continuity and Navier-Stokes equations are:

- Continuity equation

$$\frac{\partial \bar{\rho}}{\partial t} + \frac{\partial}{\partial x_i}(\bar{\rho}\tilde{u}_i) = 0 \tag{3.17}$$

- Momentum equation

$$\frac{\partial}{\partial t}(\bar{\rho}\tilde{u}_i) + \frac{\partial}{\partial x_i}(\bar{\rho}\tilde{u}_i\tilde{u}_j) = \frac{\partial \bar{\sigma}_{ij}}{\partial x_i} - \frac{\partial \bar{p}}{\partial x_j} - \bar{\rho}g_i - \frac{\partial \tau_{ij}}{\partial x_i} \tag{3.18}$$

Where σ_{ij} represents the stress tensor due to molecular viscosity; σ_{ij} is defined as:

$$\sigma_{ij} \equiv \left[\mu\left(\frac{\partial \bar{u}_i}{\partial x_j} + \frac{\partial \bar{u}_j}{\partial x_i}\right)\right] - \frac{2}{3}\mu\frac{\partial \bar{u}_l}{\partial x_l}\delta_{ij} \tag{3.19}$$

Where τ_{ij} denotes the subgrid-scale stress, which is expressed as:

$$\tau_{ij} \equiv \rho\overline{u_i u_j} - \rho\bar{u}_i\bar{u}_j \tag{3.20}$$

The filtered τ_{ij} consists of two parts that are modeled differently. The isotropic part was combined with the filtered static pressure term, while the deviator part of the filtered τ_{ij} was modeled in terms of turbulent viscosity in the form:

$$\tau_{ij} = -2\mu_t\bar{S}_{ij} \tag{3.21}$$

Where μ_t is the turbulent viscosity and S_{ij} is the strain tensor rate.

The Wall-Adapting Local Eddy-viscosity (WALE) model, used to model the turbulent viscosity, is expressed as:

$$\mu_t = \rho L_s^2 \frac{\left(S_{ij}^d S_{ij}^d\right)^{3/2}}{\left(\bar{S}_{ij}\bar{S}_{ij}\right)^{5/2} + \left(S_{ij}^d S_{ij}^d\right)^{5/4}} \quad (3.22)$$

Where the expressions for L_S and S_{ij}^d are given as:

$$L_S = \min\left(\kappa d, C_w V^{1/3}\right) \quad (3.23)$$

$$S_{ij}^d = \frac{1}{2}\left(\bar{g}_{ij}^2 \bar{g}_{ji}^2\right) - \frac{1}{3}\delta_{ij}\bar{g}_{kk}^2 \quad (3.24)$$

Where $\bar{g}_{ij} = \frac{\partial \bar{u}_i}{\partial x_j}$, κ represents the Von Karman constant, C_w represents the WALE constant, d represents the distance to the nearest wall, and V represents the volume of the computational cell.

3.4.2 Combustion model

Combustion was modeled with the thin flamelet model. It is a partially premixed option in ANSYS FLUENT, which can be modified for premixed flame by setting the inlet mixture fraction to a constant value (fuel-to-mixture ratio) to indicate that the inlet mixture is a combustible mixture and the mixture fraction variance is 0 by virtue of constant equivalence ratio. The model is a flame front topology approach assuming that the flame is made of an infinitely thin flame front in between unburnt and burnt mixtures. The flame front is indicated by the reaction progress variable, which assumes a value between 0 (unburnt mixture) and 1 (burnt mixture). The effect of turbulence on the flame brush is assumed to be purely kinematic, i.e., limited to wrinkling. Zimont turbulence flame speed model was used to close the mean reaction rate term. The chemistry, species concentration, and integrations were computed with non-chemical equilibrium-assumed shape β-PDF based on the inlet mixture composition.

The solution procedure involves solving Favre-averaged filtered transport equations for reaction progress variable $\bar{c}$ and mixture fraction $\bar{f}$and enthalpy is given as;

- Reaction progress variable equation:

$$\frac{\partial}{\partial t}(\bar{\rho}\tilde{c}) + \frac{\partial}{\partial x_i}(\bar{\rho}\tilde{u}_i\tilde{c}) = \frac{\partial}{\partial x_i}\left(\frac{\mu_t}{Sc_t}\frac{\partial \tilde{c}}{\partial x_i}\right) + \overline{\rho S_c} \quad (3.25)$$

Where Sc_t is the turbulent Schmidt number and $\overline{\rho S_c}$ is the favre-averaged reaction progress source term. The source term is expressed in terms of turbulent flame speed $\overline{S_t}$ as;

$$\overline{\rho S_c} = \overline{\rho_u}\,\overline{S_t}|\nabla\tilde{c}| \quad (3.26)$$

And the Zimont model for $\overline{S_t}$ in terms of laminar flame speed S_L is;

$$\overline{S_t} = A\overline{u'}^{3/4}{S_L}^{1/2}\alpha^{-1/4}{l_t}^{1/4} \quad (3.27)$$

Where A= 0.52, u'= $C_s\Delta|\bar{S}|$, l_t= $C_s\Delta$, α is the thermal diffusivity.

The mean reaction progress variable indicates the flame brush by assuming a value between 0 (unburnt mixture) and 1 (burnt mixture). The progress variable is defined in terms of mass fraction of species as:

$$c = \left(\frac{\sum_{i=1}^{n} Y_i}{\sum_{i=1}^{n} Y_{i,ad}}\right) \quad (3.28)$$

Where Y_i denotes mass fraction of product species i, and the subscript 'ad' represents the species after complete combustion.

- Mixture fraction equation:

$$\frac{\partial}{\partial t}\left(\bar{\rho}\tilde{f}\right) + \frac{\partial}{\partial x_i}\left(\bar{\rho}\tilde{u}_i\tilde{f}\right) = \frac{\partial}{\partial x_i}\left(\left(\frac{\mu}{Sc} + \frac{\mu_t}{Sc_t}\right)\frac{\partial \tilde{f}}{\partial x_i}\right) \tag{3.29}$$

The mixture fraction is expressed as:

$$f = \frac{sY_{fu} - Y_{ox} + Y_{ox,0}}{sY_{fu,1} - Y_{ox,0}} \tag{3.30}$$

Where s is the oxygen to fuel ratio, Y_{fu} and Y_{ox} are the fuel and oxidizer mass fraction, respectively, while 0 is the oxidizer inlet stream and 1 indicates fuel inlet stream. For premixed combustion where there is no separate inlet stream for oxidizer, the above equation can be re-written as;

$$f = \frac{sY_{fu} - Y_{ox}}{sY_{fu,1}} \tag{3.31}$$

- Enthalpy equation:

$$\frac{\partial}{\partial t}\left(\bar{\rho}\tilde{h}\right) + \frac{\partial}{\partial x_i}\left(\bar{\rho}\tilde{u}_i\tilde{h}\right) = \frac{\partial}{\partial x_i}\left(\left(\frac{k}{c_p} + \frac{\mu_t}{Pr_t}\right)\frac{\partial \tilde{h}}{\partial x_i}\right) \tag{3.32}$$

Under thin flame assumption, the thermochemical scalars such as specie fractions, density, and temperature are uniquely related to the probability density function (PDF) of f and $\bar{c}$ by:

$$\bar{\varphi} = \bar{c}\int_0^1 \varphi_b(f)\, p(f) df + (1-\bar{c})\int_0^1 \varphi_u(f)\, p(f) df \tag{3.33}$$

Where subscripts ‘b’ and ‘u’ represent burnt and unburnt mixtures, respectively. A 3D look-up table is created with the inclusion of enthalpy.

3.4.3 Radiation model

Radiative heat transfer was modeled with the radiative transport equation (RTE), which was solved using the discrete ordinate (DO) model. The DO model is suitable for oxy-fuel combustion since it is applicable over a wide optical thickness range [157]. The RTE was calculated once every five energy iteration. A field equation of the RTE in direction $\vec{s}$ is;

$$\nabla \cdot (\mathrm{I}(\vec{\mathrm{r}},\vec{\mathrm{s}})\vec{\mathrm{s}}) + (a + \sigma_{\mathrm{s}})\mathrm{I}(\vec{\mathrm{r}},\vec{\mathrm{s}}) = \mathrm{an}^2\frac{\sigma \mathrm{T}^4}{\pi} + \frac{\sigma_{\mathrm{s}}}{4\pi}\int_0^{4\pi}\mathrm{I}(\vec{\mathrm{r}},\vec{\mathrm{s}})\,\Phi(\vec{\mathrm{s}},\vec{\mathrm{s}}')\,\mathrm{d}\Omega' \tag{3.34}$$

The weighted-sum-of-gray-gases (WSGG) model was used to compute the gas mixture's absorption coefficient, as it has been applied over a wide range of operating conditions [169,170]. The total emissivity over path length L was estimated with the equation;

$$\varepsilon = \sum_{\mathrm{i}=0}^{\mathrm{i}=1} \mathrm{a}_{\varepsilon,\mathrm{i}}(\mathrm{T})[1 - \mathrm{e}^{-\kappa_{\mathrm{i}}\mathrm{PL}}] \tag{3.35}$$

Where $a_{\varepsilon,i}$ represents the emissivity weighting factors for the grey gas i, which are temperature-dependent. κ_i represents the absorption coefficient, and P represents the sum of partial pressures of absorbing gases. The temperature-dependent form of $a_{\varepsilon,i}$ is solved as;

$$\mathrm{a}_{\varepsilon,\mathrm{i}} = 1 - \sum_{\mathrm{j}=1}^{\mathrm{j}} \mathrm{b}_{\varepsilon,\mathrm{i},\mathrm{j}}\mathrm{T}^{\mathrm{j}-1} \tag{3.36}$$

Where $b_{\varepsilon,i,j}$ represents the polynomial coefficients for emissivity.

3.5 Uncertainty Analysis

Uncertainty analysis is carried out on the measurements to ascertain the credibility of experimental results and account for the errors that could arise through instrument selection, instrument calibration and environment. In this study, the uncertainty analysis was carried out with the steps outlined by Holman et al. [164]. The aggregate uncertainty in any specified measurement can be deduced from:

$$S = \left({S_{sensor}}^2 + {S_{DAS}}^2 + {S_{calib}}^2\right)^{\frac{1}{2}} \tag{3.37}$$

Where S is the total uncertainty in a measured quantity, and S_{sensor}, S_{DAS}, S_{calib} are the uncertainties in the sensor reading, data acquisition system and calibration process respectively. The uncertainties in temperature measurements and gas flow rates are presented in Table 3.1. The sets of experiments were conducted twice to check for reproducibility of results.

Table 3.1 Uncertainty in measured quantities.

Quantity	Exhaust temperature	Gas flow rate
Uncertainty, %	$\pm 0.5\ (°C)$	± 2

CHAPTER 4
NUMERICAL STUDY OF MIXING IN A SINGLE TUBE OF THE MICROMIXER BURNER

The study examines numerically the non-reacting flow and mixing characteristics inside a single tube of a micromixer burner for potential zero-emission premixed oxy-fuel combustion applications, such as gas turbines. The aim is to investigate how the geometrical parameters can affect the mixing quality in an oxy-fuel reactant mixture consisting of CH_4, O_2, and CO_2. The ranges of design parameters are fuel inlet diameter D_f (from 0.2 to 1.0 mm), number of fuel holes n, (4 and 6), and tube length L, (from 5D to 15D). The range of tube length studied is limited to 50 mm which is the maximum length of practical micromixers found in the literature [41].

4.1 Boundary Conditions

The mass flow rates were specified at the oxidizer, and fuel inlets at a common temperature of 298 K. Species mole fractions were also specified at the oxidizer inlet, while pressure outlet condition was specified at the tube outlet. No-slip and adiabatic boundary conditions were assigned at the wall. Steady-state laminar mixing flow was simulated with laminar viscous and species transport models using a pressure-based segregated solver. The pressure field was obtained using the Semi-Implicit Method for Pressure Linked Equations (SIMPLE) algorithm for pressure-velocity coupling.

Gradient for discretizing the convection and diffusion terms was evaluated with the least square cell-based method to suit the mesh's hybrid nature. The second-order upwind scheme handled spatial discretization of convection terms. Also, the density and pressure terms were discretized using the second-order upwind and standard scheme, respectively. The convergence criterion for all equations was that the level of summation of all residuals approaches the value of 10^{-6}.

4.2 Grid Independency study

The three-dimensional computational domain was discretized using a combination of tetrahedral and hexagonal elements. Tet-elements were applied close to the wall around the CH_4 inlets and up to a height of twice the tube diameter (2D) from the main flow inlet, while the downstream section was meshed with hex-elements as shown in Fig. 4.1. Mesh control was implemented to achieve efficient discretization and minimum convergence time. Finer meshes were applied at the CH_4 inlet faces as shown in Fig. 4.1. A grid-independence study was carried out with grid sizes of 341426, 477874, 679710, and 1109285 with D_f = 0.3 mm to select the grid size that has negligible influence on computational solutions as well as shortest convergence time using the CH_4 mass fraction at tube centerline, as shown in Figure 4.2a. To save computational time, while maintaining high accuracy, the 679710-cell grid size was adopted in this work. Also, Figure 4.2b shows the dependence of fuel inlet size on number of grids for D_f = 0.6, 0.4, 0.3, and 0.2 mm by comparing the radial profile of CH_4 mass fraction at tube length L = 32 mm. This confirms that the 679K mesh size chosen for this study is suitable for all fuel inlet sizes considered.

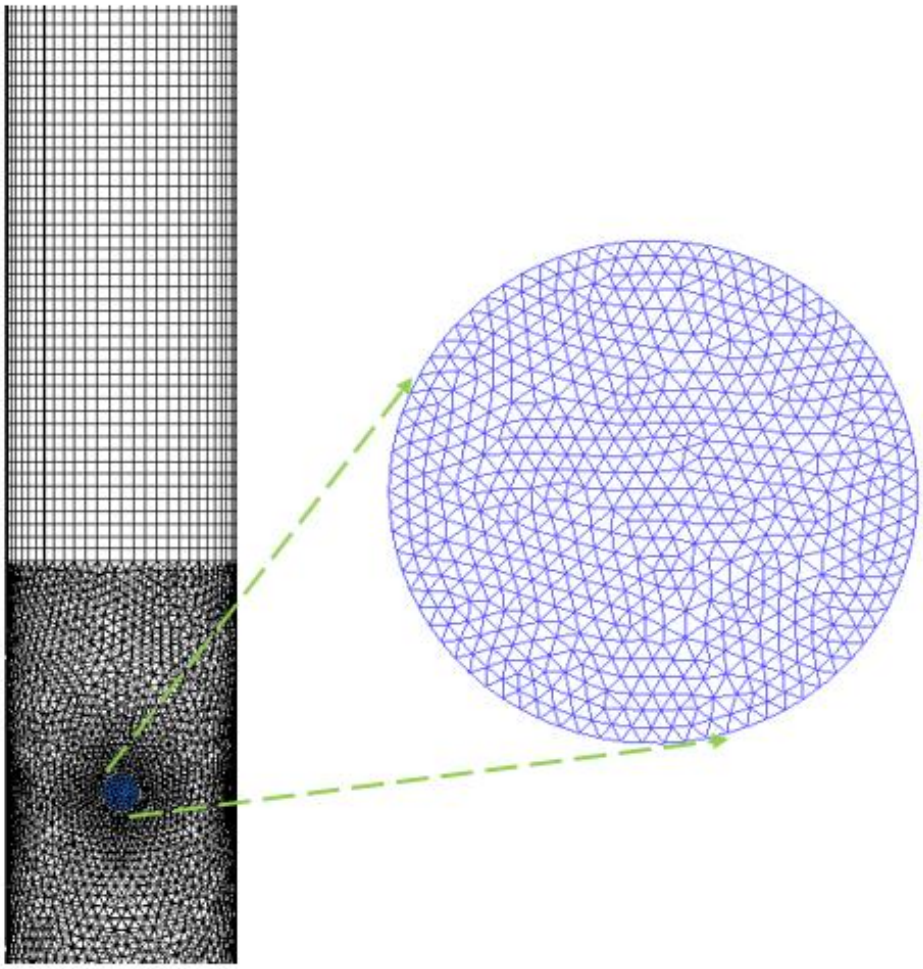

Figure 4.1 Mesh of computational domain and fuel inlet face.

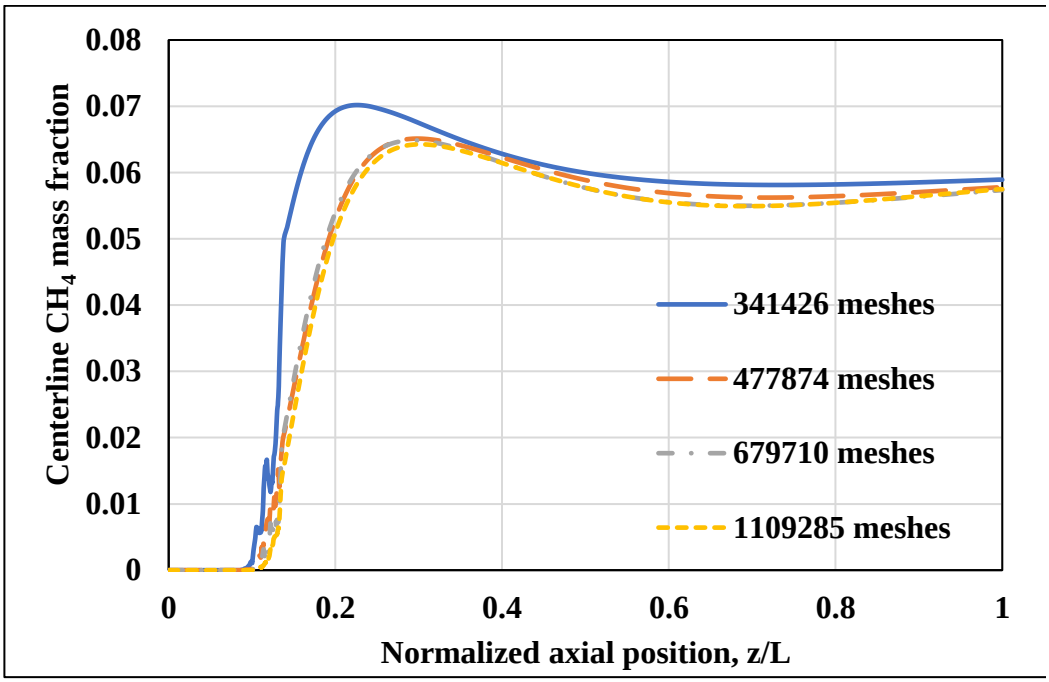
0.08
0.07
0.06
0.05
0.04
0.03
0.02
0.01
0
Centerline CH_4 mass fraction
0
0.2
0.4
0.6
0.8
1
Normalized axial position, z/L
341426 meshes
477874 meshes
679710 meshes
1109285 meshes

(a)

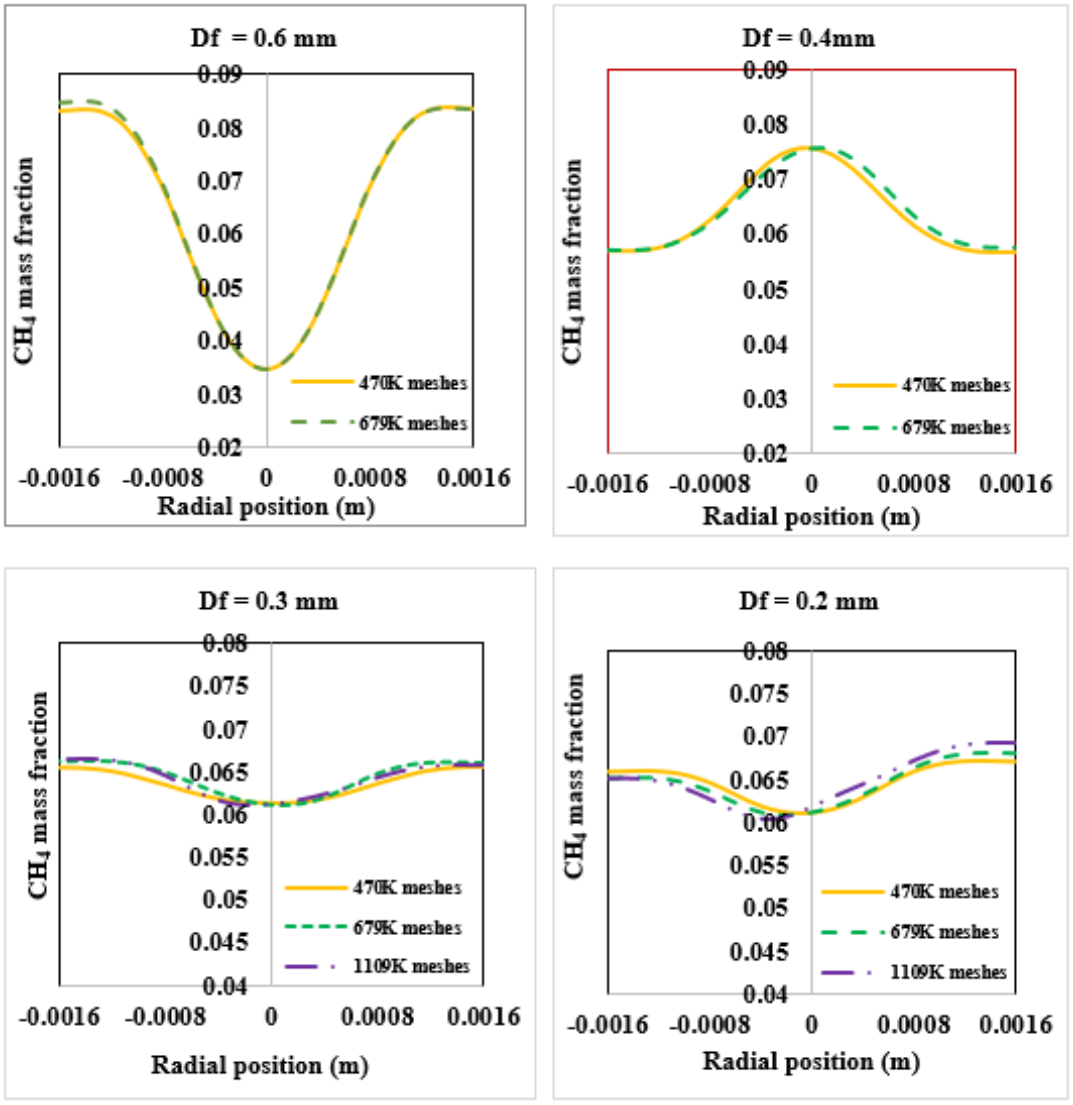

(b)

Figure 4.2 Grid-independence study considering (a) different mesh sizes 341426, 477874, 679710, and 1109285 with Df = 0.3 mm, (b) different mesh sizes 477874, 679710, and 1109285 with Df = 0.6, 0.4, 0.3 and 0.2 mm.

4.3 Model validation

A set of experiments was carried out to validate the computational model. The experimental set-up consists of a cylindrical mixing plenum of 50.4-mm diameter and 1.0-m length. It has one axial gas inlet at the base plus two radial inlets 180° apart 35 mm above the base. This plenum is an up-scaled version of the micromixer tube with a cross-jet flow mixing process to mimic the present study's simulated mixing process. CO_2, O_2, and air gases were used to prepare six different gas mixtures, as listed in Table 4.1. Mixtures A, B, C, and F comprise CO_2 and air only, while mixtures D and E consist of fixed CO_2 composition, enrichment oxygen (EnO_2), and air. Each mixture's oxygen concentration was measured using an electrochemical gas analyzer, sampling inside the plenum at 10 mm below the outlet plane, and the measured plane-average values are plotted against the inlet O_2 concentration as shown in Figure 4.3**.** All tests were carried out at a constant mixture velocity of 1.0 m/s for iso-kinetic sampling. Numerically, three different diffusion coefficient models were considered to determine the most suitable model for gas mixing. These three models are a constant dilute approximation (CDA), dilute approximation (DA), and kinetic theory (KT) [171]. As shown in Fig.4, there are negligible differences between the predictions of the three models. However, the KT model is best suitable for ideal gases; accordingly, in this study, kinetic theory model was implemented.

Table 4.1 Compositions and flow rates of different gas mixtures used in the model-validation experiment.

Mixtures	CO_2%	O_2%	N_2% (air-based)	CO_2 SLPM	EnO_2 SLPM	Air SLPM
A	10%	19%	71%	12.16	0	108.95
B	25%	16%	59%	30.40	0	90.79
C	40%	13%	47%	48.64	0	72.63
D	40%	17%	43%	48.64	6.47	66.20
E	40%	21%	39%	48.64	12.93	59.77
F	50%	11%	39%	60.80	0	59.77

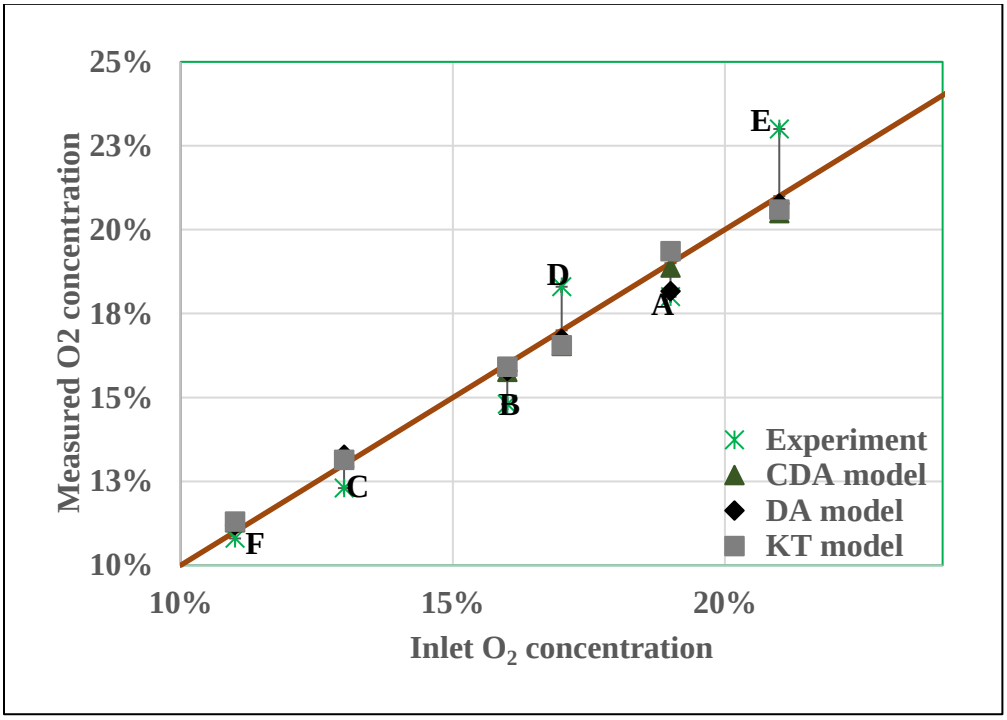

Figure 4.3 Numerical model validation.

4.4 Parameter for evaluating mixing quality

Several methods have been used in the literature to quantify the degree of mixing. One standard method is determining the mixing quality from the contour plots of fluid and flow properties. Fang and Bakhiter [172] assessed the mixing quality of two gases by considering the symmetric pattern of contour plots of density at the channel centerline. Mansour et al. [173] determined the fuel-air mixture's mixing homogeneity through the contour plots of mixture fraction and its gradient. This method is, however, susceptible to visual error because symmetry is sight biased [174]. Another method is to define statistical parameters in terms of flow composition, such as mass fraction or mole fraction. The statistical parameters are usually in the form of mean deviation, standard deviation, or probability density function (pdf). Some of the most common methods to evaluate the mixing quality are defined below.

- **Mean deviation**

Gobby et al. [175] evaluated the quality of a two-gas mixing process in a T-shaped micromixer using each species' deviation from the equilibrium composition since complete mixing is attained when equilibrium composition is achieved. A deviation value of ± 0.01 was used, and the relation was expressed in terms of mass fraction as:

$$Y_{eq}(k) - 0.01Y_{eq}(k) \leq Y(k,z) \leq Y_{eq}(k) + 0.01Y_{eq}(k) \quad (4.1)$$

Where, $Y_{eq}(k)$ is the mass fraction of the equilibrium composition of specie k, $Y(k,z)$ is the mass fraction of specie k at any location z in the domain.

- **Composition deviation coefficient (ζ)**

Le-Hassan [174] studied the mixing progress in a similar T-shaped micromixer and defined the composition deviation coefficient, ζ. It is expressed as follows and is expected to decrease asymptotically to zero along the channel centerline:

$$\zeta = \frac{max\left|Y(i,z) - Y_{eq}(i)\right|}{Y_{eq}(i)} \tag{4.2}$$

- **Uniformity index (U)**

Zhang et al. [128] defined a Uniformity index, U, to quantify mixing quality as follows:

$$U = 1 - \left(\frac{1}{N}\sum_{i=1}^{N}\left(\frac{\emptyset_i - \overline{\emptyset}}{\overline{\emptyset}}\right)^2\right)^{1/2} \tag{4.3}$$

Where ∅ represents any variable such as velocity, mass fraction, or temperature. The term, $\emptyset_i$, represents ith cell value, $\overline{\emptyset}$ represents the mean value, and N represents the total number of cells. A uniformity index value of 1.0 means complete uniformity.

- **Mixing index (I_m)**

Zhang et al. [176] investigated the mixing quality of a binary mixture using the mixing index, I_m, which is calculated as:

$$I_m = \frac{\sum(Y_i - \bar{Y})^2}{N.\bar{Y}.(1-\bar{Y})} \quad (4.4)$$

Where, Y_i is the mass fraction of ith component of the mixture, $\bar{Y}$ is the average mass fraction of ith component of the mixture in a plane, and N is the number of cells on a plane. The range of values for I_m is between 0.0 and 1.0, signifying complete mixing and no mixing (full segregation), respectively.

4.5 Results and discussion

The CFD simulation results investigating the mixing quality inside the micromixer tube will be analyzed here in terms of the CH_4 mass fraction because it has the least mass flow rate, i.e., evaluating mixing with the smallest mass fraction gives better accuracy. The CH_4 mass fraction is expressed as follows:

$$\overline{x}_{CH_4} = \frac{\dot{m}_{CH_4}}{\dot{m}_{CH_4} + \dot{m}_{O_2} + \dot{m}_{CO_2}} \quad (4.5)$$

Also, a dimensionless number is employed to characterize the flow process in the tube. The Schmidt number is a dimensionless number suitable for characterizing fluid flow defined mainly by the momentum and mass transfer processes. It is defined as the ratio of the transfer rate of molecular diffusion to transfer rate of mass diffusion, as:

$$Sc = \frac{\mu}{\rho D_{k,m}} \quad (4.6)$$

Where, $\frac{\mu}{\rho}$ represents the kinematic viscosity and $D_{k,m}$ represents the mass diffusion coefficient.

The Schmidt number portrays a clear picture of the dominant process in mixing. Sc > 1 implies mixing is governed by momentum diffusion, Sc = 1 implies mixing is controlled by both momentum and mass diffusion, while Sc < 1 shows mixing is dominated mainly by mass diffusivity.

4.5.1 Effect of fuel inlet tube diameter (Df) on mixing quality

The size of fuel inlet diameter (D_f) was varied as 1.0 mm, 0.6 mm, 0.4 mm, 0.3 mm, and 0.2 mm, to investigate its effect on mixing while keeping the other tube dimensions constant. The flow rates of all gases were kept constant while examining the effect of D_f. Four fuel inlets were considered, which are equally spaced circumferentially (90° apart). A fixed fuel mass flow rate, $\dot{m}_f = 7.3771 \times 10^{-7} kg/s$ per inlet was introduced. Figure 4.4 shows the profiles of CH_4 mass fraction at the micromixer tube outlet for all D_f values considered. It can be observed that as D_f decreases, the difference between the peak and crest values decreases (approximately 620% and 15% for D_f = 1.0 mm and 0.3 mm, respectively), which indicates better mixing at lower D_f.

The large difference between the peak and crest values observed for larger D_f may be attributed to the high difference between the oxidizer inlet velocity and fuel inlet velocity. The latter decreases with increasing fuel inlet area. Therefore, the CH_4 specie cannot effectively penetrate and mix hydro-dynamically with the main oxidizer stream near the jet cross-flow; thereby, the fuel flow is restricted to the wall region.

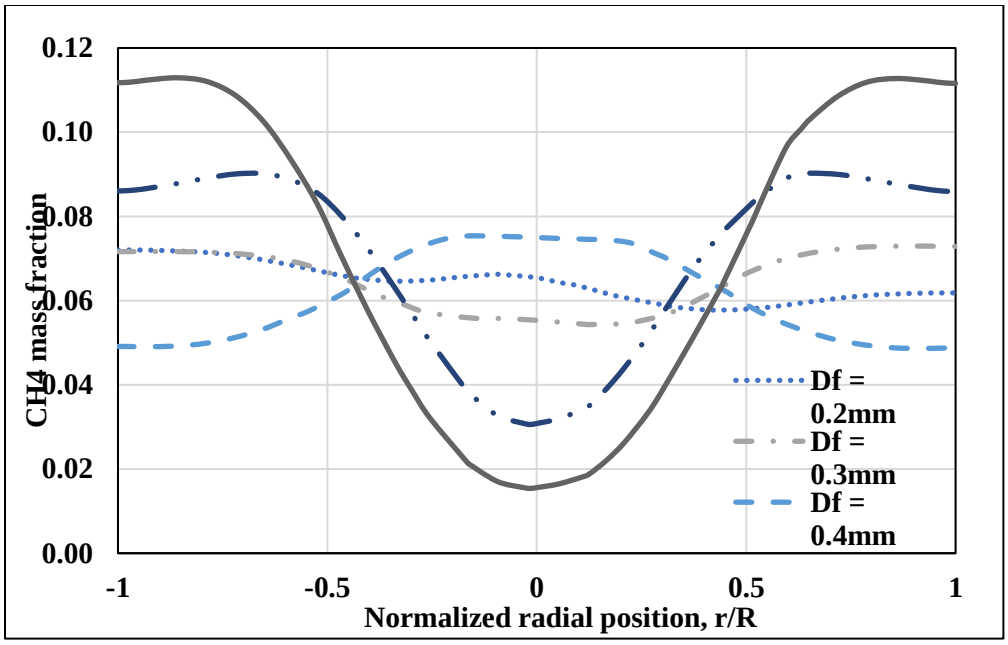

Figure 4.4 Variation of CH_4 mass fraction at micromixer tube outlet for different fuel inlet diameters: 1.0, 0.6, 0.4, 0.3, and 0.2 mm for a tube length of 32 mm, considering four fuel inlets.

This is clearly illustrated in Figure 4.5, showing the velocity vector plots colored with CH_4 mass fraction near the fuel inlets for Df's different values. Furthermore, the tube length is not long enough to enable adequate molecular diffusion before the mixture reaches the outlet. This may explain the peak values observed near the wall at the outlet. On the other hand, as D_f decreases, the fuel jet velocity increases, causing more effective hydrodynamic mixing close to the fuel-injection points, which compliments the molecular diffusion process further downstream, resulting in better mixing, as the velocity vectors for D_f = 0.3 mm indicate in Figure 4.5.

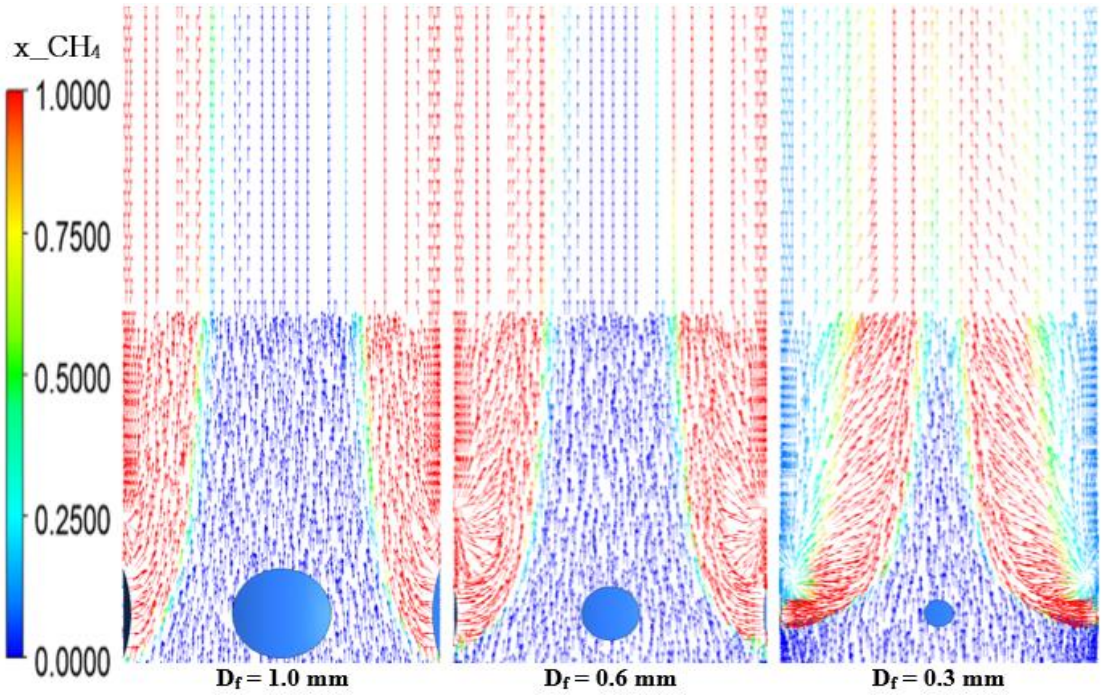

Figure 4.5 Velocity vectors colored with CH_4 mass fraction plotted on centerline plane for fuel inlet diameter: 1.0, 0.6, and 0.3 mm considering four fuel inlets.

Hence, there is a lower concentration of CH_4 near the tube wall, and the profile skewness is smaller, which implies better mixing. Interestingly, although the D_f = 0.2 mm case produced a CH_4 mass fraction profile with the least difference between the peak and crest values, the profile is not axisymmetric, which will be explained later.

The CH_4 Schmidt number (Sc_{CH4}) profiles at the outlet are shown in Figure 4.6 for the different D_f values. The average outlet Sc_{CH4}value for all D_f values is 0.575 (<1), indicating that mass diffusivity has more influence on mixing near the outlet region. Moreover, the profiles are similar to those of CH_4 mass fraction presented in Fig.5, which supports the observation that the mixing process near the outlet is majorly influenced by mass diffusivity.

Among the considered D_f values, the smaller diameters, 0.2 mm and 0.4 mm, showed better mixing, which indicates that the optimum fuel diameter for the examined tube length of 32 mm falls between these two sizes. Accordingly, the mixing uniformity for D_f = 0.25, 0.30, 0.35, and 0.40 mm was investigated, and the results are displayed in Figure 4.7 in terms of CH_4 mass fraction profiles at the outlet section. The CH_4 profiles for D_f = 0.25 – 0.35 mm are closest to the mean ideal mixing profile. Thus, it is expected to have the optimum D_f, for the 32-mm micromixer tube with four fuel inlet holes, in the range of 0.3 mm $\pm$ 0.05 mm.

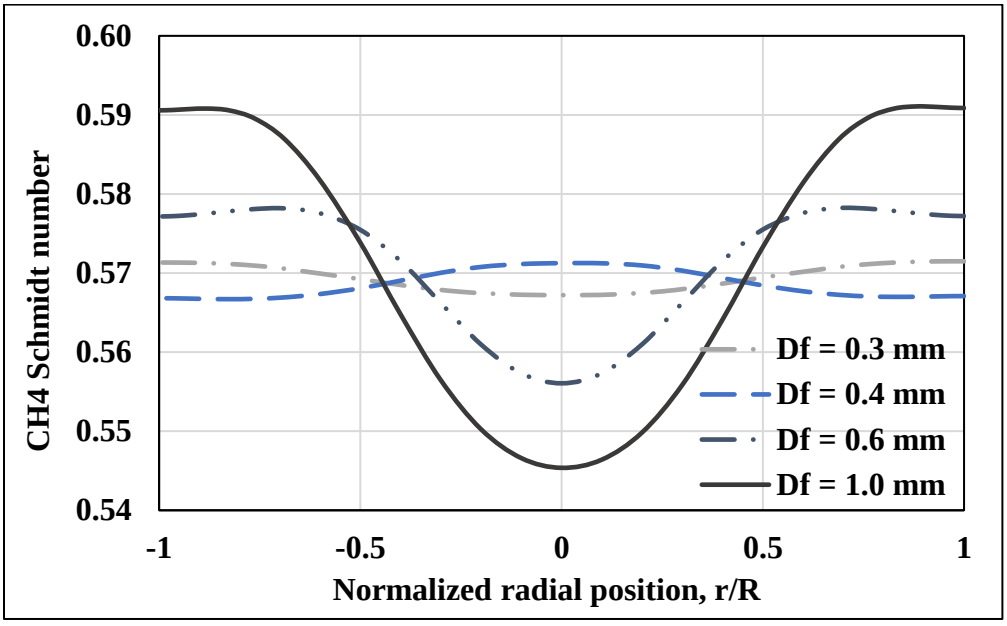

Figure 4.6 Variation of CH_4 Schmidt number at micromixer tube outlet for different fuel inlet diameters: 1, 0.6, 0.4, 0.3, and 0.2 mm for a tube length of 32 mm, considering four fuel inlets.

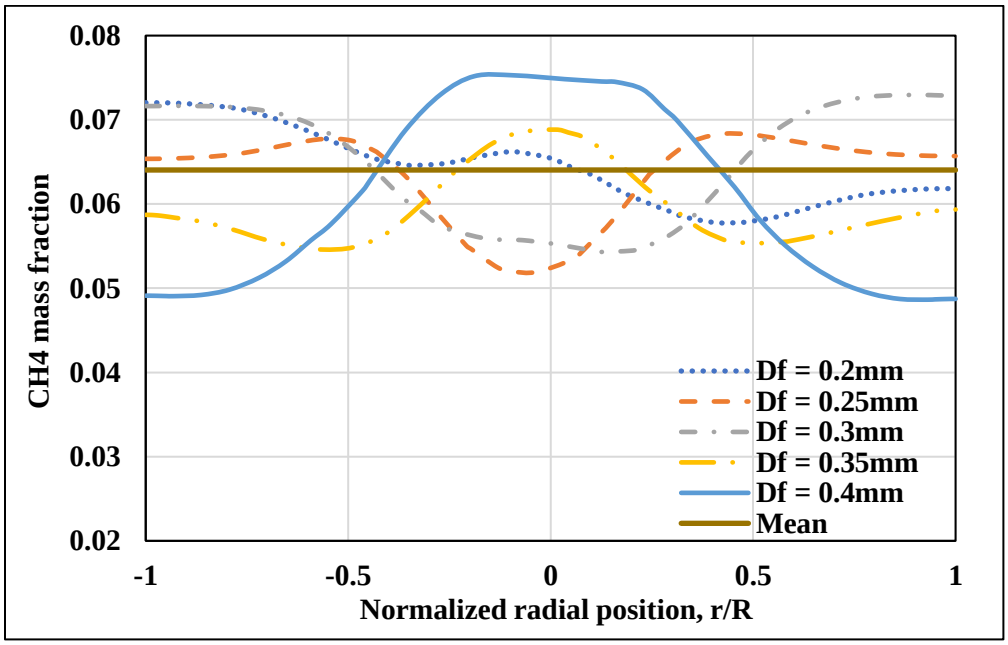

Figure 4.7 Variation of CH_4 mass fraction at outlet of the micromixer tube for different fuel inlet diameters: 0.4, 0.35, 0.3, 0.25, and 0.2 mm for a tube length of 32 mm, considering four fuel inlets.

Mixing quality for $D_f \leq 0.4$ mm was further assessed by computing the mean deviation at L = 10D inside the micromixer tube. This quantifies mixing quality in terms of uniformity by setting a minimum deviation (as expressed in Equation (4.1)) of specie composition from its equilibrium composition in the mixture. A 10% deviation value has been adopted, and the contour plots on plane L = 10D are shown in Figure 4.8. The contours display the portion of the circular plane with CH_4 concentration within the specified deviation only. It is observed that the contours of the small diameter nozzles ($D_f = 0.2 – 0.35$) with corresponding higher velocity inlet have asymmetry deviation pattern. This signifies an increasing influence of unsteady effects due to convection or inertia on mixing in addition to mass diffusion effects that are prevalent bear the outlet.

It can be deduced that the tube with $D_f = 0.25$mm produced the best mixing quality, judging by the largest contoured area and least contoured variation. Thus, supporting the inference made earlier from the outlet radial profiles of CH_4 mass fraction. This also implies that mixing quality is not a direct function of inlet fuel hole size, as $D_f = 0.25$ mm produced better mixing than $D_f = 0.2$ mm.

Figure 4.9 shows the variation of mixing quality with D_f at L = 10D. Here, mixing quality is expressed in terms of the Uniformity Index (U) and mixing index (I_m), which are statistical parameters defined in terms of CH_4 mass fraction, as defined in Equations (4.3) and (4.4), respectively. Both parameters quantify mixing with the uniformity of constituents.

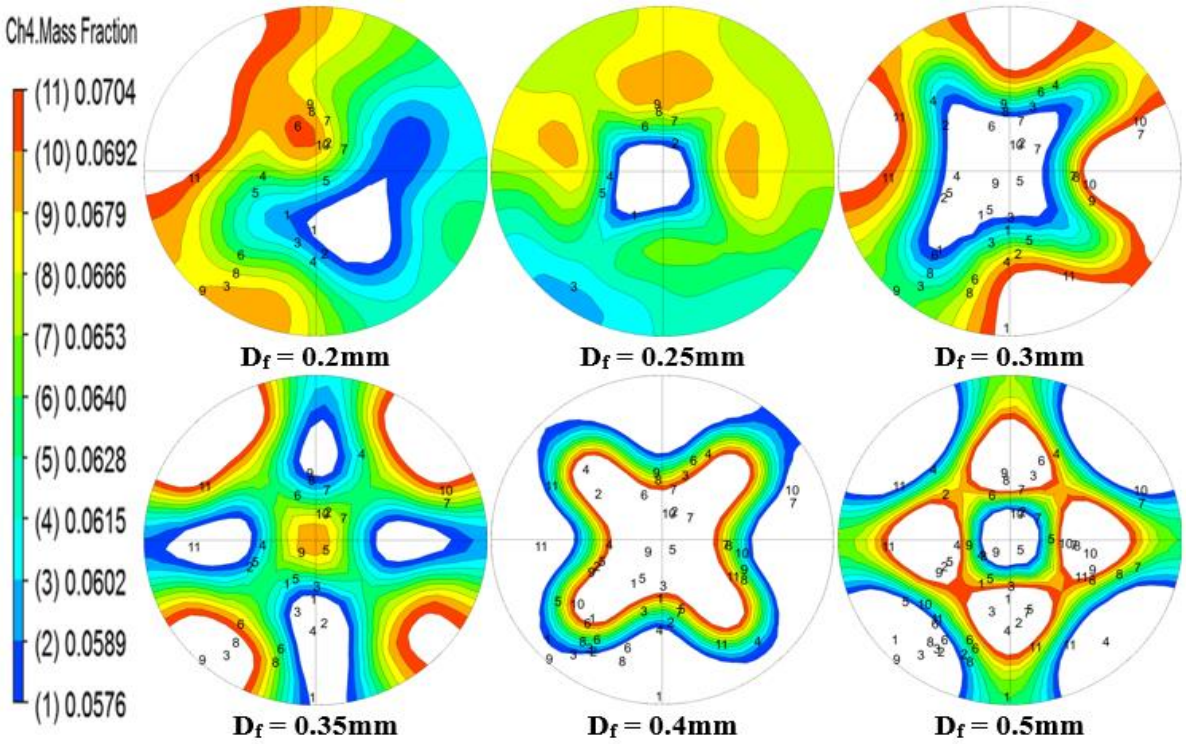

Figure 4.8 Contour plots of mean deviation of CH_4 mass fraction at L = 10D inside the micromixer tube for different fuel inlet diameters: 0.5, 0.4, 0.35, 0.3, 0.25, and 0.2 mm, considering four fuel inlets.

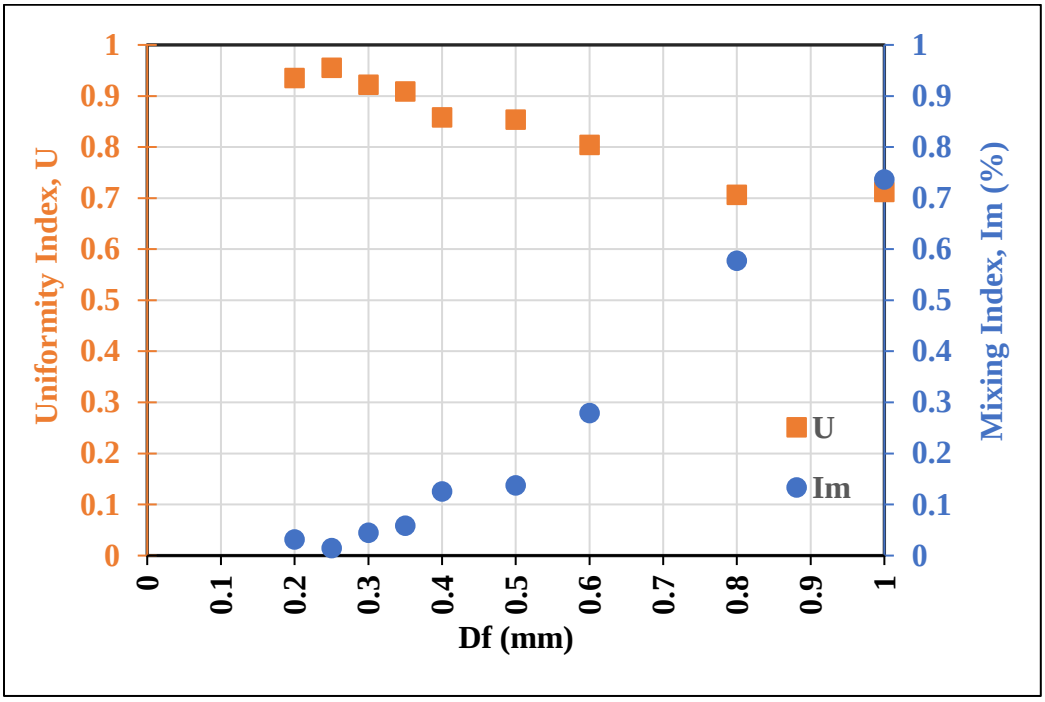

Figure 4.9 Uniformity Index and Mixing Index calculated at L =10D inside the micromixer tube for Df = 0.2 - 1 mm, considering four fuel inlets.

However, U varies from 0.0 to 1.0, while I_m varies from 1.0 to 0.0, from complete segregation to complete uniformity. The trend is similar for both parameters, as they show that mixture uniformity improves with decreasing fuel hole size, and this can again be attributed to the higher jet velocity produced by the smaller jet sizes (since the mass flow rate per inlet is constant), which enhances the interaction of the jet flow with the main stream. A mixing quality greater than 90% was achieved in the range of D_f = 0.2 - 0.35 mm. Moreover, both parameters predict D_f = 0.25 mm as the hole size with the best mixing quality at L = 10D, thereby corroborating the results obtained earlier based on the mean deviation parameter.

4.5.2 Effect of tube length (L) on mixing quality

The effect of micromixer tube length (L) on mixing quality was studied by varying L (32, 40, and 48 mm) at fixed fuel inlet diameter, D_f = 0.25 mm. From the CH4 mass fraction profile results at the tube outlet, shown in Figure 4.10, it can be inferred that increasing L improves mixing quality, judging by the closeness of the profiles to the mean x_CH_4 profile. This is because a longer tube length creates more space for more molecular diffusion to take place. Figure 4.11 examines the transition from mass to molecular diffusion along the micromixer tube. The figure illustrates the contour plots of 10% mean deviation of CH_4 mass fraction for D_f < 0.4 mm at L = 16 mm (5D), 32 mm (10D), 40 mm (12.5D), and 48 mm (15D). The contours show the axial variation in mixing due to varying interaction between the main flow and fuel jet flow for the various fuel hole sizes considered.

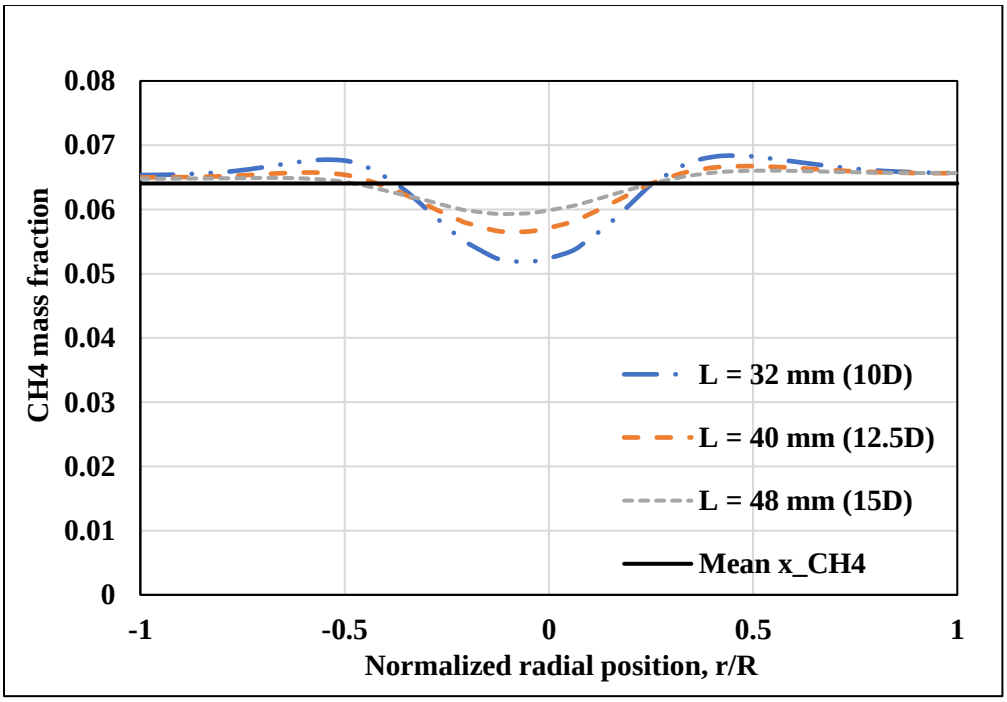

Figure 4.10 Variation of CH_4 mass fraction at the micromixer outlet for tube lengths 32, 40, and 48 mm at constant D_f = 0.25 mm, considering four fuel inlets.

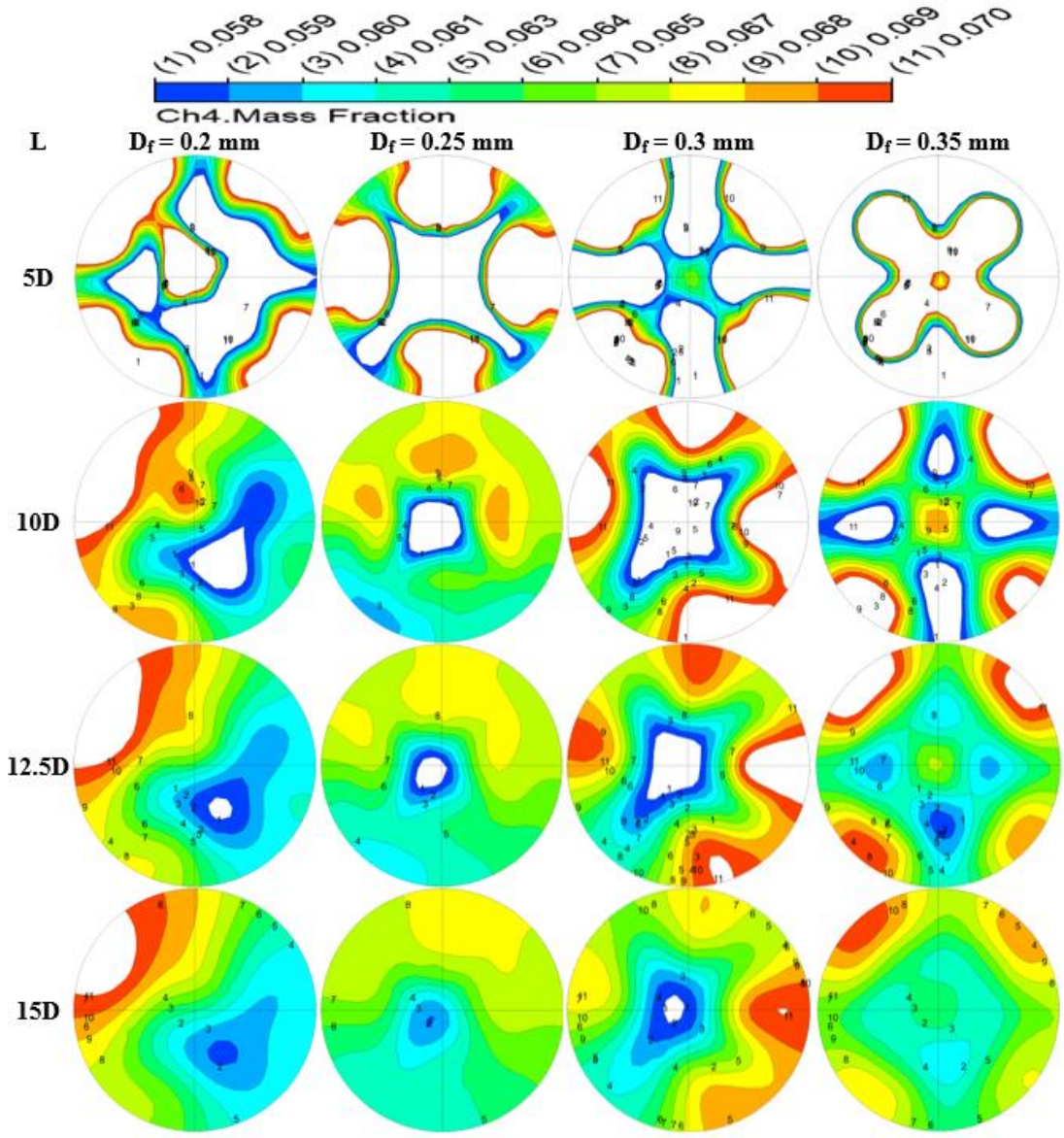

Figure 4.11 Contour plots of mean deviation of CH_4 mass fraction at lengths L = 5D, 10D, 12.5D and 15D for different fuel inlet diameters D_f = 0.2, 0.25, 0.3 and 0.35 mm, considering four fuel inlets.

At L = 5D, the mixing process is at an early stage, and the species are barely distributed across the plane, as shown by the scanty contour plots. Improved distribution of species can be seen in contours at L = 10D. Unlike the contour patterns at L = 5D, those at L = 10D are like the ones at 12.5D and 15D. This indicates diffusion-controlled mixing from L =10D upwards instead of momentum-dominated mixing near L = 5D. At L =15D, the mixture is most uniform for all the fuel hole sizes, showing mixing quality improvement with tube length. Also, the fuel inlet with D_f = 0.25 mm shows the best mixing quality with minimum variation, judging by the least contour numbers at L = 15D, which agrees with the findings of Figure 4.8 and Figure 4.9.

The composition deviation coefficient (ζ) was calculated at the tube centerline to show the mixing progress of CH_4 species. It is expected to decrease asymptotically to 0.0 along the length of the tube. Figure 4.12 shows the composition deviation coefficient of CH_4 for the tube with four fuel holes of inlet diameters (0.2 mm - 1 mm). The mixing progress curves for all the fuel diameters represented in the figure are characterized by a zero-gradient portion at ζ = 1.0 (initial non-mixing condition) and a negative gradient curve approaching ζ = 0.0 (complete mixing condition). The size of the zero gradient portion signifies the rate at which CH_4 specie reaches the tube center. Also, the magnitude/steepness of the negative gradient afterward indicates the mixing rate.

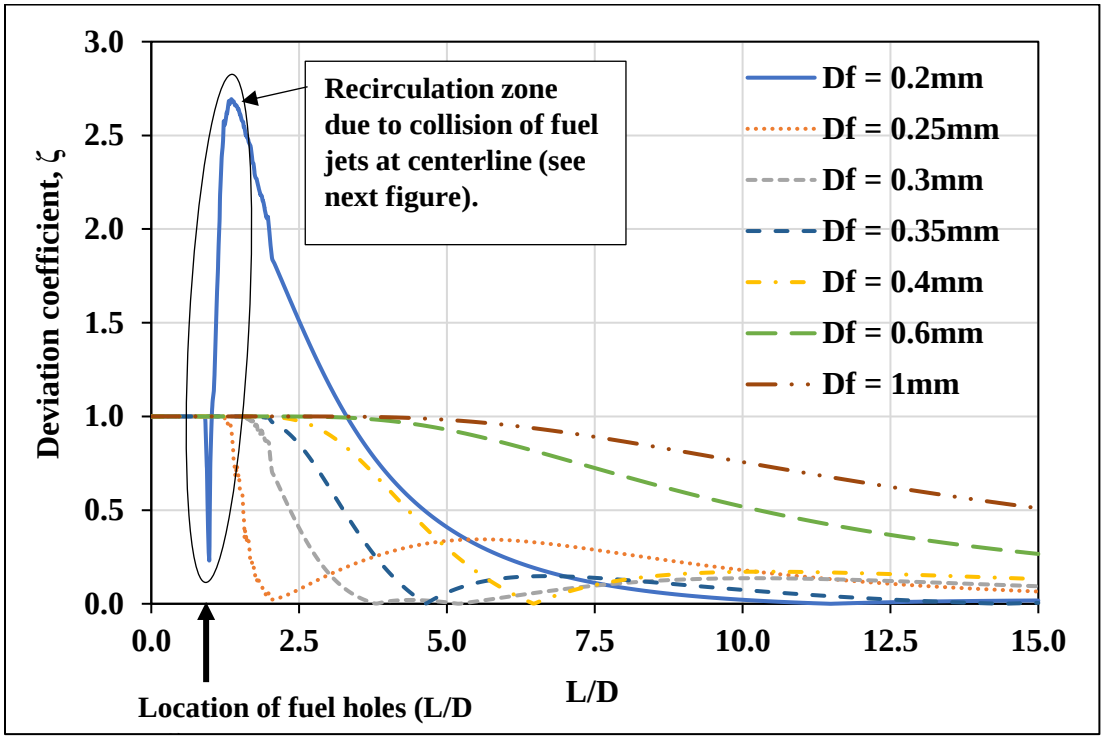

Figure 4.12 Tube centerline CH_4 composition deviation coefficient for different fuel inlet diameters D_f = 0.2 – 1 mm up to L = 15D, considering four fuel inlets.

Based on these facts, faster main flow penetration and greater mixing rate occur with decreasing fuel inlet diameter due to the increased jet velocity since the fuel mass flow rate is kept constant for all cases.

Little difference in mixing profile and rate is observed for Df > 0.4 mm, whereas Df < 0.4 mm' fuel holes show higher mixing rates and distinct mixing profiles. Note the points of inflection at $\zeta = 0$ followed by a secondary peak, as observed for D_f = 0.25, 0.3, 0.35, and 0.4 mm. Downstream these points, the mixing pattern can be said to steadily improve towards the tube outlet, as indicated by the less steep profiles. The inflection points indicate axial locations where the CH_4 mass fraction equals its equilibrium value, resulting from the displacement of the main oxidizer flow due to the high jet flux/penetration strength produced by the smaller fuel diameters $D_f < 0.4$ mm. The outlier is the profile of $D_f = 0.2$, with a sharp drop in ζ below 1 just before the point of CH_4 injection at L = 1D, followed by a steep rise to peak ζ, before the curve behaves as expected at $L \approx 2D$, as seen in Figure 4.12. This anomaly is attributed to a recirculation region created by the collision of fuel jet flows at the tube center below the CH_4 injection points (L < 1D). This is explained in more detail in the next figure.

Figure 4.13 illustrates the three-dimensional side and plan views of absolute helicity vortex for D_f = 0.2 - 0.4 mm, showing the magnitude of the interaction between the oxidizer main flow and fuel jet flows. Absolute helicity vortex quantifies vortex structures created by fluid-fluid and fluid wall interactions [171]; this represents the fluid-fluid interaction.

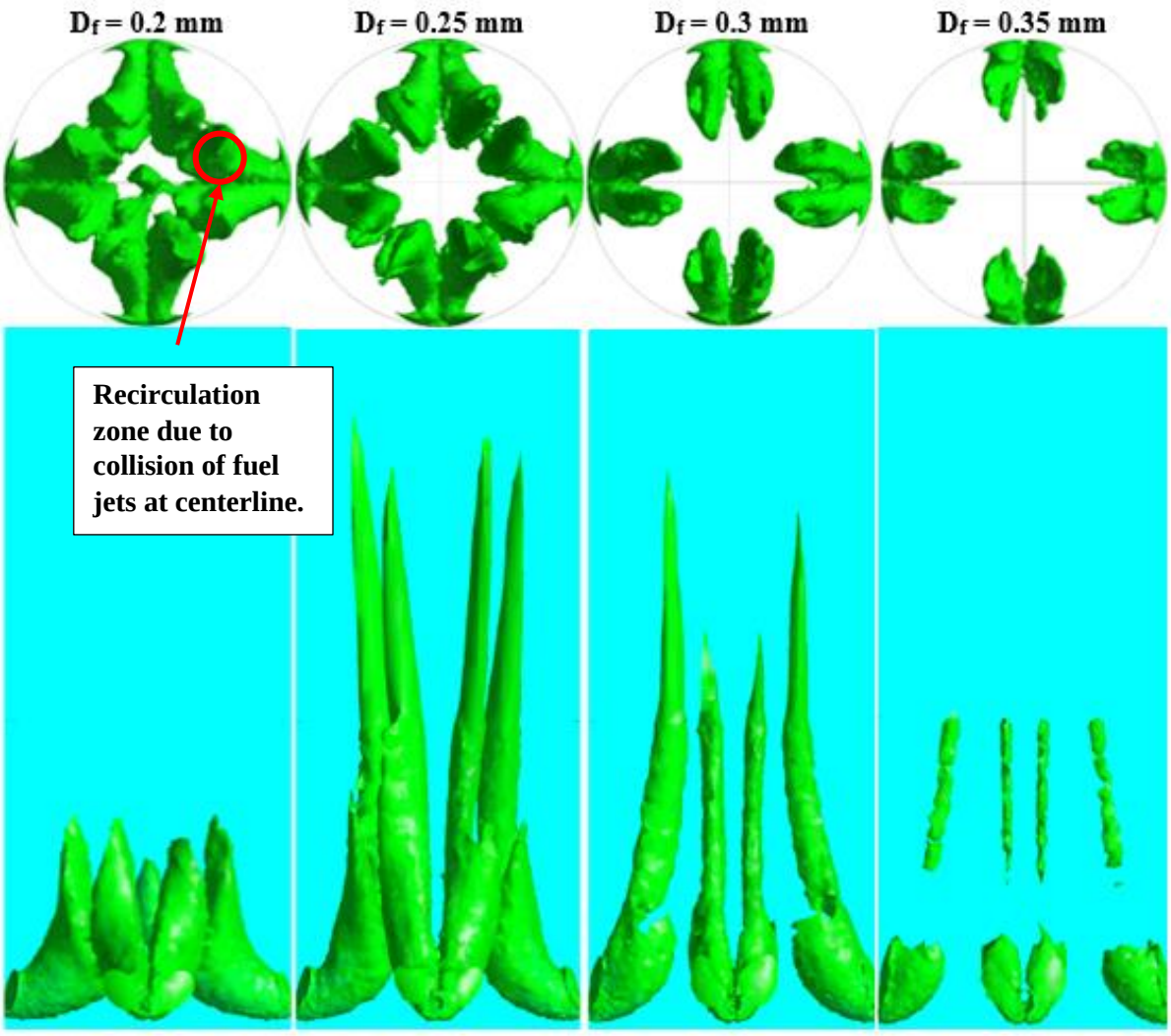

Figure 4.13 Three-dimensional absolute helicity vortex for different fuel inlet diameters D_f = 0.2, 0.25, 0.3 and 0.4 mm, considering four fuel inlets.

The plan view of helicity for D_f = 0.2 mm indicates fluid interaction at the tube center, absent in other cases. This interaction happens in the form of a recirculation zone, which explains the anomaly in Figure 4.12 and justifies the lack of axisymmetry of the 0.2-mm profiles in Figure 4.4 and Figure 4.7.

It is also observed from the side views in Figure 4.13 that D_f = 0.25 mm has the tallest helicity structures indicating longer fluid-fluid interaction and sufficient unsteady effects, which are responsible for the case producing the best mixing uniformity. Unsteady effects due to convection or inertia play an important role on mixing quality. The magnitude of the unsteady effects depends on the size of fuel inlets. Still, the sufficient magnitude to produce the best mixing quality relies on the relative size of fuel inlets to the main inlet. The helicity structure size decreases with increasing fuel hole size, explaining why mixing quality is worse at larger fuel hole diameters. Generally, the mixing process can be described as thus; the upstream region near the fuel-injection holes is the high-vortex region, where momentum change represented by steeper slopes drive mixing, and the region further downstream towards the tube outlet is the low-vortex region dominated by molecular diffusive mixing. For all fuel inlet diameters considered, mixing improved with mixing tube length L. Based on a ζ = 1% criterion, the optimum fuel inlet diameter is D_f = 0.25 mm, as observed at L = 15D in Figure 4.12 for the examined micromixer tube with four fuel inlets.

4.5.3 Effect of number of fuel holes on mixing quality

In addition to the previously discussed four-hole arrangement, a six-hole one was also analyzed with six equally spaced fuel holes (60° apart) at the height of 3.2mm (one tube diameter) from the main flow inlet to study the effect of the number of fuel jets on mixing quality. Figure 4.14 shows a plot of centerline deviation coefficient (ζ) with respect to tube length, considering the four- and six-hole arrangements. For similar hole sizes, the plot shows that the 4-hole arrangement has a higher mixing rate (curve gradient). This is because, at the same D_f and total fuel mass flow rate, the flow rate per hole is greater for the case of 4 holes, resulting in higher fuel jet velocity, which causes more penetration and interaction with the main flow. Unlike in the 4-hole arrangement at D_f = 0.2, 0.25, and 0.3 mm, the ζ profiles of the 6-hole micromixer tube have no inflection points along the centerline, indicating a lack of equilibrium composition points.

Based on the value of ζ at the outlet, the optimum D_f for the 6-hole tube is 0.2 mm with ζ = 16 %, while that of the 4-fuel hole tube is 0.25 mm with ζ = 1.2 %. Figure 4.15 shows the comparison of mixing quality between number of fuel holes of 4 and 6 for D_f range of 0.2 – 0.4 mm using Uniformity Index parameter. This corroborates the results shown in Figure 4.14 and shows that for $D_f \geq 0.25\,mm$, 4 fuel hole-tube produced better mixing quality while $D_f < 0.25\,mm$ 6 fuel hole-tube yielded better mixing quality.

Based on parameters such as Uniformity Index (U_A) and Deviation coefficient (ζ), it can be concluded that 4 fuel holes is recommended for $D_f \geq 0.25\ mm$ while 6 fuel holes is recommended for $D_f < 0.25\ mm$ to achieve optimum mixing with this micomixer-tube design.

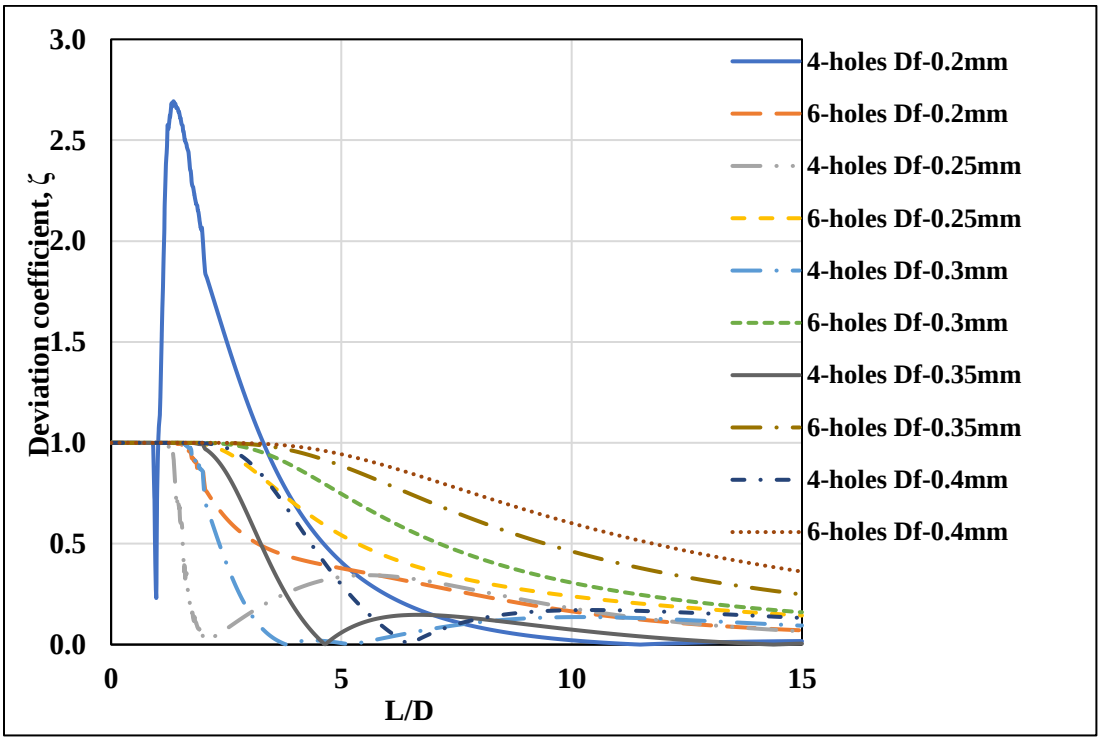

Figure 4.14 CH_4 composition deviation coefficient for different fuel inlet diameters D_f = 0.2 – 0.4 mm for the micromixer tubes of four and six holes.

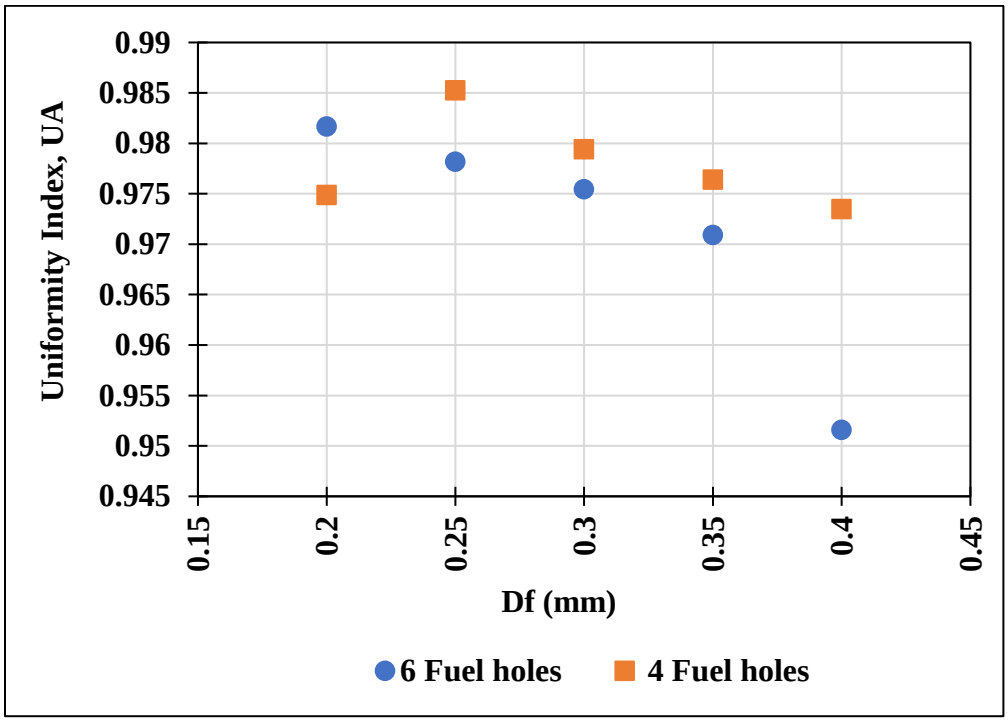

Figure 4.15 Uniformity Index for different fuel inlet diameters Df = 0.2 – 0.4 mm for the micromixer tubes of four and six holes.

CHAPTER 5

EXPERIMENTAL INVESTIGATION OF COMBUSTION CHARACTERISTICS IN A PREMIXED MICROMIXER COMBUSTOR

5.1 Introduction

This chapter presents the results and discussion of the experimental investigation of premixed oxy-combustion of hydrogen-enriched methane under atmospheric conditions in a multi-hole burner mimicking gas-turbine micromixers. The experiments were conducted at a fixed oxygen fraction (OF) of 30% by volume in the O_2/CO_2 oxidizer since this OF produces similar flame characteristics to air combustion. The hydrogen fraction (HF) in the fuel mixture was varied within the range of 25-70%. The equivalence ratio (ϕ) was varied from 0.1 to 1.0 at each target value of HF to determine the blowout limit. A stability map showing the region where the stable flame is achievable is defined in terms of the stoichiometric and blowout limits and plotted within the HF-ϕ space. To gain more insight into the flame extinction mechanism, flame shapes were imaged and compared over a range of HF. Furthermore, flame shapes were captured at constant adiabatic flame temperature (AFT = 2200K) to study the influence of chemical kinetics rates on flame shapes.

5.2 Combustor stability maps

The stable operating zone of the micromixer-like multi-hole burner holding premixed H_2-CH_4/O_2/CO_2 flames was mapped over ranges of fuel hydrogen fraction (HF=25-70%) and equivalence ratio (ϕ=0.1-1.0) by identifying the static stability limits as shown in Fig. 5.1. These limits were investigated at fixed OF=30% and jet velocity of 5.2 m/s.

The lower flammability (blowout) limit was identified by decreasing the equivalence ratio at each HF until the flame blew out. No upper flammability (flashback) limit was encountered because of the flame arrestors built in the multi-hole burner. The stable combustion zone is delineated by the stoichiometric limit at the top and the blowout limit at the bottom, while the blowout zone falls below the blowout limit. The stability map was superimposed on numerically generated contours of different operability parameters, such as adiabatic flame temperature (AFT), combustor power density (PD), Reynolds number (Re), and pressure drop across burner headend (Δp), to investigate their correlation with the stability limits.

Figure 5.2 shows the stability map plotted against the contours of constant AFT. Multiple observations can be made:

- Blowout occurs at leaner equivalence ratios with hydrogen addition. This is attributed to the enhanced chemical kinetics and higher flame speed with hydrogen enrichment, as reviewed earlier.

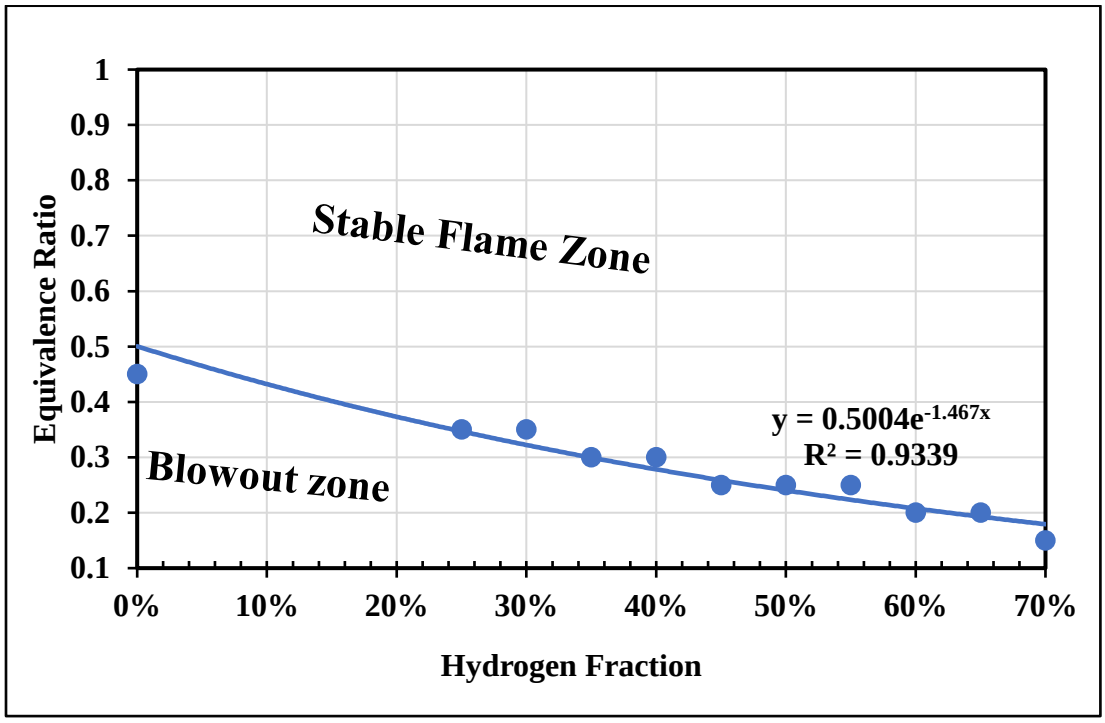

Figure 5.1 Stability map of micromixer gas combustor mapped over equivalence ratio (ϕ) and hydrogen fraction (HF).

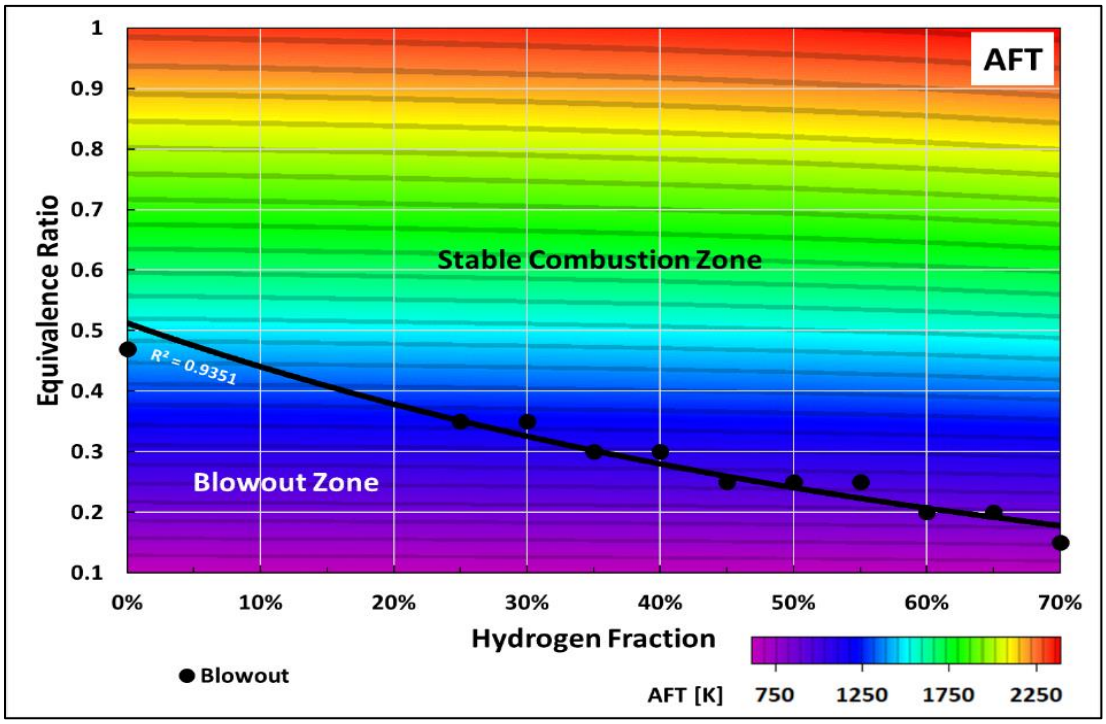

Figure 5.2 Flame stability map at fixed jet velocity of 5.2 m/s and oxygen fraction of 30% superimposed on contours of constant adiabatic flame temperature.

The flame base speed reduces to a critical value where its axial component is overtaken by the unburnt mixture velocity, resulting in flame blowout [95]. Invariably, the blowout limit is greatly dependent on flame speed and Damkohler number [177]. Hydrogen enrichment has a minuscule effect on AFT, as seen in Figure 5.2, so the observed enhancement in blowout with hydrogen addition is not related to an increase in flame temperature; on the contrary, blowout occurs at lower AFT with hydrogen addition. The positive effect of hydrogen is attributed to the fact that it saturates the reaction zone with OH, O, and H radicals, which boosts the reaction rates and burning velocity, as reviewed earlier.

- In terms of AFT, blowout shifts from ~1430 K at 0% HF to ~770 K at 70% HF. The fact that an oxy-fuel combustor can remain lit down to ~800 K (~530 °C or ~990 °F) is a remarkable pioneering finding that has never been attained in past studies, which highlights the strong positive effect of hydrogen enrichment on the stability of oxy-fuel flames. Even without hydrogen enrichment, the combustor remains lit down to ~1450 K (~1180 °C or ~2150 °F), which is comparable to lean-premixed air-flames in gas turbines and significantly better than most reported limits in past swirl-based oxy-fuel studies, as reviewed earlier. This highlights the effective flame stabilization of micromixer technology and makes it the technology of choice for oxy-fuel combustors.

- The fact that AFT is almost insensitive to HF at constant equivalence ratios facilitates great operational flexibility in adjusting the HF to sustain flame stability without affecting the gas-turbine-cycle peak temperature or impacting the turbine health. A similar relationship was reported for low swirl-stabilized premixed H_2-CH_4/O_2/CO_2 flames [178]. The stability map plot against the contours of constant power density (PD, MW/m^3/bar) is depicted in Figure 5.3. The PD represented within the stable combustion zone covers the lower operating power range of industrial gas turbines, which have typical ratings of 3.5-20 MW/m^3bar [179]. It can be observed that PD increases with increasing equivalence ratio because PD is directly proportional to the mass flow rates of CH_4 and H_2, see Equation 3, and both flow rates increase with equivalence ratio. Remarkably, hydrogen enrichment has almost no effect on PD, which leads to two important findings:
- The lack of correlation between PD and HF again facilitates great operational flexibility in adjusting the HF to sustain flame stability without affecting the cycle power input or the turbine health.
- The combustor remains lit down to a PD of 1.8 MW/m^3/bar at 70% HF, which is significantly lower than the typical minimum of industrial gas turbines. This offers the operational freedom not to flame out some premixers at engine part loads, but to keep them lit at low power density and sustained by hydrogen addition.

Avoiding premixer flameout at part loads and relight at higher loads is beneficial in avoiding the instabilities associating relight due to acoustic interference and/or flame-to-flame interaction.

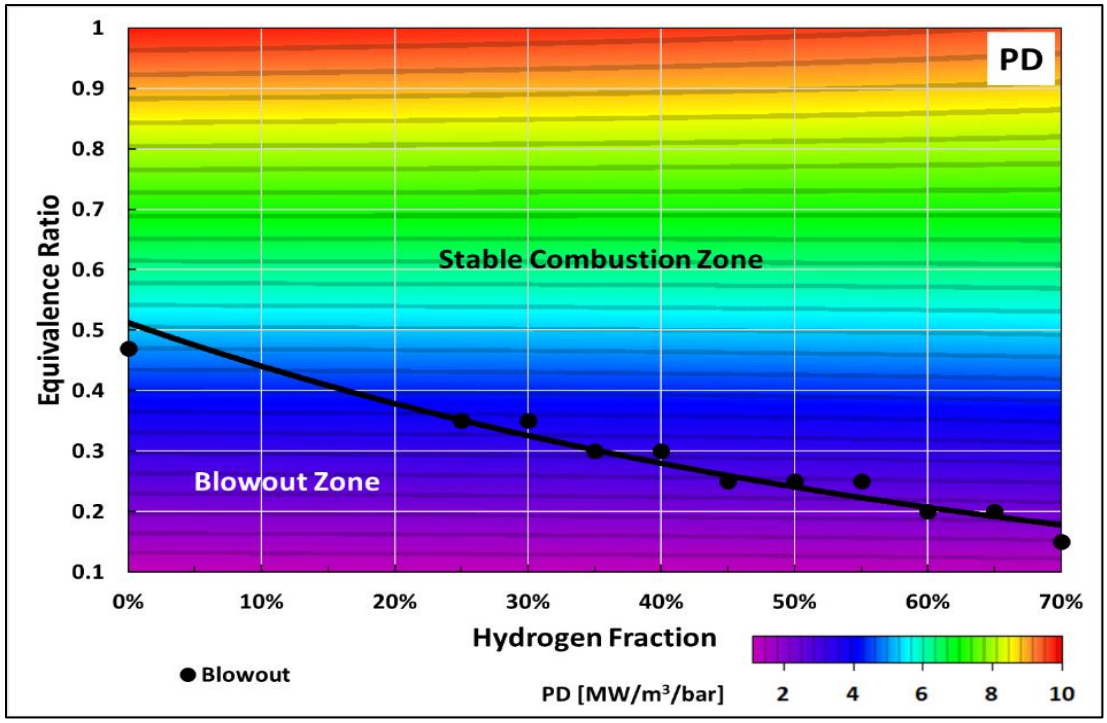

Figure 5.3 Flame stability map at fixed jet velocity of 5.2 m/s and oxygen fraction of 30% superimposed on contours of constant power density.

To investigate the relationship between the blowout limit and mixture Reynolds number (Re), the stability map was replotted against the contours of constant Re, as shown in Figure 5.4. The Re map extends over the range 1300-1600, with maximum Re at minimum HF and ϕ, and vice versa. It can thus be deduced that excessively high Reynolds numbers characterize the blowout zone.

Interestingly, the Re map is a strong reflection of the ρ_{mix} map, because μ_{mix} varies from 16.0 to 16.5 μPa·s, i.e., by 3% only. Hydrogen enrichment might not affect AFT or PD, but it surely affects ρ_{mix}, because hydrogen is significantly less dense than methane.

The flow parameters directly affected by hydrogen addition are thus ρ_{mix} and Re. Increasing Re increases flow turbulence, which should boost the burning velocity and thus flame stability. However, decreasing HF and ϕ (in the direction of higher Re) reduces the burning velocity.

This infers that the contours of constant burning velocity are close to those of constant Re, especially within the blowout region, which explains why blowout nearly occurs at constant Re. The blowout limit is mainly a function of Damkohler number, Da [28,177,178]. Since the flow time scale can be assumed constant because of the fixed jet velocity, then a constant reaction time scale (and thus burning velocity) results in constant Da. This confirms that the burning velocity is nearly constant along the blowout limit.

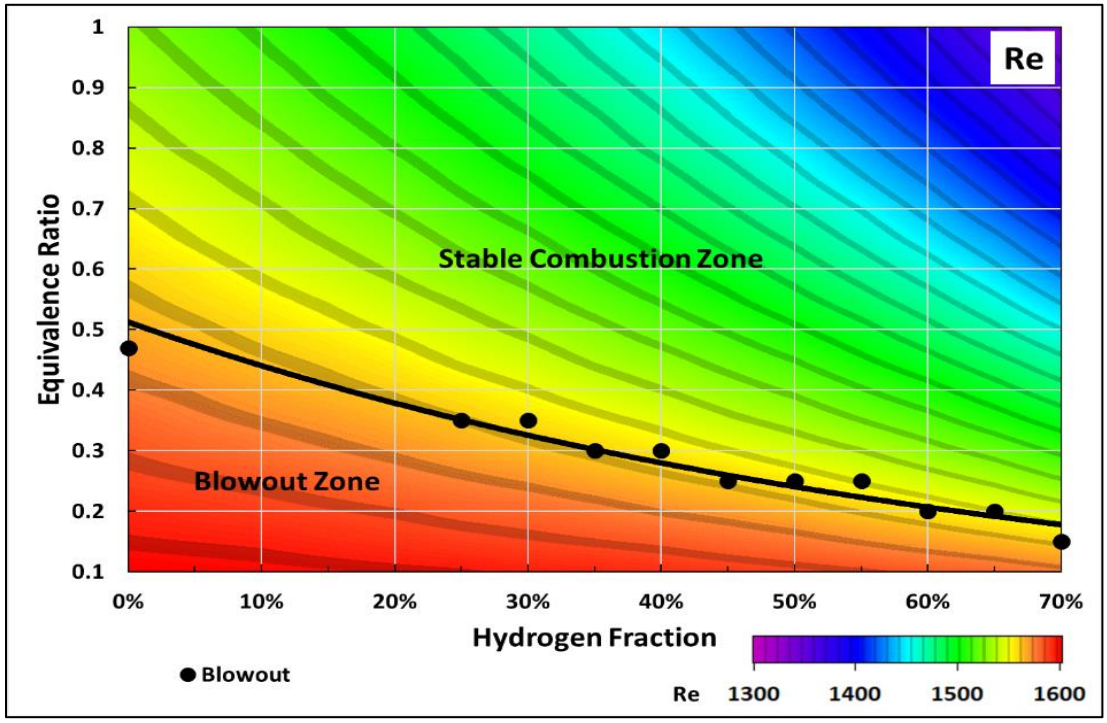

Figure 5.4 Flame stability map at fixed jet velocity of 5.2 m/s and oxygen fraction of 30% superimposed on contours of constant mixture Reynolds number.

To zoom in on the effect of Re, and to de-convolute the effects of ρ_{mix} and μ_{mix}, Figure 5.5 depicts the stability map plotted against the contours of constant pressure drop across burner headend (Δp), which is directly proportional to ρ_{mix} at constant jet velocity, according to Equation 7. It can be seen that the blowout limit coincides with a contour of Δp, which infers that ρ_{mix} is the primary parameter within the Re, as analyzed earlier. ρ_{mix} is analyzed in Figure 5.5 in the form of Δp because the latter has a unique importance in the operation of lean-premixed air-fuel gas turbines. The compressor discharges air at a given pressure and temperature, so air density is typically constant at combustor inlet.

The Δp across combustor headend is thus a direct measure of jet velocity and, consequently, air mass flow rate through the headend. Since the rate of airflow reflects engine load, Δp is monitored as a direct indicator of load.

5.3 Flame macrostructure

Flame shapes at specific points within the stable combustion zone were imaged to help understand and analyze the effects of different parameters on flame macrostructure. Figure 5.6 shows the locations of these selected flames within the Δp stability map. Flames 1-3 examine the effect of HF at constant ϕ=0.912, while flames 4-6 investigate the effect of ϕ at constant HF=50%.

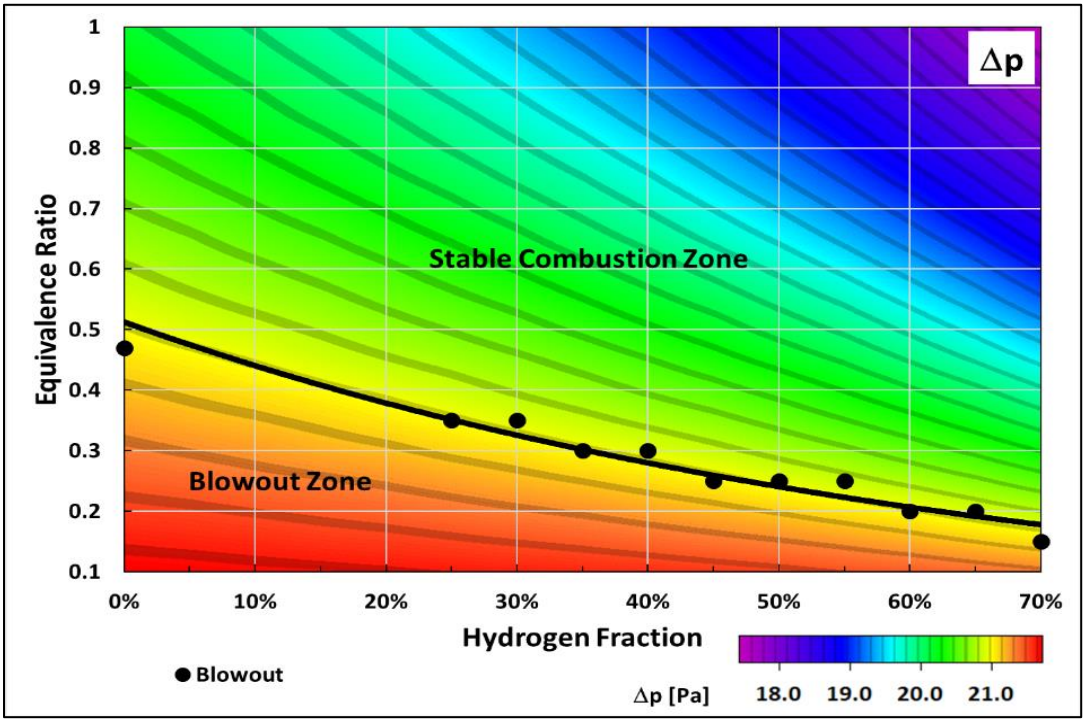

Figure 5.5 Flame stability map at fixed jet velocity of 5.2 m/s and oxygen fraction of 30% superimposed on contours of constant pressure drop across burner headend.

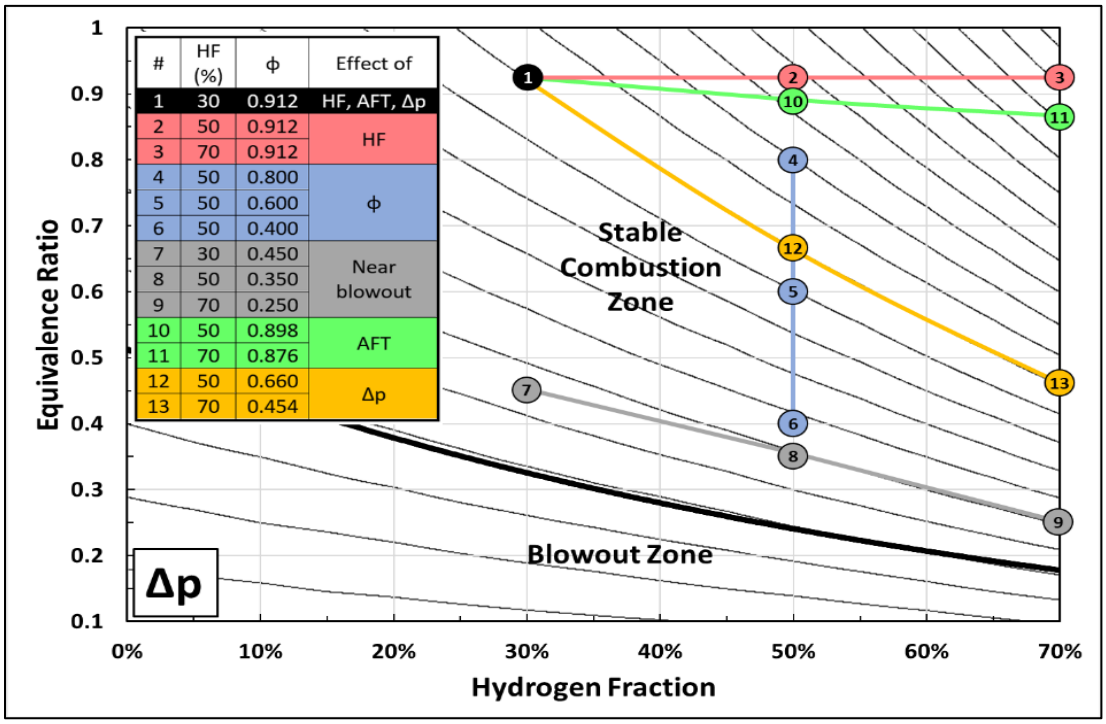

Figure 5.6 Flames selected for imaging shown on Δp map.

Flame macrostructure close to the blowout limit is studied in flames 7-9. The correlation (if any) between AFT and flame shape is tested in flames 1, 10, and 11 at AFT=2200 K. Finally, since the blowout limit coincided with a constant Δp contour, flames 1, 12, and 13 were selected to have a common Δp=19.6 Pa to check for any potential correlation between Δp and flame shape.

The effect of hydrogen enrichment on flame structure at constant ϕ=0.912 is shown in Figure 5.7. The flamelets in the primary reaction zone become shorter and more robust, while the flame plume (secondary reaction zone) becomes brighter and more intense as the HF increases.

This is attributed to the improved chemical kinetics and increased turbulent flame speed. Recall from the analysis of Figure 5.2 that HF has a marginal effect on AFT, where < 100 K change in AFT is recorded for 70% hydrogen enrichment at constant ϕ. Thus, the observed changes in flame shape with hydrogen enrichment in Figure 5.7 are induced primarily by enhanced reaction kinetics and not by higher flame temperature. It can also be observed from Figure 5.7 that the flame plume becomes longer with hydrogen addition, which could be explained by delayed CO burnout in the presence of excess hydrogen, as reported in past studies [180]; further quantification is needed here. On the effect of ϕ on flame characteristics at fixed HF of 50%, Figure 5.8 shows that the flame becomes stronger, brighter, more intense, and more stable with increasing ϕ, as expected.

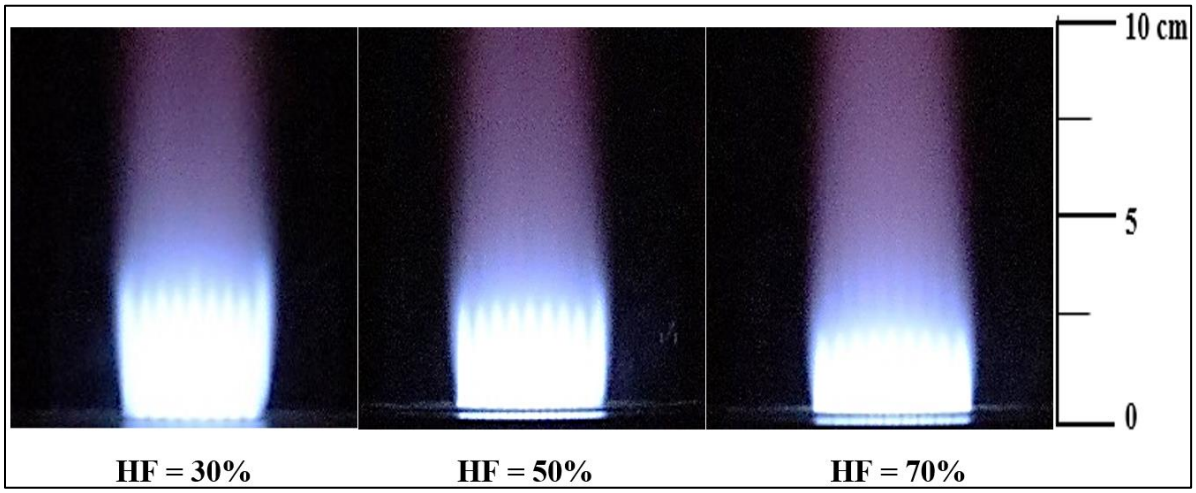

Figure 5.7 Flame shapes captured at constant ϕ = 0.912, fixed jet velocity = 5.2 m/s, and three different values of HF: 30%, 50%, and 70%.

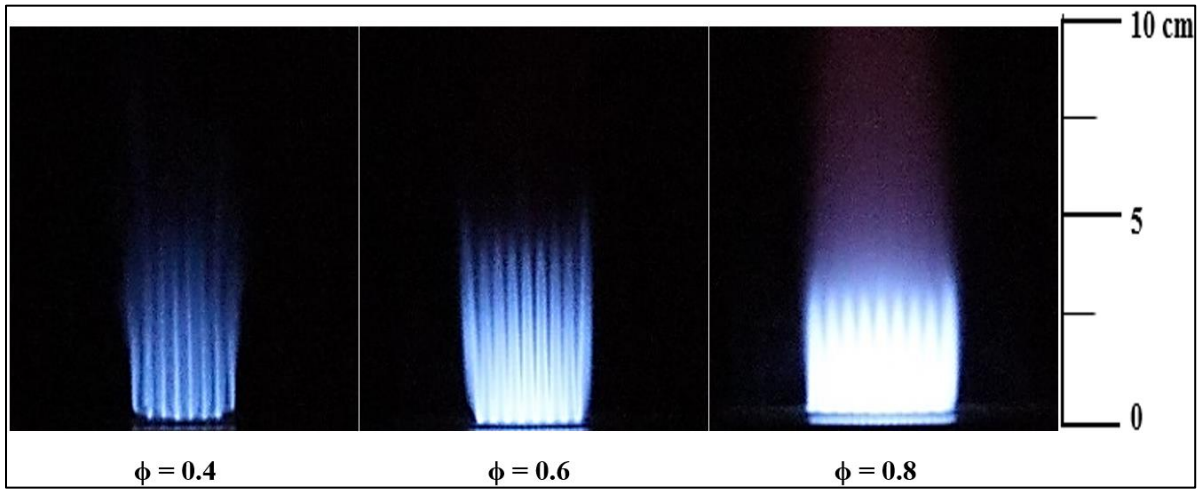

Figure 5.8 Flame shapes captured at constant HF = 50%, fixed jet velocity = 5.2 m/s, and three different values of ϕ: 0.4, 0.6, and 0.8.

The negative effect of CO_2 dilution also subsides by increasing the fuel flow with respect to CO_2. Flame/plume length is observed to increase with ϕ, which could be again explained by delayed CO burnout as the fuel flow increases.

Flame shapes near the blowout limit are displayed in Figure 5.9. To conform to the slope of blowout limit, ϕ had to be reduced from 0.45 – 0.25 as HF increased from 30% to 70%. Near lean blowout, the flames are dimmer, signifying lower strength and stability. The flamelets become longer at low ϕ due to reduced reaction rates at low AFT and greater effect of CO_2 dilution. It can also be observed that the inner flamelets are attached, while the outer ones are lifted and burn in random island flames further downstream, where the average flow velocity is favorable and comparable to the reduced flame speed. As HF increases, the flamelet length decreases, indicative of faster reaction rates with hydrogen addition. Interestingly, as HF is more than doubled (30% to 70%), flame brightness does not increase, which infers that ϕ (and AFT) has a greater influence on flame strength and intensity than HF. In other words, HF has weak effects on Temperature within about 10% changes over a given range of HF tested, there is an effect, but it is insignificant compared to equivalent ratio.

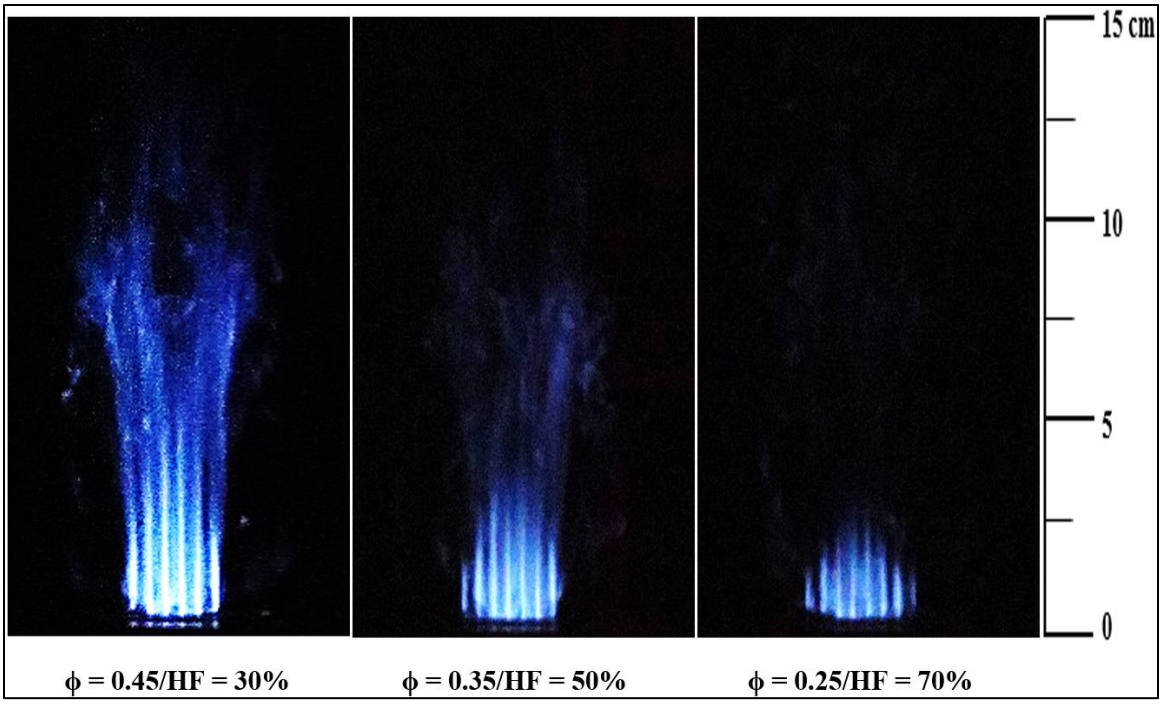

Figure 5.9 Flame shapes captured near the blowout limit at fixed jet velocity of 5.2 m/s.

To decouple the effects of AFT and hydrogen enrichment on chemical kinetics, flame shapes at fixed AFT of 2200K were imaged, as shown in Figure 5.10. Constant AFT was maintained by slightly decreasing ϕ as HF was increased. It can be observed that the flame structures are not identical despite the constant AFT, in contrast to methane flames without hydrogen enrichment [118,157], which exhibited identical structures at fixed AFT. This clearly demonstrates the effect of hydrogen enrichment on the reaction kinetics and, consequently, flame structure. Flamelet length decreases with H_2 addition because of greater reaction rates and higher flame speed, despite the reduction in ϕ.

Since the analyses of Figure 5.4 andFigure 5.5 revealed the primary role of unburnt-mixture density, ρ_{mix}, in the effects of jet Reynolds number, Re, and headend pressure drop, Δp, three flames of common Δp (i.e., constant ρ_{mix}) but different HF and ϕ were imaged, as seen in Figure 5.11. These flames are numbered 1, 12, and 13 in Figure 5.6. It can be observed from Figure 5.11 that maintaining constant Δp does not result in identical flame structures, even though the blowout limit follows a Δp contour in Figure 5.5. However, the remarkable observation is that the flamelet length is approximately constant in Figure 5.11 in spite of reducing ϕ from 0.912 to 0.454 (50% reduction) and increasing HF from 30% to 70% (133% increase). Since flamelet length is a reflection of reaction rate, and consequently Da at constant jet velocity (same flow time scale), it can be assertively concluded here that the contours of constant burning velocity and constant Da are close to those of constant Δp, as analyzed earlier in Figure 5.4 and Figure 5.5.

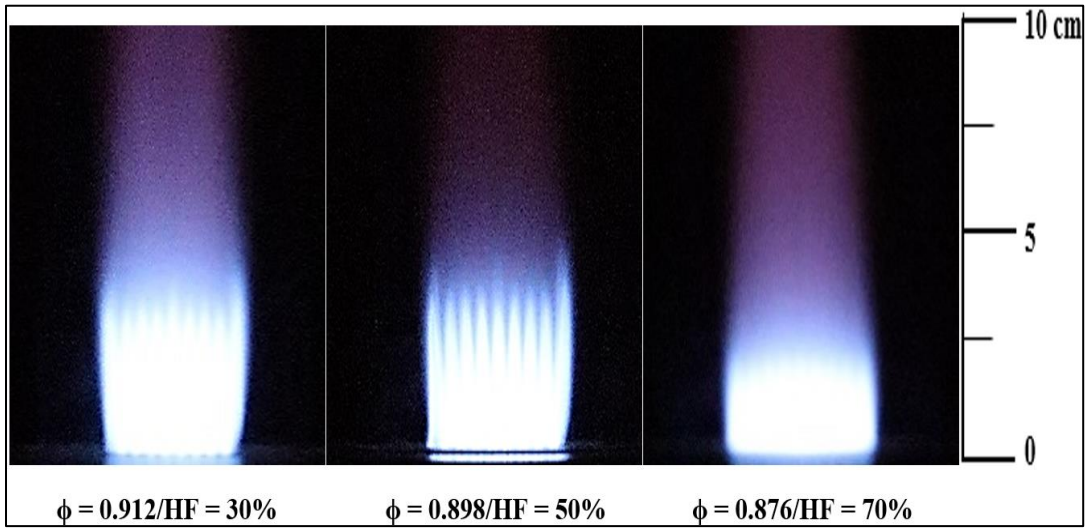

Figure 5.10 Flame shapes captured at constant AFT of 2200 K and fixed jet velocity of 5.2 m/s.

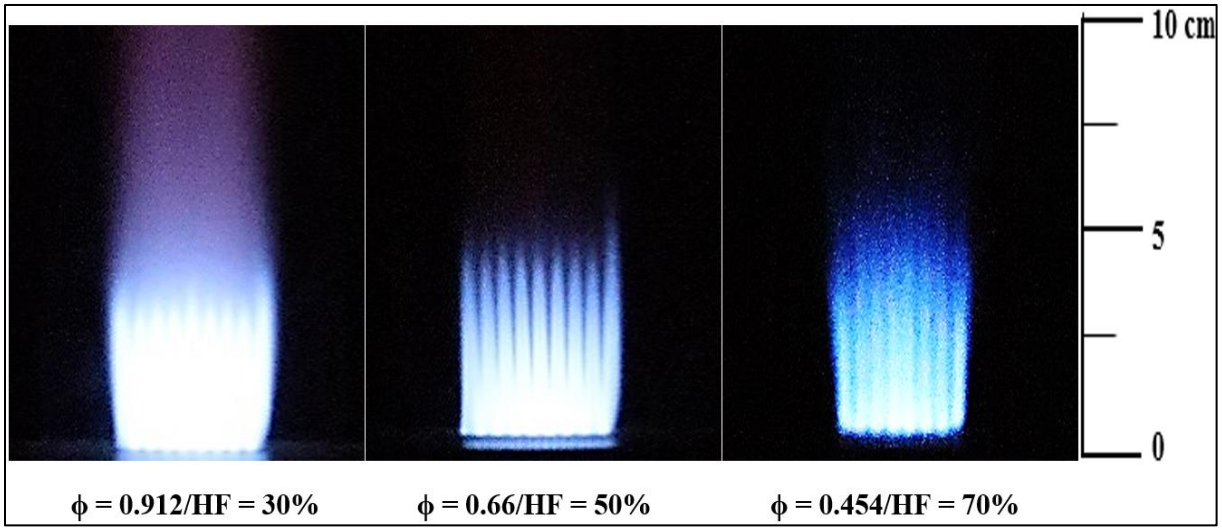

Figure 5.11 Flame shapes captured at a constant Δp of 20 Pa and fixed jet velocity of 5.2 m/s.

This is also an additional affirmation that hydrogen-enriched oxy-methane flames are kinetics-limited and blow out at constant Da, which explains why the blowout limit follows a Δp contour. On the other hand, flame brightness does not correlate with Δp, as observed in Figure 5.11, but correlates with ϕ and AFT, as discussed earlier in the analysis of Figure 5.8.

5.4 Temperature measurements

Temperature measurements were performed in the plumes of selected flames to give an insight into the reaction progress, quantify the effects of different parameters, and provide a reference for validating numerical models. The temperature readings were taken as close as possible to the flame, as allowed by the limit of the utilized R-type thermocouple. The axial measurements were made along the combustor centerline, while the radial readings were taken at a specific axial location of $z/L = 0.833$ as shown in Figure 5.12. Figure 5.13 shows the temperature distributions along the combustor centerline for three flames of different ϕ but common HF=50%. Increasing ϕ clearly results in hotter flames, as expected, because of the corresponding increase in the rate of reaction, heat-release rate, power density, flame speed, and AFT.

The temperature profile increases by an average of 18.62% and 10.18% as ϕ increases from 0.454 to 0.660 and 0.912, respectively. This also agrees with the observation of brighter flames at higher ϕ in Figure 5.8. Changing HF at constant ϕ, however, does not have a similar effect with an average 3.5% difference in temperature for HF of 70% and 40% at ϕ=0.454 as seen in Figure 5.14.

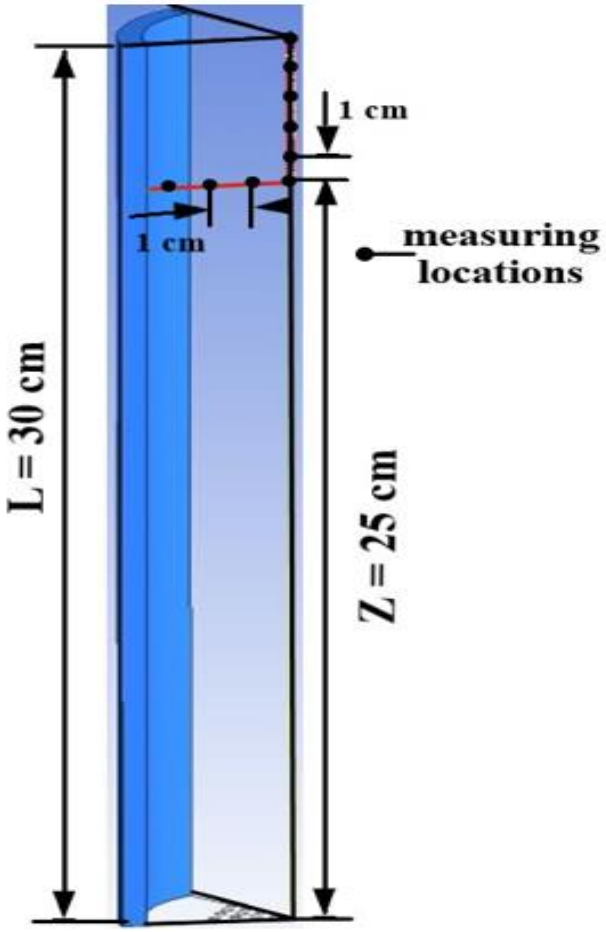

Figure 5.12 Sketch of combustion domain with dimensions and measuring locations.

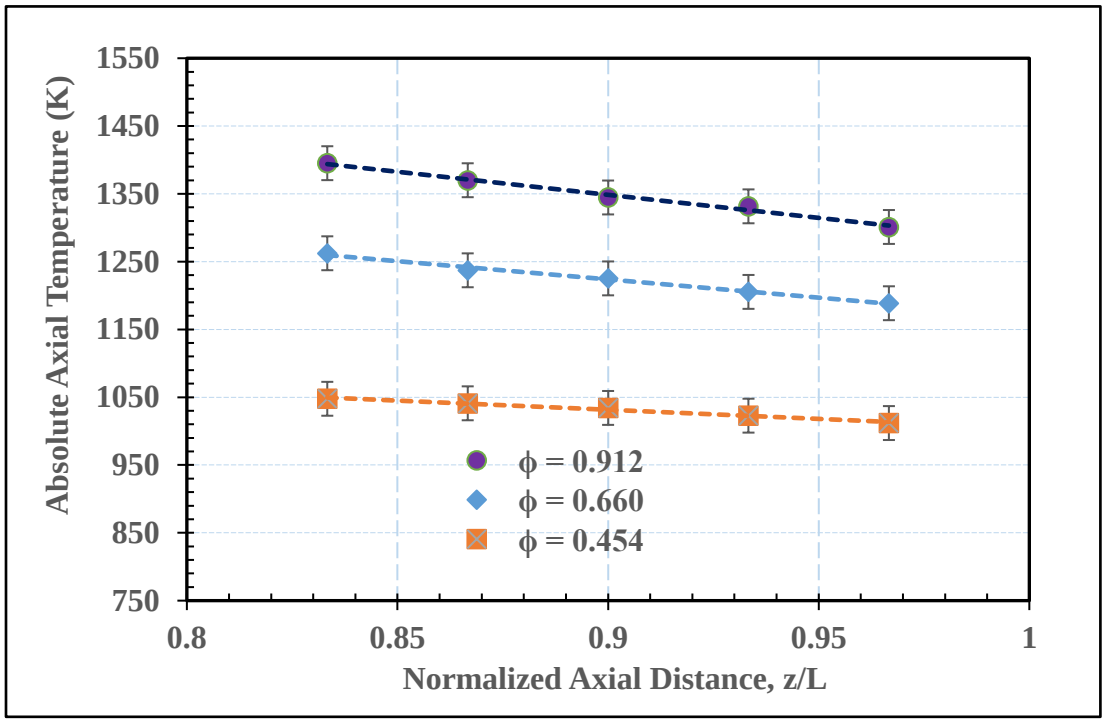

Figure 5.13 Temperature distributions along combustor centerline at 50% HF and different equivalence ratios.

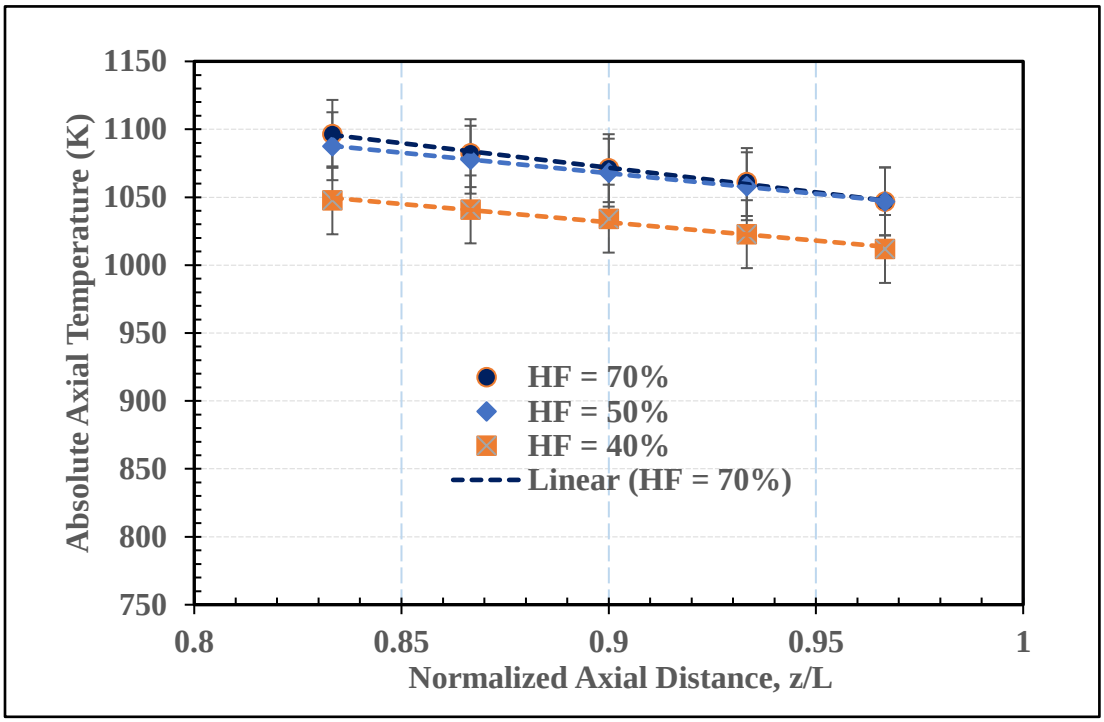

Figure 5.14 Temperature distributions along combustor centerline at ϕ=0.454 and different hydrogen fractions.

No discernable correlation between HF and the temperature data can be detected, which strengthens the findings mentioned above (Figure 5.7), namely that (a) hydrogen enrichment has a negligible effect on AFT and (b) the stabilizing effect of hydrogen is purely due to reaction kinetics effects other than making the flames hotter such as enhanced production of radicals.

Figure 5.15 provides additional proof that the data in Figure 5.14 is not a spurious artifact limited to the centerline; again, no discernable correlation between HF and the radial temperature data can be detected. Figure 5.16 and 5.17 revisit the effect of maintaining constant burner-headend Δp, which was discussed earlier in Figure 5.11. Local temperatures were measured in three flames of common Δp=19.6 Pa but different ϕ and HF (0.78/40%, 0.66/50% and 0.454/70%).

It can be observed in Figure 5.16 and 5.17 that the effect of ϕ clearly overtakes that of HF; higher ϕ results in hotter flames (higher AFT) despite the reduction in HF. The difference in axial temperature profiles between Flames 0.78/40% and 0.66/50% is averagely 9.76% and between Flames 0.66/50% and 0.454/70% is averagely 14.18%. This aligns very well with the analysis of Figure 5.11 and confirms all findings mentioned above on the effects of ϕ and hydrogen enrichment. An additional interesting observation in Figure 5.17 is that hydrogen addition flattens the combustor radial temperature profile as HF increases from 30% to 70%. A uniform, non-skewed profile is advantageous for avoiding turbine damage due to the absence of hot spots. Thus, in addition to enhancing flame stability, hydrogen enrichment is beneficial for maintaining good turbine health.

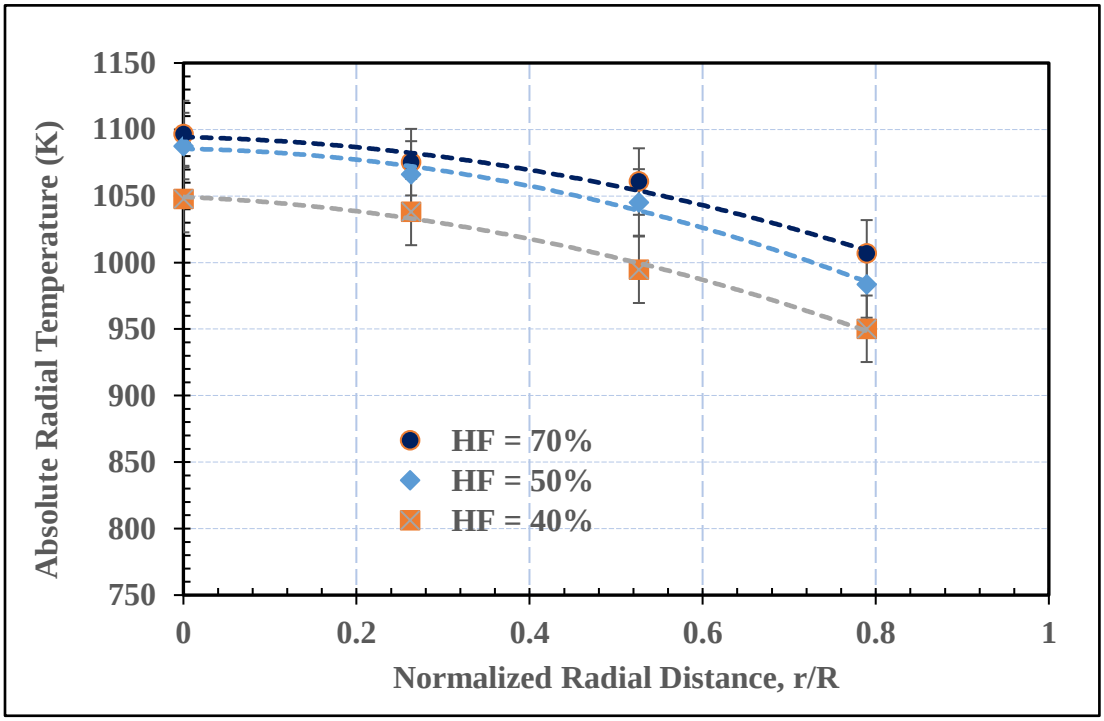

Figure 5.15 Radial temperature profiles at ϕ=0.454 and different hydrogen fractions. All profiles are at z/L=0.833.

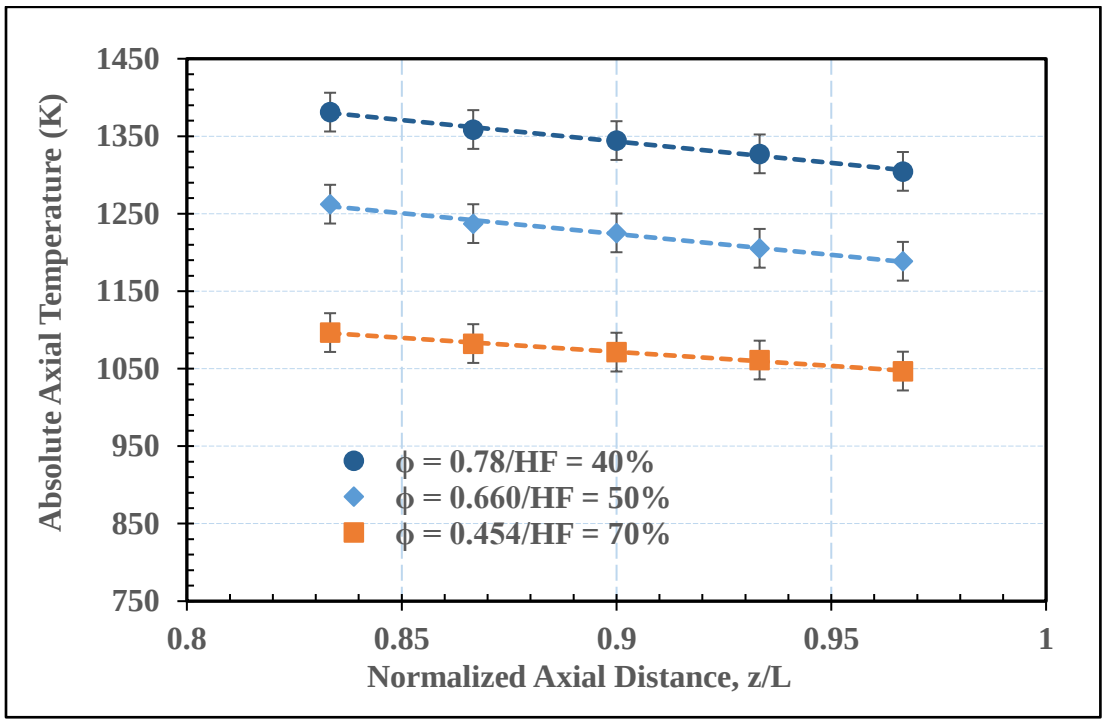

Figure 5.16 Temperature distributions along combustor centerline at constant Δp = 19.6 Pa and different equivalence ratios and hydrogen fractions.

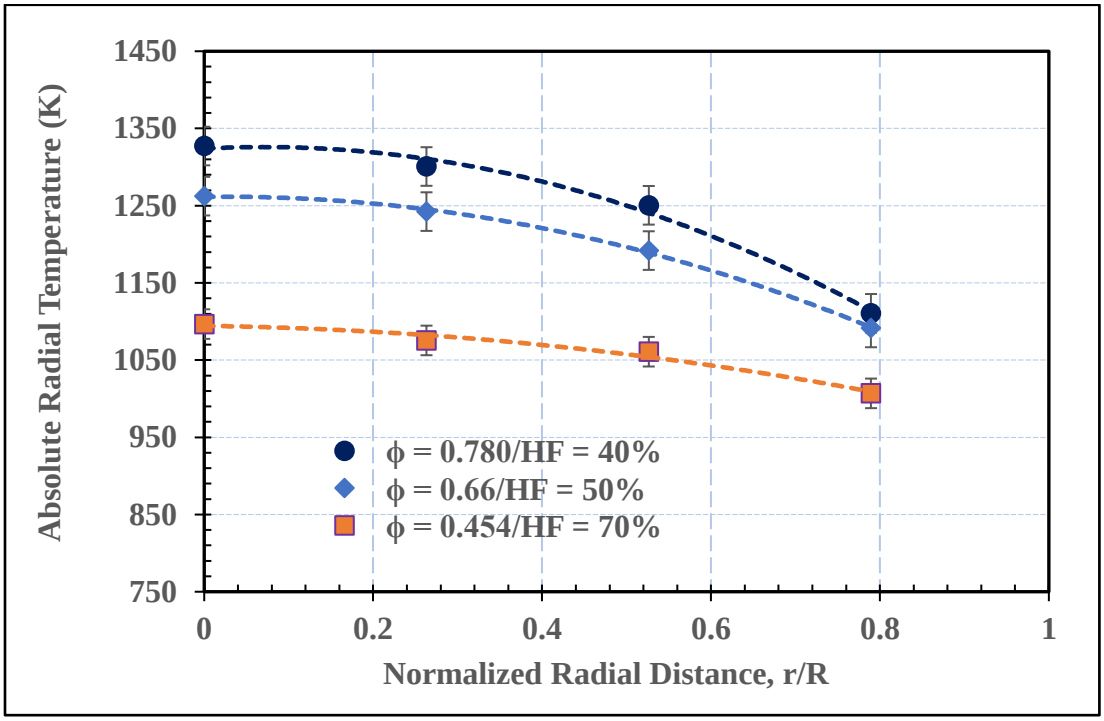

Figure 5.17 Radial temperature profiles at constant Δp = 19.6 Pa and different equivalence ratios and hydrogen fractions. All profiles are at z/L=0.833.

CHAPTER 6

NUMERICAL MODELLING OF OXY-COMBUSTION CHARCATERISTICS IN A PREMIXED MICROMIXER-LIKE COMBUSTOR

This chapter presents the numerical study of the combustion and emission characteristics for a micromixer-like model gas combustor operating on oxy-combustion technology. A thin flame-front topology-based LES premixed combustion model with the DO-WSGGM radiation model was implemented to predict the combustor's oxy-combustion characteristics. The numerical results were validated against the data obtained from experiments conducted on the combustor. Finally, the effects of hydrogen enrichment on combustion features and emissions.

6.1 Computational domain and Boundary conditions

Taking advantage of the micromixer burner's hexagonal hole pattern, only a 60° sector of the combustor was adopted and discretized in a 3D mesh, as shown in Fig. 6.1. This sector comprises of 6 full-holes, 8 half-holes, and one quarter-hole. All holes were set as velocity inlets introducing the same premixed $CH_4/H_2/O_2/CO_2$ mixture at a constant inlet velocity of 5.2 m/s and inlet temperature of 300 K. The *HF* was varied from one case to another by manipulating the values of inlet mixture fractions. A pressure-outlet condition was assigned to the combustor outlet.

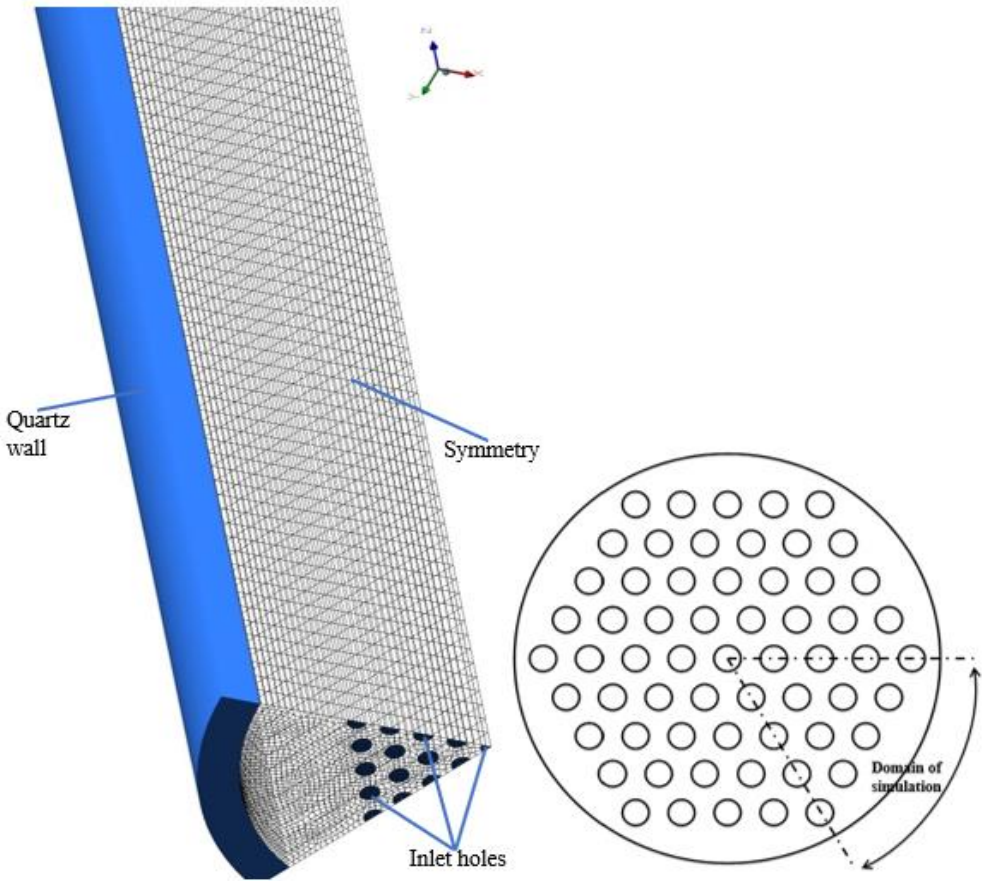

Figure 6.1 Mesh of computational domain representing one-sixth of the combustor.

Since the combustor confinement is made of quartz glass, a mixed thermal boundary condition was assigned to the combustor wall to cater for the convective and radiative modes of heat transfer to the surroundings, with values of convective heat-transfer coefficient and free-stream temperature of 20 $W/m^2/K$ and 298 K, respectively. The 6-mm-thick quartz wall was modeled as semi-transparent, and the radiative heat transfer through it was modeled with four-wavelength non-gray band model. A periodic boundary condition was imposed at the symmetry faces adjoining the wall. A parametric study was conducted targeting HF's effect at fixed Ø=1 (stoichiometric) and *OF*=30%. The hydrogen component of the fuel blend was varied between 10-50%.

6.2 Grid independence study

A mesh-independence study was conducted by comparing the LES simulation results of three meshes containing 100k, 150k, and 200k cells, as shown in Figure 6.2. The 3D mesh has finer cells near the burner, and cell size gradually grows coarser towards the outlet and wall, with inflation at the wall. The differences in the predicted radial temperature between these meshes at an axial height Z=3.3D above the burner were negligible near the combustor centerline and grew marginally significant towards the wall, as seen in Figure 6.2. The mesh of 150k cells was adopted for this computational work.

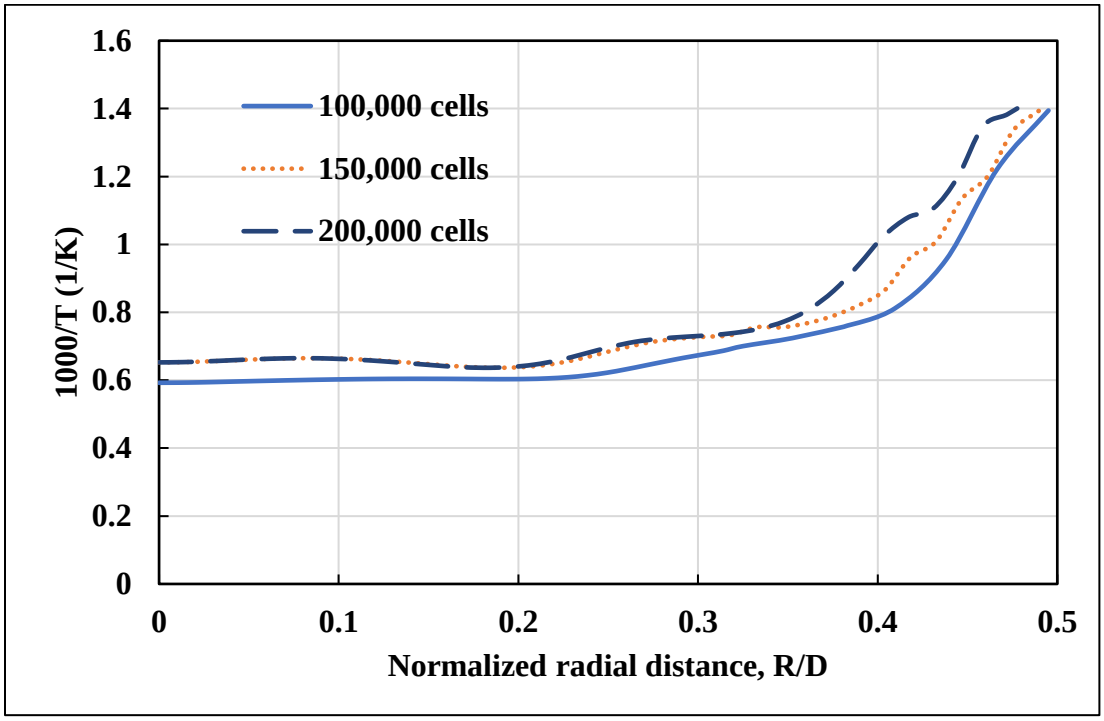

Figure 6.2 Mesh independence test with radial temperature profile at axial height Z=3.3D for mesh sizes of 100k, 150k, and 200k cells.

6.3 Model Validation

The numerical model was validated with the measured temperature data at Ø = 0.78, HF = 40%, and OF = 30%. Figure 6.3a compares experimental and numerical axial temperature along the combustor axis for temperature readings at Z/D > 3.3, and there is a good agreement between the two methods. Although temperature readings for Z/D < 3.3, which contains the flame core, could not be measured due to the limited operating range of the thermocouple, such temperature values were calculated numerically as seen in Figure 6.3a while the radial temperature profile at Z/D = 3.3 for both experimental and numerical results is presented in Figure 6.3b. The experimental results are slightly overpredicted by a maximum/average values of 16.51%/15.09% and 11.78%/9.18% for the axial and radial profiles respectively within the region where experimental data have been taken. This may be attributed to the fact that the heat transfer to the micromixer burner is not included in the computational model. The micromixer burner conducts heat from the flame, which raises the reactants' temperature through preheating, resulting in reduced combustor temperature.

Figure 6.4 compares the experimental and numerical flame image for set point Ø = 0.78, HF = 40% and OF = 30%. OH contour plots represent the numerical flame shape. The primary reaction zone represented by the mini-flames and secondary reaction zone represented by the plume above the mini-flames is captured in both images. The heights of the micro-flames are comparable visually.

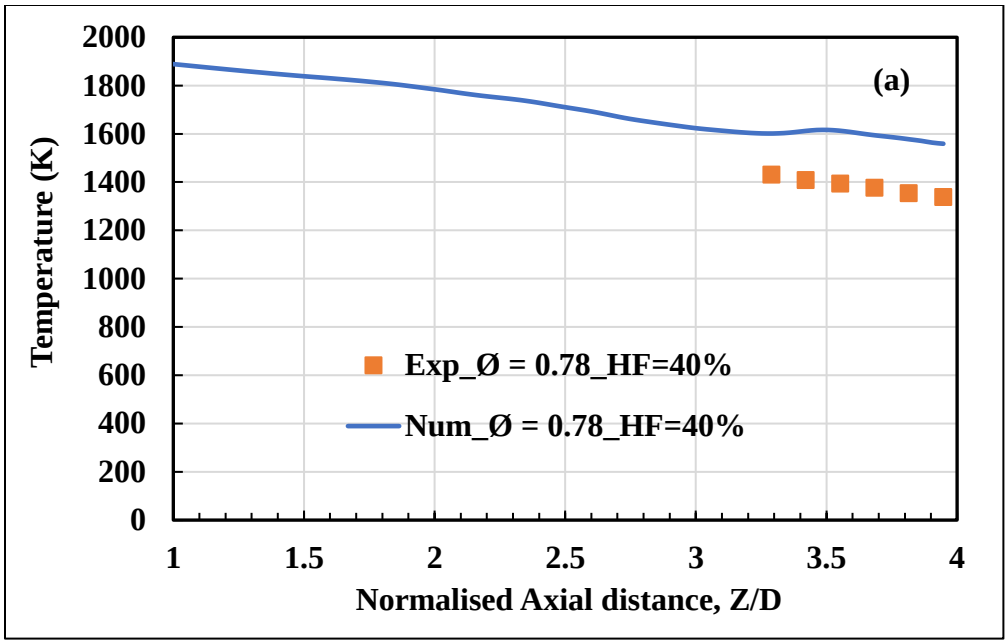

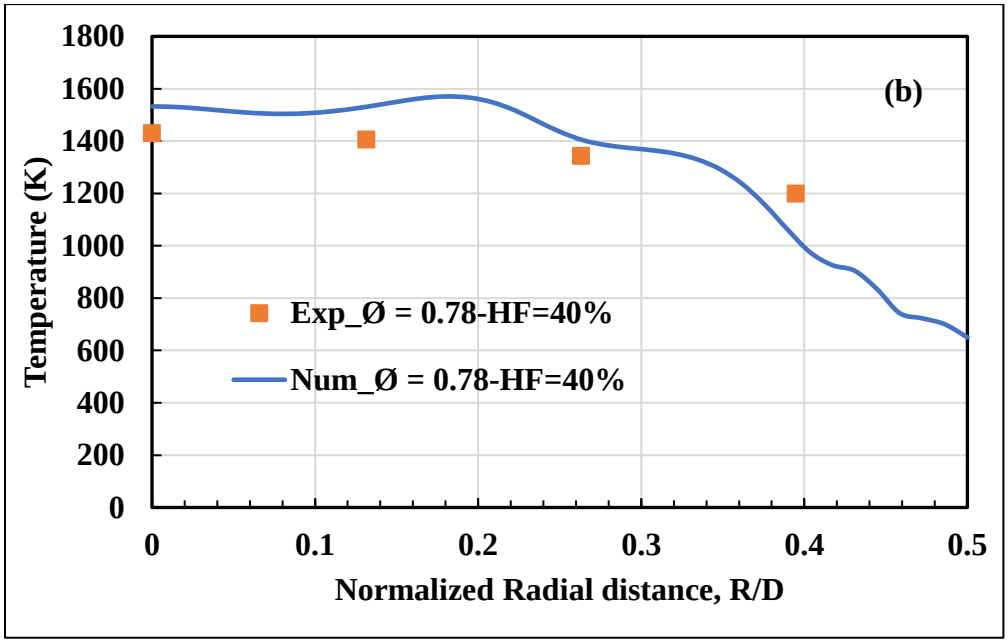

Figure 6.3 Comparison of experimental and numerical temperature profiles inside the combustor at Ø = 0.78, HF = 40% and OF 30% (a) axial temperature along combustor axis (b) radial temperature at Z/D = 3.3.

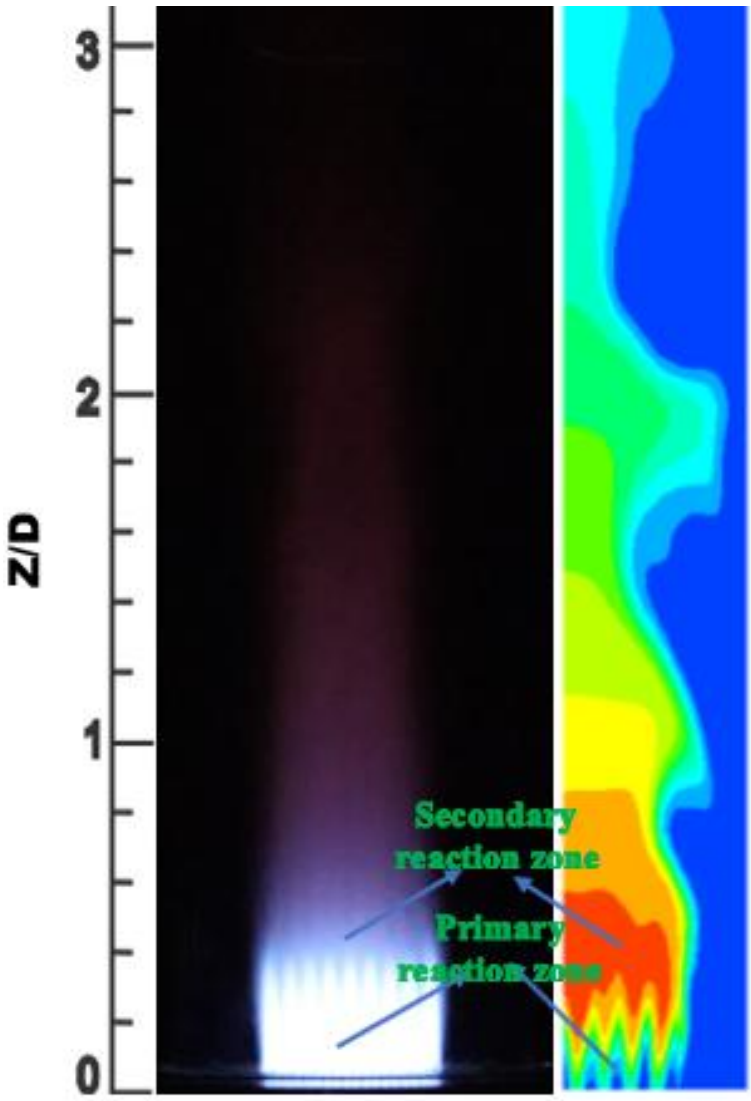

Figure 6.4 Comparison of experimentally captured flame image and numerical OH contour plot at Ø = 0.78, HF = 40% and OF 30%.

Reaction zone exists in the spacing between mini-flames, but it is non-existent in the region between the flame base and the wall. This is because the global flame shape consists of multiple jet flames that mainly propagate axially, unlike swirl flames.

6.4 Parameters defining flame characteristics.

Some parameters that were used to define the characteristics of the flame are defined as follows:

- Heat release factor (γ): To quantify the heat release during the combustion process, a non-dimensional parameter known as heat-release factor γ is expressed as:

$$\gamma = \frac{T_{ad} - T_0}{T_{ad}} = 1 - \frac{T_0}{T_{ad}} \tag{6.1}$$

Where T_{ad} is the adiabatic flame temperature and T_0 is the unburnt gas-mixture temperature.

- Flame thickness (δ): This represents the length of the preheat zone and inner-layer part of the laminar flame front, has been calculated with the correlation:

$$\delta = \frac{\lambda_u}{\rho_u c_p S_L} \tag{6.2}$$

Where λ_u and ρ_u represent the thermal conductivity and density of the unburnt reactant mixture, respectively.

- Damköhler number (Da): This is a non-dimensional parameter defined as the ratio of reaction rate to diffusion rate, and is expressed as:

$$Da = \frac{\left(l_t/u'\right)}{\left(\delta/S_L\right)} \tag{6.3}$$

Where l_t represents the integral length scale and *u'* represents the root mean square of velocity fluctuation.

- Karlovitz number (Ka): this is a non-dimensional ratio of chemical time scale to Kolmogorov time scale, represented as:

$$Ka = \frac{\sqrt{\varepsilon/\upsilon}}{S_L/\delta} \tag{6.4}$$

Where ε is the turbulent dissipation rate and υ is the kinematic viscosity.

6.5 Results and discussions

6.5.1 Stability and structure of premixed $CH_4/H_2/O_2/CO_2$ flames

An experimental investigation of the behavior of premixed $CH_4/H_2/O_2/CO_2$ flames was performed, considering various fuel compositions in a micromixer-adapted model gas-turbine combustor. A fixed jet velocity of 5.2 m/s ensured that (a) a constant volumetric flow rate of reactant mixture was maintained, and (b) all flames have similar cold-flow (non-reacting) conditions and turbulence intensities. To identify the combustor's static stability limits, Ø and *HF* were varied over the ranges 0.1-1.0 and 25-70%, respectively. Then, the flame stability was mapped on a Ø versus HF plot, as seen in Figure 6.5, which shows the lean blowout (LBO) limit. This signifies that the stable flame region is only delineated by the LBO limit for the operating conditions under consideration.

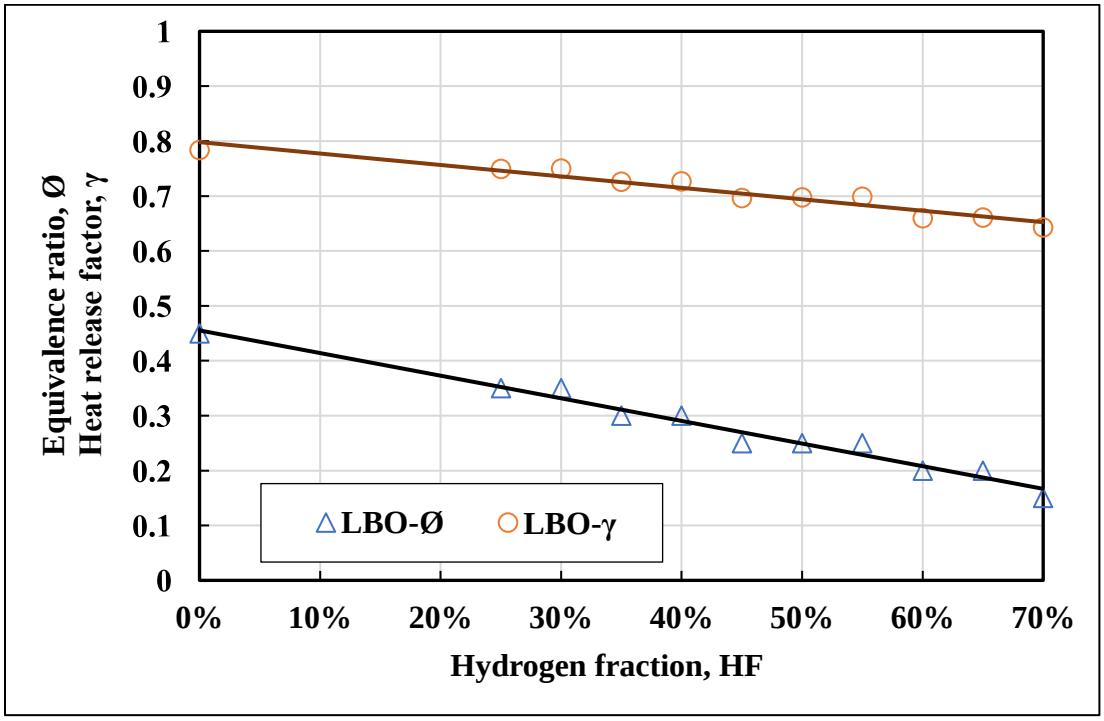

Figure 6.5 Experimentally recorded lean blowout (LBO) limit, mapped as plots of equivalence ratio (Ø) and heat release factor (γ) vs. hydrogen fraction (HF), at a fixed inlet jet velocity and oxygen fraction (OF) of 5.2 m/s and 30%, respectively.

The variations of calculated heat release factor (γ) with HF are also presented in Figure 6.5. As HF increases from 0-70%, the LBO limit extends linearly from 0.45-0.15 towards lower Ø, thereby widening the operating space with a slight decrease of up to 0.14 in the heat release factor (γ).

The extended LBO limit indicates that flames are stabilized at lower temperature due to high reaction rate and faster laminar flame speed of hydrogen. The addition of hydrogen increases the laminar flame speed of the mixture, which balances or offsets the inlet flow velocity and prevents the flame from migrating downstream, thereby restricting the early occurrence of blowout at low Ø. Blowout sets in when the inlet flow velocity exceeds the laminar flame speed. The expanded operability space of heat release factor can be attributed to the improved adiabatic flame temperature with hydrogen addition.

Numerically computed temperature profile along the combustor axis is plotted in Figure 6.6a for different hydrogen fractions at Ø = 1.0 and OF = 30%. There is a marginal increase in temperature with an increase in hydrogen concentration. This can be attributed to a boost in fuel reactivity and diffusivity as well as slightly increased adiabatic flame temperature due to hydrogen addition. For all the HFs, the axial temperature increases from the jet inlet until it reaches the maximum temperature at the flame core and then decreases downstream towards the exit. Radial temperature profiles for different HFs at axial distance Z = D are shown in Figure 6.6b.

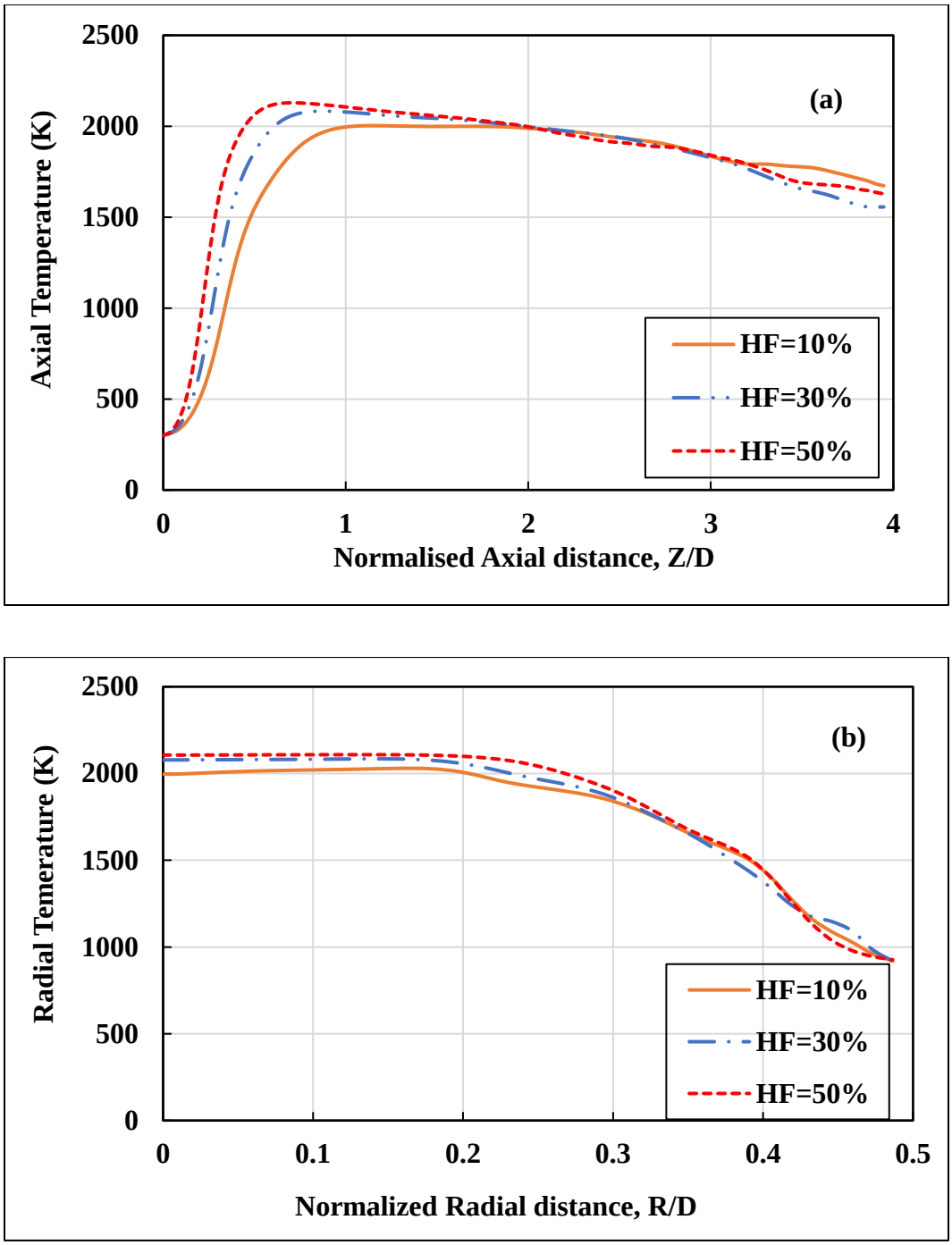

Figure 6.6 Comparison of (a) axial temperature along the combustor axis, and (b) radial temperature profile at Z/D = 1.0, for various hydrogen fraction at Ø = 1 and OF = 30%

A marginal increase in radial temperature with hydrogen addition is also observed, showing that hydrogen enrichment has little impact on the flame temperature. As r/D increases, the radial temperature profile transitions from a relatively constant value near the combustor axis to a lower value at a high r/D value close to the wall. This is due to the conical shape of the flame and heat loss at the combustor wall. It can also be seen from Figure 6.6a that the axial location of the peak flame temperature from the burner decreases with increasing hydrogen fraction. This is due to the higher laminar flame speed that ensues from hydrogen addition and thereby produces a shorter primary reaction zone.

Figure 6.7 shows the contour plots of static temperature and vorticity magnitude for various hydrogen fractions. The temperature field shows a distribution of high-temperature zone at the flame core to the lower temperature towards the combustor exit. Vorticity indicates shear layers where turbulent eddies are formed, as seen at the combustor base between the mini-flames. The shear layers in the primary reaction zone occupy the hole spacing and contribute to the mini-flames' stabilization. In contrast, outer shear layer at the edge of the plume stabilizes the flame core in the secondary reaction zone. The height of the shear layers in-between the mini-flames decreases with increasing hydrogen fraction due to increased burning velocity which reduces the flame height. Also, the vorticity magnitude of the outer shear layer increases with increasing hydrogen concentration due to enhanced eddy formation. In general, hydrogen addition makes the flame shorter and more intense.

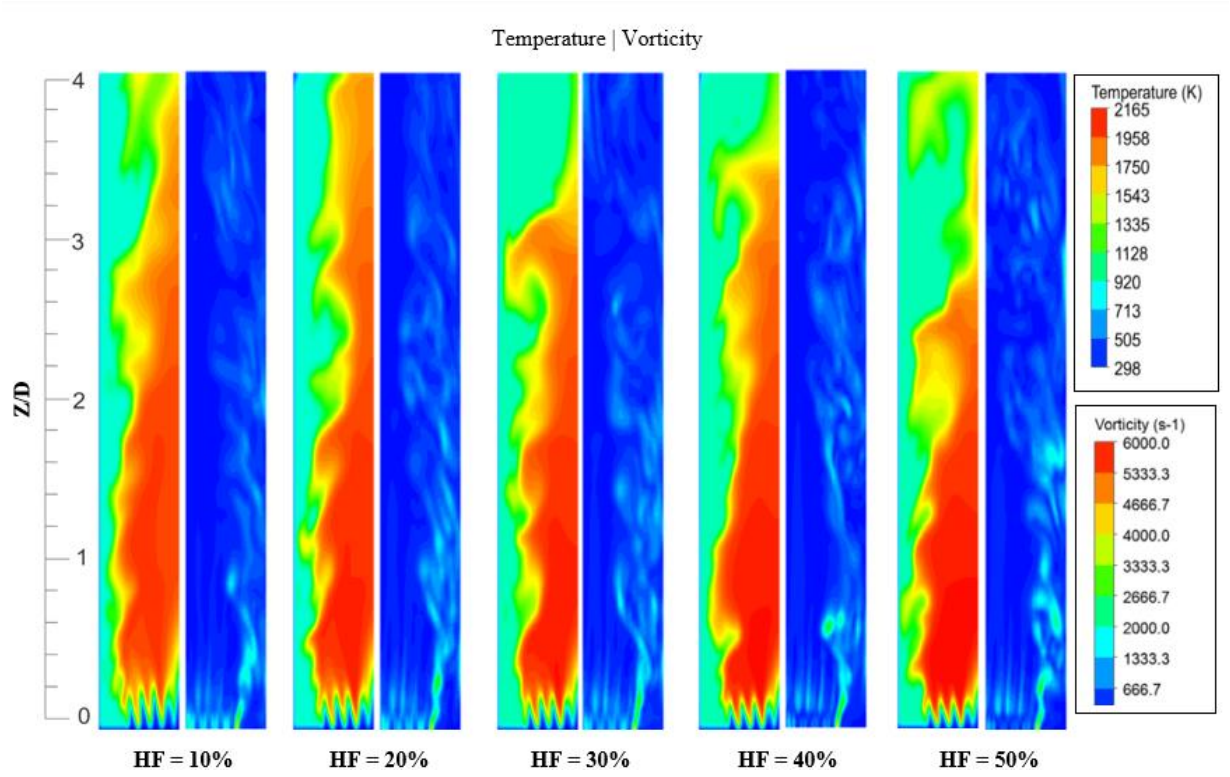

Figure 6.7 Contour plots of temperature field (left) and vorticity magnitude (right) for various HFs under stoichiometric condition and fixed oxygen fraction of 30%

6.5.2 Combustion and emission characteristics of CH_4-H_2-O_2-CO_2 flames

The effect of hydrogen addition on the flames' combustion characteristics was also investigated through the contours of product formation rate (PFR) and reaction progress variable shown in Figure 6.8. The reaction zone exists in the shear layers at the hole spacing and stabilizes the mini-flames. Hydrogen addition increases the PFR in the shear regions which makes the flame more compact. The progress variable contours also show the compactness of the flames with increasing hydrogen fraction which is due to enhanced reaction rates. Figure 6.9 presents the variation of flame thickness with hydrogen addition.

Flame thickness represents the length of both the preheat zone and inner layer of the flame front which accounts for chemical reaction, heat release and radical recombination. It is observed that the flame thickness decreases with increasing hydrogen fraction due to faster reaction rate and rapid consumption of fuel species.

The increased reaction rate with hydrogen addition is evident in the plot of the variation of Damköhler number (Da) with hydrogen fraction represented in Figure 6.10. As hydrogen fraction increases, the composition of fuel mixture (CH_4/H_2) varies from CH_4-rich to H_2-rich mixture and the ignition delay time and laminar flame speed increases and decreases respectively due to the increasing concentration of H_2 which significantly increase the reactivity of the mixture [181–184]. The Karlovitz number (Ka) for different hydrogen fractions was also calculated, and it was found that Ka decreases from 0.69 for pure CH_4 to 0.225 for 50% HF. This implies that the flames become thinner with hydrogen addition.

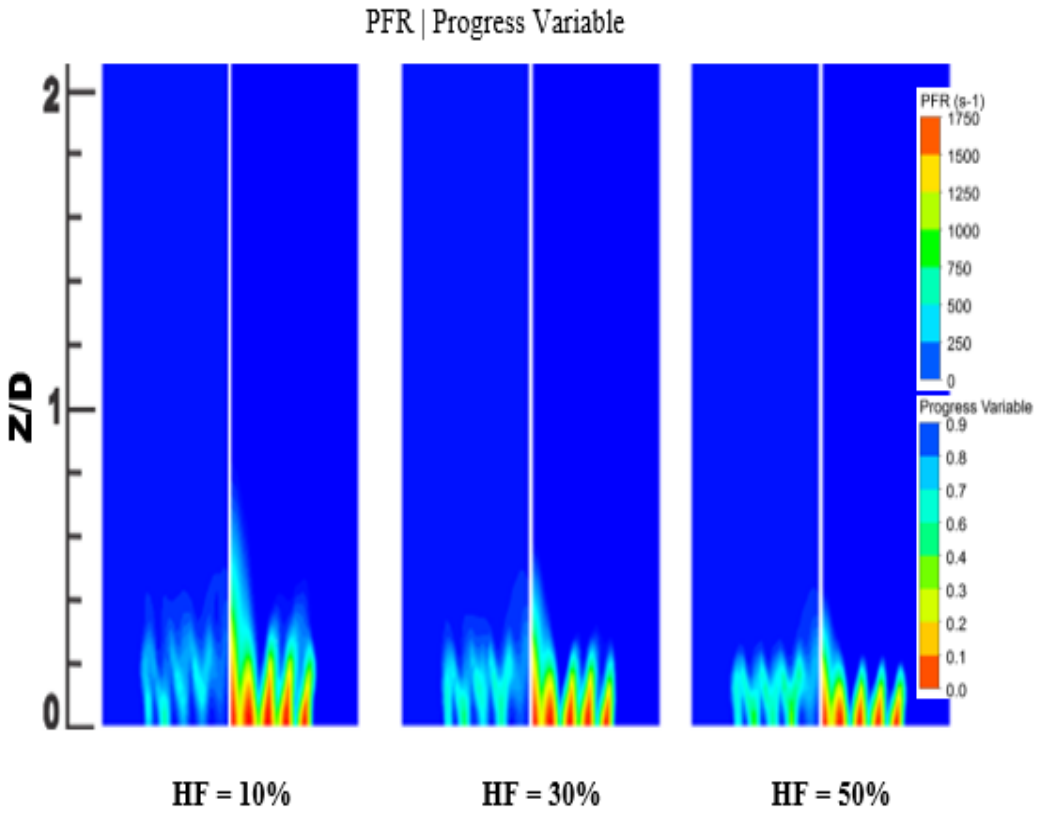

Figure 6.8 Contour plots of product formation rate (left) and progress variable (right) for various HFs under stoichiometric condition and fixed oxygen fraction of 30%.

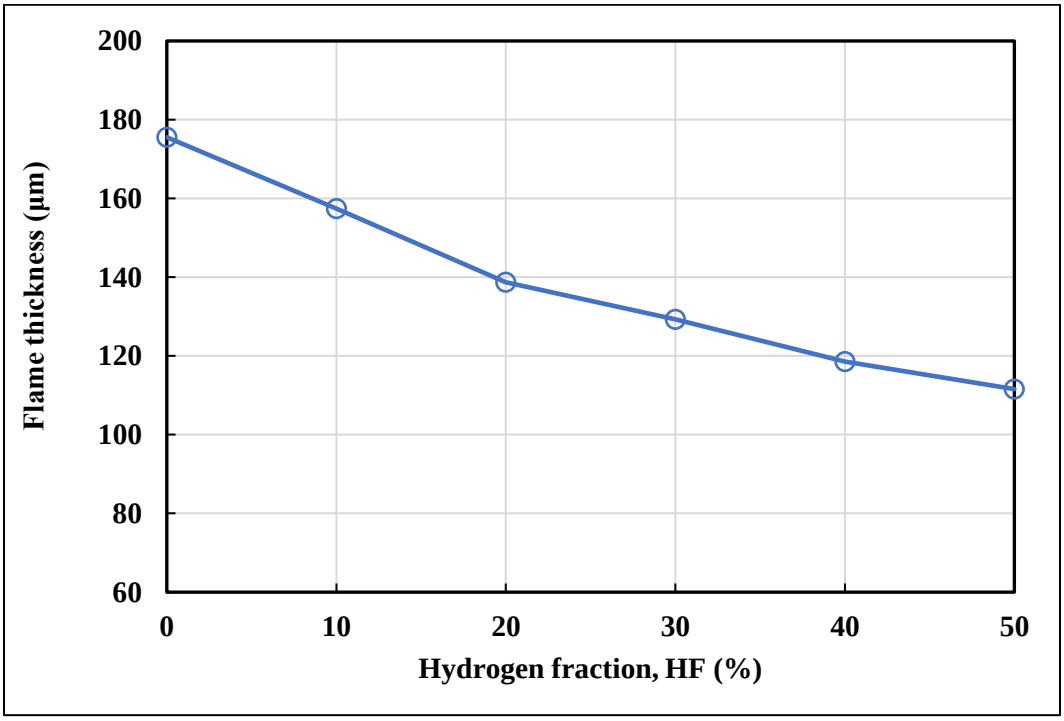

Figure 6.9 Variation of flame thickness with hydrogen fractions at equivalence ratio of 1.0 and oxygen fraction of 30%.

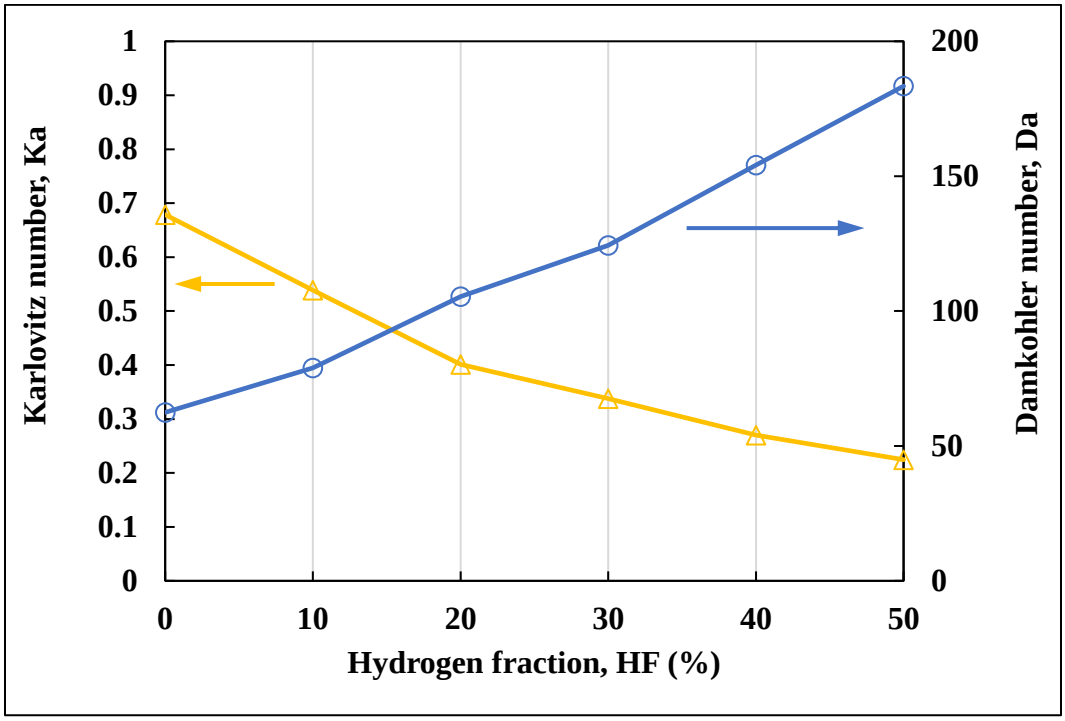

Figure 6.10 Variations of Karlovitz and Damköhler numbers with hydrogen fraction under stoichiometric condition and at fixed oxygen fraction of 30%.

The condition of Ka<1, which represents all the cases, shows that the laminar flame thickness is smaller than the smallest eddies and as such the flame fronts are embedded inside the scales. This means that the small eddies can only wrinkle the flame and cannot penetrate the flames' inner layer to alter reactions. Hence, the laminar burning rate controls the reaction rates.

Figure 6.11 shows the contours of mole fractions of OH and CO radicals for hydrogen fractions of 10%, 30% and 50%. It is observed that increasing hydrogen fractions enhances OH and CO radicals' formation in the inner layer of the flame front. CO emission becomes significant at equivalence ratio > 0.95 in both air- and oxy-combustion with higher emission observed in the latter as reported by Williams et al. [185]. This can be as a result of the chemically active CO_2 diluent in oxy-combustion which competes with O_2 for H radicals thereby increasing CO emission [186]. Glarborg and Bentzen [187] identified three reaction pathways for CO formation from CO_2; $(I)\ CO_2 + H \leftrightarrow CO + OH$, $(II)\ CO_2 + O \leftrightarrow CO + O_2$, $(III)\ CO_2 + OH \leftrightarrow CO + HO_2$ with path (I) being relatively faster. Hydrogen addition increases the number of H species thereby increasing the production of CO through traction pathway (I).

The competition for H radical by CO_2 is also responsible for the lower laminar speed and overall reaction rate in oxy-combustion as compared to air combustion [188]. Also, the high-temperature field associated with hydrogen-enriched combustion expedites the dissociation of CO_2 into CO and O species, thereby increasing the CO concentration in the oxidation zone of the flame front.

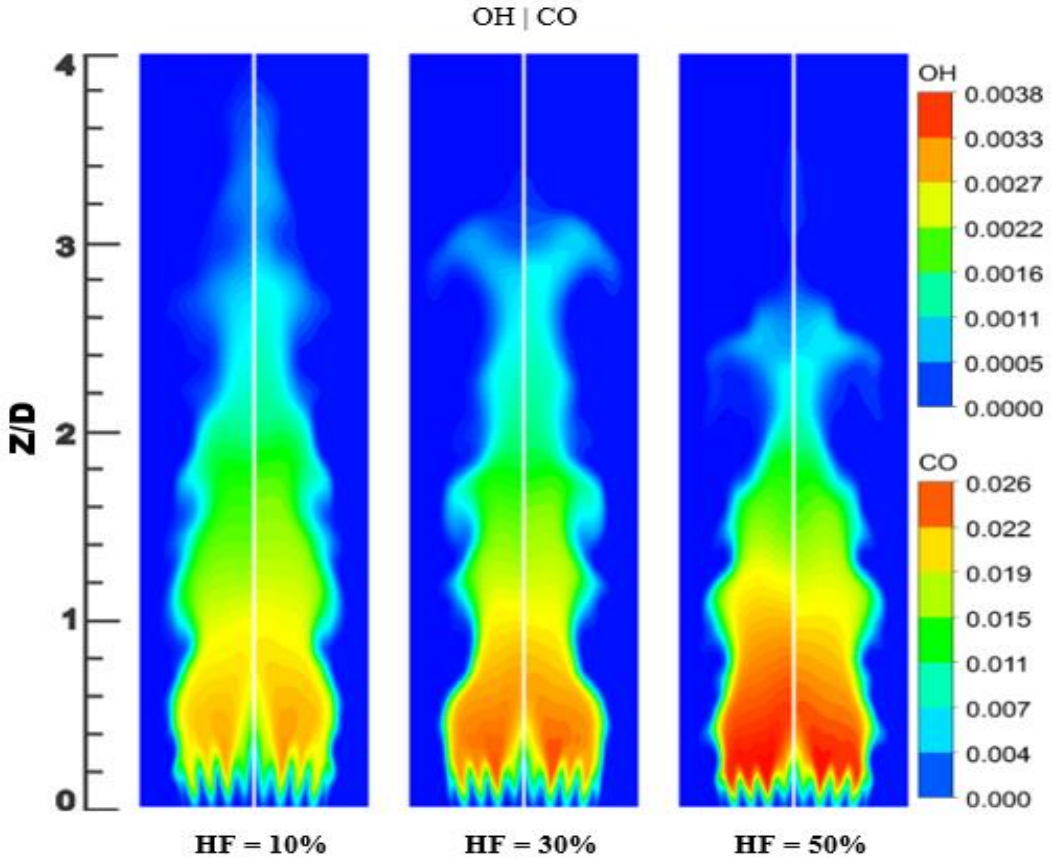

Figure 6.11 Contour plots of mole fraction distributions of OH (left) and CO (right) radicals within the combustor for hydrogen fraction of 10%, 30% and 50% under stoichiometric condition and fixed oxygen fraction of 30%.

The computed CO emitted from the combustor for different HF's is presented in Figure 6.12. The emitted CO increases from 33 ppm at 10% HF to 364 ppm at 50% ppm, indicating increased CO emission with hydrogen addition.

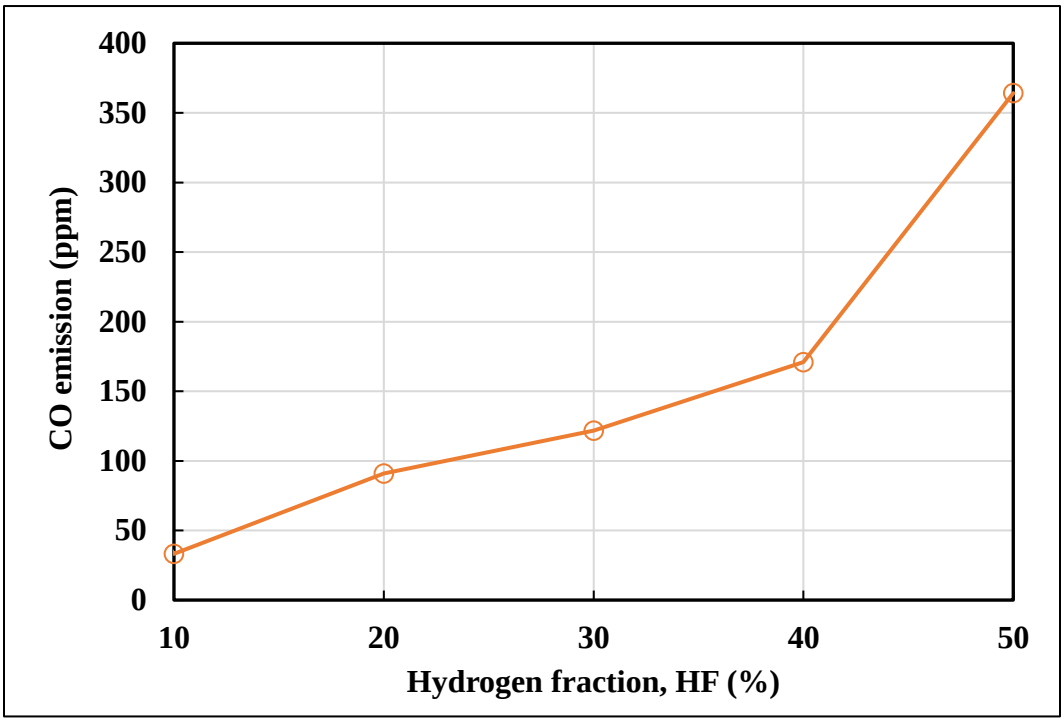

Figure 6.12 CO emission for various hydrogen fractions under stoichiometric condition and fixed oxygen fraction of 30%.

CHAPTER 7

CONCLUSIONS AND RECOMMENDATIONS

7.1 Conclusions

The global shift towards hydrogen fuel as a clean energy source has made the micromixer burner technology more relevant to flame stabilization due to its flexibility in accommodating different degrees of hydrogen enrichment without experiencing instabilities or flashbacks, as well as its compactness for usage in portable combustors. The micromixer burner has been successfully implemented by various gas turbine manufacturers and researchers, mainly for air-fuel combustion of hydrogen and syngas. Thus, this research investigated the implementation of a micromixer-like burner in a model gas turbine combustor for premixed hydrogen-enriched methane flame under oxy-combustion conditions by studying the combustor stability, combustion characteristics, and emissions.

In the first part of this work, the mixing quality of CH_4 fuel jets injected in the laminar main crossflow of O2/CO2 oxidizer has been studied numerically in a single micromixer tube a unit to be repeated abundantly to form potential oxy-fuel micromixer headends in zero-emission combustion applications. Mixing quality was examined in terms of uniformity in reactant composition, which is critical to the stability of premixed flames in gas turbines and other applications.

Numerical assessment of the quality of mixing was carried out through various mixedness parameters available in the literature. The effects of tube length, fuel hole size, and number of fuel holes on the mixing quality were investigated. Results showed that the mixing quality improves with increasing tube length because more mass diffusion occurs as the tube gets longer. It was observed that momentum-driven diffusion has a lesser influence on mixing than mass diffusion at length L > 10D. The fuel hole diameter also affects mixing, which improves with decreasing hole diameter. This can be attributed to the increased jet velocity that allows for easier penetration of the main flow and enhances mixing through intense fluid-fluid interaction. An optimum fuel hole diameter of 0.25mm was obtained for the 4-hole micromixer tube arrangement; smaller diameters resulted in inferior mixing. This indicates that the main factor affecting the mixing quality is the main flow ratio to jet flow momenta and not the fuel hole size. Increasing the number of fuel holes from four to six at a fixed total fuel mass flow rate and similar hole size resulted in reduced mixing quality for hole sizes greater than 0.2 mm and enhanced mixing quality for smaller hole sizes. This can again be attributed to both the penetration strength and ratio of the main flow to jet flow momenta. The results show that micromixers can achieve high mixing quality at a reasonable burner height.

The second part of this research involved experimental investigation of the stability and structure of premixed CO_2-diluted oxy-H_2-CH_4 flames in a micromixer-like stabilized combustor. Equivalence ratio sweep test was carried out, combustor temperature profile was measured, and flame images were captured.

The stable combustion zone was established over ranges of fuel hydrogen fraction (HF: 25-70%) and equivalence ratio (ϕ: 0.1-1) at fixed oxidizer oxygen fraction (OF) of 30% and fixed jet velocity of 5.2 m/s. To understand the concept of flame extinction mechanism, the blowout limit was plotted within the HF-ϕ space over the contours of adiabatic flame temperature (AFT), combustor power density (PD), Reynolds number (Re) and pressure drop across the burner headend (Δp). The study revealed some valuable conclusions regarding micromixer burners' operability under H_2-enriched oxy-combustion conditions for gas-turbine applications. Hydrogen addition widens the stable combustion zone by extending the blowout limit into the leaner zone. The blowout limit coincides with a contour of constant Δp, indicating the existence of a strong correlation between flame stability and the pressure difference across burner headend at constant jet velocity. A relative correlation was also found to exist with Re.

The combustor blows out at constant burning velocity and Damkohler number. However, no correlation existed between the blowout limit and AFT or PD. The stabilizing effect of hydrogen is proven a purely reaction-kinetics effect and not attributed to hotter flames. As the HF increases, the flamelets in the primary reaction zone become shorter and more robust, while the flame plume (secondary reaction zone) becomes brighter and more intense. Flame structure was also analyzed at constant Δp, in light of the blowout-limit trend, and it was found that the effect of ϕ clearly overtakes that of HF; higher ϕ results in hotter, brighter flames (higher AFT), despite the reduction in HF.

The temperature readings were used as validation for the numerical work.

Numerical studies using Large-eddy simulation (LES) were performed as well to predict the structure, emission, and combustion characteristics of turbulent premixed $H_2/CH_4/O_2/CO_2$ flame for HF=10-50%, at a fixed jet velocity of 5.2 m/s, stoichiometric condition (*Ø=1) and OF=30%*. Thin flame-front topology model, non-chemical equilibrium-presumed PDF approach, and Zimont turbulent flame speed model were used for combustion modeling. The OH contour plots showed that flame length becomes shorter and more attached to the burner as HF increases from 10-50% This is due to the faster consumption rate of the fuel mixture and heightened vorticity within the hole spacing. Hydrogen addition of 50% by volume caused a 38% reduction in flame thickness and a 193.7% increase in Damköhler number (Da) due to increased rates of chemical reactions. The Karlovitz number (Ka) decreased by 20.6% and 66.9%, with 10% and 50%, respectively. These imply that the flame becomes thinner and more embedded in the small eddies such that small eddies cannot penetrate the flame's inner layers. Hence, the reactions in the cases studied are controlled by the laminar burning rate. CO emission increased from 33.3 ppm to 364.2 ppm for hydrogen enrichment values of 10 and 50% by volume, respectively. This is due to the superior competition of CO_2 for H radicals to yield more CO and possible decomposition of CO_2 at high temperatures prevalent in the combustor.

7.2 Recommendations

1. In this study, the experimental and numerical investigation of oxy-fuel combustion in multi-hole burner combustors has been conducted at fixed mixture inlet velocity, atmospheric pressure, and room temperature—effects of inlet velocity, high pressure, and preheating on multi-hole stabilized hydrogen-enriched oxy-methane flames should be investigated.
2. The numerical model validated with experimental data and employed for the numerical study is based on a thin flamelet combustion model. Robust combustion models such as composition -Transport-PDF, Flamelet Generated Manifold can be explored for more accurate results.
3. Laser diagnostic tools such as 3D-PIV, PLIF can be deployed to measure velocity components, species concentrations, and temperature inside the combustor for detailed flame characterization.
4. Hydrogen-enriched methane flame has been considered in this study. Combustion of other fuels such as compressed natural gas (CNG), propane, syngas, and biomass should be studied to ascertain the fuel flexibility characteristics of multi-hole burners for gas turbine applications.
5. Numerical study of the effects of burner geometry in terms of hole spacing, hole pattern and hole sized on the characteristics of multi-hole stabilized turbulent oxy-flame can be studied.
6. Economic analysis of the micromixer gas turbine combustor operating on premixed oxy-fuel combustion should be investigated.

REFERENCES

[1] IEA, World Energy Statistics 2019, IEA, Paris. (2019). https://www.iea.org/reports/world-energy-statistics-2019.

[2] World Resources Institute, Climate Analysis Indicators Tool, 2017.

[3] IEA, Key World Energy Statistics, IEA, Paris. (2020). https://www.iea.org/reports/key-world-energy-statistics-2020.

[4] S. Nader, Paths to a Low-Carbon Economy-The Masdar Example., Energy Procedia. 1 (2009) 3951–3958. https://doi.org/http://dx.doi.org/10.1016/j.egypro.2009.02.199.

[5] J. Goldemberg, The promise of clean energy, Energy Policy. 34 (2006) 2185–2190. https://doi.org/10.1016/j.enpol.2005.03.009.

[6] L. Yildiz, Fossil Fuels, Compr. Energy Syst. 1 (2018) 521–567. https://doi.org/10.1016/B978-0-12-809597-3.00111-5.

[7] United States Environmental Protection, Inventory og U.S. Greenhouse Gas Emissions and Sinks: 1990-2018, 2020.

[8] M. Welch, B. Igoe M, Gas Turbine Fuel and Fuel Quality Requirements for use in Industrial Gas Turbine Combustion, in: Proc. Second Middle East Turbomach. Symp., Doha, Qatar, 2013.

[9] IPCC Fourth Assessment Report, Climate Change 2007, Clim. Chang., (Geneva, Switzerland), 2007.

[10] J. Rizza, L. Alvarez, M. V Gil, C. Pevida, J.J. Pis, F. Rubeira, Effect of oxy-fuel combustion with steam addition on coal ignition and burnout in an entrained flow, Energy. 36 (2011) 5314–9.

[11] T. Wall, R. Gupta, B. Buhre, S. Khare, Oxy-fuel (O2/CO2, O2/RFG) technology for sequestration-ready CO2 and emission compliance, in: Proc. 30th Int. Tech. Conf. Coal Util. Fuel Syst., 2005: pp. 523–534.

[12] A.F. Ghoneim, Needs, resources and climate change: clean and efficient combustion technologies, Prog. Energy Combust. Sci. 37 (2011) 15–51.

[13] R.J. Allam, J.E. Fetvedt, B.A. Forrest, D.A. Freed, The oxy-fuel, supercritical CO2 allam cycle: new cycle developments to produce even lower-cost electricity from fossil fuels without atmospheric emissions, in: Proc. ASME Turbo Expo 2014 Turbine Tech. Conf. Expo., ASME, Düsseldorf, Germany, n.d.: p. 26952. https://doi.org/https://doi.org/10.1115/GT2014-26952.

[14] N. Perrin, C. Paufique, M. Leclerc, Latest performances and improvement perspective of Oxycombustion for carbon capture on coal power plants, Energy Procedia. 63 (2014) 524–531. https://doi.org/10.1016/j.egypro.2014.11.057.

[15] M.A. Nemitallah, M.A. Habib, Experiemntal and numerical investigations of an atmospheric diffusion oxy-combustion flame in a gas turbine model combustor, Appl. Energy. 111 (2013) 401–15.

[16] C.Y. Liu, G. Chen, N. Sipöcz, M. Assadi, X.S. Bai, Characteristics of oxy-fuel combustion in gas turbines, Appl. Energy. 89 (2012) 387–394. https://doi.org/10.1016/j.apenergy.2011.08.004.

[17] F. Liu, H. Guo, G.J. Smallwood, The chemical effect of CO2 replacement of N2 in air on the burning velocity of CH4 and H2 premixed flames, Combust. Flame Flame. 133 (2003). https://doi.org/10.1016/S0010-2180(03)00019-1.

[18] J. Oh, D. Noh, Laminar burning velocity of oxy-methane flames in atmospheric condition, Energy. 45 (2012) 669–675. https://doi.org/10.1016/j.energy.2012.07.027.

[19] A.A. Konnov, I. V. Dyakov, Measurement of propagation speeds in adiabatic cellular premixed flames of CH4 + O2 + CO2, Exp. Therm. Fluid Sci. 29 (2005) 901–907. https://doi.org/10.1016/j.expthermflusci.2005.01.005.

[20] T. Nozaki, S. Takano, T. Kiga, Analysis of the flame formed during oxidation of pulverised coal by an O2-CO2 mixture, Energy. 22 (1997) 199–205.

[21] A. Amato, B. Hudak, P. D'Souza, P. D'Carlo, D. Noble, D. Scarborough, J. Seitzman, T. Lieuwen, Measurements and analysis of CO and O2 emissions in CH 4/CO2/O2 flames, Proc. Combust. Inst. 33 (2011) 3399–3405. https://doi.org/10.1016/j.proci.2010.07.015.

[22] I.A. Ramadan, A.H. Ibrahim, T.W. Abou-Arab, S.S. Rashwan, M.A. Nemitallah, M.A. Habib, Effects of oxidizer flexibility and bluff-body blockage ratio on flammability limits of diffusion flames, Appl. Energy. 178 (2016). https://doi.org/10.1016/j.apenergy.2016.06.009.

[23] M.A. Nemitallah, S.S. Rashwan, I.B. Mansir, A.A. Abdelhafez, M.A. Habib, Review of Novel Combustion Techniques for Clean Power Production in Gas Turbines, Energy Fuels. 32 (2018) 979–1004. https://doi.org/https://doi.org/10.1021/acs.energyfuels.7b03607.

[24] S.S. Rashwan, A.H. Ibrahim, T.W. Abou-Arab, M.A. Nemitallah, M.A. Habib, Experimental investigation of partially premixed methane-air and methane-oxygen flames stabilized over a perforated-plate burner, Appl. Energy. 169 (2016) 126–137. https://doi.org/10.1016/j.apenergy.2016.02.047.

[25] F. Gong, Y. Huang, X. Huang, Size effect on the flame base locations after V-gutters for premixed flames, Int. J. Heat Mass Transf. 82 (2015) 406–418. https://doi.org/10.1016/j.ijheatmasstransfer.2014.11.031.

[26] E. V Jithin, V.R. Kishore, R.J. Varghese, Three-Dimensional Simulations of Steady Perforated-Plate Stabilized Propane − Air Premixed Flames, (2014). https://doi.org/10.1021/ef401903y.

[27] B. Roy Chowdhury, B.M. Cetegen, Effects of fuel properties and free stream turbulence on characteristics of bluff-body stabilized flames, Combust. Flame. 194 (2018) 206–222. https://doi.org/10.1016/j.combustflame.2018.04.027.

[28] B.A. Imteyaz, M.A. Nemitallah, A.A. Abdelhafez, M.A. Habib, Combustion behavior and stability map of hydrogen-enriched oxy-methane premixed flames in a model gas turbine combustor, Int. J. Hydrogen Energy. 43 (2018) 16652–16666. https://doi.org/10.1016/j.ijhydene.2018.07.087.

[29] S. Taamallah, K. Vogiatzaki, F.M. Alzahrani, E.M.A. Mokheimer, M.A. Habib, A.F. Ghoniem, Fuel flexibility , stability and emissions in premixed hydrogen-rich gas turbine combustion : Technology , fundamentals , and numerical simulations, Appl. Energy. 154 (2015) 1020–1047. https://doi.org/10.1016/j.apenergy.2015.04.044.

[30] A.A. Subash, R. Collin, M. Alden, A. Kundu, J. Klingmann, Investigation of hydrogen enriched methane flame in a dry low emission Industrial prototype burner at atmospheric pressure conditions, Proc. ASME Turbo Expo. 4A-2017 (2017). https://doi.org/10.1115/GT201763924.

[31] IEA, The Future of Hydrogen, IEA. (2019). www.iea.org/reports/the-future-of-hydrogen (accessed July 3, 2021).

[32] J. Wang, Z. Huang, C. Tang, H. Miao, X. Wang, Numerical study of the effect of hydrogen addition on methane-air mixtures combustion, Int. J. Hydrogen Energy. 34 (2009) 1084–1096.

[33] H.S. Kim, V.K. Arghode, A.K. Gupta, Flame characteristics of hydrogen-enriched methane-air premixed swirling flames, Int. J. Hydrogen Energy. 34 (2009) 1063–1073. https://doi.org/10.1016/j.ijhydene.2008.10.035.

[34] S. Abdelwahid, M. Nemitallah, B. Imteyaz, A. Abdelhafez, E ff ects of H 2 Enrichment and Inlet Velocity on Stability Limits and Shape of CH 4 / H 2 − O 2 / CO 2 Flames in a Premixed Swirl Combustor, Energy & Fuels. 32 (2018) 9916–9925. https://doi.org/10.1021/acs.energyfuels.8b01958.

[35] S.R. Bell, M. Gupta, Extension of the lean operating limit for natural gas fueling of a spark ignited engine using hydrogen blending, Combust. Sci. Technol. 123 (1997) 23–48. https://doi.org/10.1080/00102209708935620.

[36] S.J. Shanbhogue, Y.S. Sanusi, S. Taamallah, M.A. Habib, E.M.A. Mokheimer, A.F. Ghoniem, Flame macrostructures, combustion instability and extinction strain scaling in swirl-stabilized premixed CH4/H2 combustion, Combust. Flame. 163 (2016) 494–507. https://doi.org/10.1016/j.combustflame.2015.10.026.

[37] F. Halter, C. Chauveau, I. Gökalp, Characterization of the effects of hydrogen addition in lean premixed methane/air flames, Int. J. Hydrogen Energy. 32 (2007) 2585–2592. https://doi.org/https://doi.org/10.1016/j.ijhydene.2006.11.033.

[38] F. Cozzi, A. Coghe, Behavior of hydrogen-enriched non-premixed swirled natural gas flames, Int. J. Hydrogen Energy. 31 (2006) 669–677. https://doi.org/10.1016/j.ijhydene.2005.05.013.

[39] T. Tahtouh, F. Halter, E. Samson, C. Mounaïm-Rousselle, Effects of hydrogen addition and nitrogen dilution on the laminar flame characteristics of premixed methane-air flames, Int. J. Hydrogen Energy. 34 (2009) 8329–8338. https://doi.org/10.1016/j.ijhydene.2009.07.071.

[40] M.H. du Toit, A. V. Avdeenkov, D. Bessarabov, Reviewing H2 Combustion: A Case Study for Non-Fuel-Cell Power Systems and Safety in Passive Autocatalytic Recombiners, Energy Fuels. 32 (2018) 6401–6422.

[41] H.H.W. Funke, N. Beckmann, J. Keinz, S. Abanteriba, Numerical and Experimental Evaluation of a Dual-Fuel Dry-Low-NOx Micromix Combustor for Industrial Gas Turbine Applications, J. Therm. Sci. Eng. Appl. 11 (2019) 011015.

[42] T. Asai, S. Dodo, M. Karishuku, N. Yagi, Y. Akiyama, A. Hayashi, Performance of Multiple-Injection Dry Low-NOx Commbustors on Hydrogen-Rich Syngas Fuel in an IGCC Pilot Plant, J. Eng. Gas Turbines Power. 137 (2015) 091504.

[43] W.D. York, W.S. Ziminsky, Development and Testing of a Low NO x Hydrogen Combustion System for Heavy-Duty Gas Turbines, J. Eng. Gas Turbines Power. 135 (2013) 1–8. https://doi.org/10.1115/1.4007733.

[44] P.H. LEE, S.S. HWANG, Formation of Lean Premixed Surface Flame Using Porous Baffle Plate and Flame Holder, J. Therm. Sci. Technol. 8 (2013) 178–189. https://doi.org/10.1299/jtst.8.178.

[45] M.A. Habib, H.M. Badr, S.F. Ahmed, R. Ben-Mansour, K. Mezghani, S. Imashuku, G.J. la O', Y. Shao-Horn, N.D. Mancini, A. Mitsos, P. Kirchen, A.F. Ghoneim, A review of recent developments in carbon capture utilizing oxy-fuel combustion in conventional and ion transport membrane systems, Int. J. Energy Res. 35 (2011) 741–764. https://doi.org/10.1002/er.1798.

[46] H. Watanabe, S.J. Shanbhogue, A.F. Ghoneim, Impact of Equivalence Ratio on the Macrostructure of Premixed Swirling CH 4 /Air and CH 4 /O 2 /CO 2 Flames., in: Vol. 4B Combust. Fuels Emiss., ASME International, 2015. https://doi.org/10.1115/gt2015-43224.

[47] M.A. Habib, H.M. Badr, S.F. Ahmed, K. Mezghani, S. Imashuku, A review of recent developments in carbon capture utilizing oxy-fuel combustion in conventional and ion transport membrane systems, Int. J. Energy Res. 35 (2011) 741–764. https://doi.org/10.1002/er.

[48] S.S. Rashwan, A.H. Ibrahim, T.W. Abou-arab, M.A. Nemitallah, M.A. Habib, Experimental study of atmospheric partially premixed oxy-combustion fl ames anchored over a perforated plate burner, Energy. 122 (2017) 159–167. https://doi.org/10.1016/j.energy.2017.01.086.

[49] Mixture Properties n.d., (n.d.). http://navier.engr.colostate.edu/dandy/code/code-2/.

[50] M. Ditaranto, J. Hals, Combustion instabilities in sudden expansion oxy-fuel flames, Combust. Flame. 146 (2006) 493–512. https://doi.org/10.1016/j.combustflame.2006.04.015.

[51] M. Ditaranto, R. Anantharaman, T. Weydahl, Performance and NOx emissions of refinery fired heaters retrofitted to hydrogen combustion, Energy Procedia. 37 (2013) 7214–7220. https://doi.org/10.1016/j.egypro.2013.06.659.

[52] H. Liu, R. Zailani, B.M. Gibbs, Comparison of pulverized coal combustion in air and in mixtures of O2/CO2, Fuel. 84 (2005) 833–40.

[53] K. Andersson, R. Johansson, S. Hjartstam, F. Johnsson, B. Leckner, Radiation intensity of lignite-fired oxy-fuel flames, Exp. Therm. Fluid Sci. 33 (2008) 67–76.

[54] Y. Song, C. Zou, Y. He, C. Zheng, The chemical mechanism of the effect of CO2 on the temp in methane oxy-fuel combustion, Int. J. Heat Mass Transf. 86 (2015) 622–8.

[55] K. Andersson, F. Johnsson, Flame and radiation charcteristics of gas-fired O2/CO2 combustion, Fuel. 86 (2007) 656–68. https://doi.org/http://doi.org/10.1016/j.fuel.2006.08.013.

[56] B. Imteyaz, M.A. Habib, R. Ben-Mansour, The characteristics of oxycombustion of liquid fuel in a typical water-tube boiler, Energy & Fuels. (2017). https://doi.org/https://doi.org/10.1021/acs.energyfuels.7b00489.

[57] J. Wang, Z. Huang, C. Tang, H. Miao, X. Wang, Numerical study of the effect of hydrogen addition on methane-air mixtures combustion, Int. J. Hydrogen Energy. 34 (2009) 1084–1096. https://doi.org/10.1016/j.ijhydene.2008.11.010.

[58] X. Hu, Q. Yu, J. Liu, N. Sun, Investigation of laminar flame speeds of CH4/O2/CO2 mixtures at ordinary pressure and kinetic simulation, Energy. 70 (2014) 626–634. https://doi.org/DOI: 10.1016/j.energy.2014.04.029.

[59] W. JERZAK, M. Kuźnia, Experimental study of impact of swirl number as well as oxygen and carbon dioxide content in natural gas combustion air on flame flashback and blow-off, J. Nat. Gas Sci. Eng. (2016) 46–54. https://doi.org/10.1016/j.jngse.2015.12.054.

[60] M. Ball, M. Wietschel, The future of hydrogen – opportunities and challenges 5, Int. J. Hydrogen Energy. 34 (2009) 615–627. https://doi.org/10.1016/j.ijhydene.2008.11.014.

[61] P.P. Edwards, V.L. Kuznetsov, W.I.F. David, N.P. Brandon, Hydrogen and fuel cells : Towards a sustainable energy future, Energy Policy. 36 (2020) 4356–4362. https://doi.org/10.1016/j.enpol.2008.09.036.

[62] F. Halter, C. Chauveau, I. Gökalp, Characterization of the effects of hydrogen addition in premixed methane / air flames, Int. J. Hydrogen Energy. 32 (2007) 2585–2592. https://doi.org/10.1016/j.ijhydene.2006.11.033.

[63] T. Boushaki, Y. Dhue, L. Selle, B. Ferret, T. Poinsot, Effects of hydrogen and steam addition on laminar burning velocity of methane e air premixed flame : Experimental and numerical analysis, Int. J. Hydrogen Energy. 37 (2012) 0–10. https://doi.org/10.1016/j.ijhydene.2012.03.037.

[64] E. Hu, Z. Huang, J. He, C. Jin, J. Zheng, Experimental and numerical study on laminar burning characteristics of premixed methane – hydrogen – air flames, Int. J. Hydrogen Energy. 34 (2009) 4876–4888. https://doi.org/10.1016/j.ijhydene.2009.03.058.

[65] V. Di Sarli, A. Di Benedetto, Laminar burning velocity of hydrogen – methane / air premixed flames, Int. J. Hydrogen Energy. 32 (2007) 637–646. https://doi.org/10.1016/j.ijhydene.2006.05.016.

[66] C. Tang, Z. Huang, C. Jin, J. He, J. Wang, X. Wang, H. Miao, Laminar burning velocities and combustion characteristics of propane – hydrogen – air premixed flames, Int. J. Hydrogen Energy. 33 (2008) 4906–4914. https://doi.org/10.1016/j.ijhydene.2008.06.063.

[67] R. Sankaran, H.G. Im, H.G. Im, Effects of Hydrogen addition on the Markstein Length and Flammability Limit of Stretched methane / air premixed flames, Combust. Sci. Technol. 178 (2006) 1585–1611. https://doi.org/10.1080/00102200500536217.

[68] M. Nakahara, H. Kido, Study on the Turbulent Burning Velocity of Hydrogen Mixtures Including Hydrocarbons, AIAA J. 46 (2008). https://doi.org/10.2514/1.23560.

[69] M. Zhang, J. Wang, Z. Huang, Turbulent flame structure characteristics of hydrogen enriched natural gas with CO 2 dilution, Int. J. Hydrogen Energy. 45 (2019) 20426–20435. https://doi.org/10.1016/j.ijhydene.2019.12.015.

[70] S. Daniele, P. Jansohn, J. Mantzaras, K. Boulouchos, Turbulent flame speed for syngas at gas turbine relevant conditions, Proc. Combust. Inst. 33 (2011) 2937–2944. https://doi.org/10.1016/j.proci.2010.05.057.

[71] E.R. Hawkes, J.H. Chen, Direct numerical simulation of hydrogen-enriched lean premixed methane – air flames, Combust. Flame. 138 (2004) 242–258. https://doi.org/10.1016/j.combustflame.2004.04.010.

[72] O. Tuncer, S. Acharya, J.H. Uhm, Dynamics , NO x and flashback characteristics of confined premixed hydrogen-enriched methane flames, Int. J. Hydrogen Energy. 34 (2009) 496–506. https://doi.org/10.1016/j.ijhydene.2008.09.075.

[73] S. Guo, J. Wang, W. Zhang, M. Zhang, Z. Huang, Effect of hydrogen enrichment on swirl / bluff-body lean premixed flame stabilization, Int. J. Hydrogen Energy. 45 (2020) 10906–10919. https://doi.org/10.1016/j.ijhydene.2020.02.020.

[74] M. Emadi, D. Karkow, T. Salameh, A. Gohil, A. Ratner, Flame structure changes resulting from hydrogen-enrichment and pressurization for low-swirl premixed methane-air flames, Int. J. Hydrogen Energy. 37 (2012) 10397–10404. https://doi.org/10.1016/j.ijhydene.2012.04.017.

[75] F. Cammarota, A. Di Benedetto, V. Di Sarli, E. Salzano, G. Russo, Journal of Loss Prevention in the Process Industries Combined effects of initial pressure and turbulence on explosions of hydrogen-enriched methane / air mixtures, J. Loss Prev. Process Ind. 22 (2009) 607–613. https://doi.org/10.1016/j.jlp.2009.05.001.

[76] R.W. Schefer, D.M. Wicksall, A.K. Agrawal, Combustion of Hydrogen-enriched methane in a lean premixed swirl-stabilized burner, Proc. Combust. Inst. 29 (2002) 843–851.

[77] J.L. Gauducheau, B. Denet, G. Searby, A Numerical Study of Lean CH 4 / H 2 / Air Premixed Flames at High Pressure A Numerical Study of Lean CH 4 / H 2 / Air Premixed Flames at High Pressure, Combust. Sci. Technol. 137 (1998) 81–99. https://doi.org/10.1080/00102209808952046.

[78] F.H. V Coppens, J. De Ruyck, A.A. Konnov, Effects of hydrogen enrichment on adiabatic burning velocity and NO formation in methane + air flames, Exp. Therm. Fluid Sci. 31 (2007) 437–444. https://doi.org/10.1016/j.expthermflusci.2006.04.012.

[79] A.E.E. Khalil, A.K. Gupta, Hydrogen addition effects on high intensity distributed combustion, Appl. Energy. 104 (2013) 71–78. https://doi.org/10.1016/j.apenergy.2012.11.004.

[80] V.K. Arghode, A.K. Gupta, Hydrogen addition effects on methane e air colorless distributed combustion flames, Int. J. Hydrogen Energy. 36 (2011) 6292–6302. https://doi.org/10.1016/j.ijhydene.2011.02.028.

[81] M. Nemitallah, B. Imteyaz, A. Abdelhafez, M.A. Habib, Experimental and computational study on stability characteristics of hydrogen-enriched oxy-methane premixed flames, Appl. Energy. 250 (2019). https://doi.org/10.1016/j.apenergy.2019.05.087.

[82] Q. S., B. A. H., B. T., Methane Air Equivalence Ratio E ect on Premixed Turbulent Low Swirl Stabilized Flame, ACTA Phys. Pol. A. 126 (2014). https://doi.org/10.12693/APhysPolA.126.717.

[83] Y.A. Eldrainy, K.M. Saqr, S.H. Aly, M.N. Jaafar, CFD insight of the flow dynamics in a novel swirler for gas turbine combustors, Int. Commun. Heat Mass Transf. 36 (2009) 936–941.

[84] Y. Huang, H.-G. Sung, S.-Y. Hsieh, V. Yang, Large-Eddy Simulation of Combustion Dynamics of Lean-Premixed Swirl-Stabilized Combustor, J. Propuls. Power. 19 (2003) 782–794.

[85] A.H. Lefebvre, D.R. Ballal, Gas Turbine Combustion: Alternative Fuels and Emissions, THIRD EDIT, CRC Press, Taylor & Francis Group, Boca Raton, 2010.

[86] H.M. Abdelgayed, W.A. Abdelghaffar, K. El Shorbagy, Main flow characteristics in a lean premixed swirl stabilized gas turbine combustor – Numerical computations, Am. J. Sci. Ind. Res. 4 (2013) 123–136. https://doi.org/10.5251/ajsir.2013.4.1.123.136.

[87] K. Thomas, L. Tay-wo-chong, Z. Mathieu, A. Huber, P. Wolfgang, Modeling The Effect of Heat Loss on Flame, in: Int. Conf. Jets, Wakes Seperated Flows, ICJWSF, 2008.

[88] L. Tay-wo-chong, M. Zellhuber, T. Komarek, H.G. Im, W. Polifke, Combined Influence of Strain and Heat Loss on Turbulent Premixed Flame Stabilization, Flow, Turbul. Combust. 97 (2016) 263–294. https://doi.org/10.1007/s10494-015-9679-0.

[89] O. Tuncer, The Effect of Hydrogen Enrichment of Methane Fuel on Flame Stability and Emissions, in: Int. Conf. Renew. Energy Res. Appl., Madrid, Spain, 2013: pp. 103–108. https://doi.org/10.1109/ICRERA.2013.6749734.

[90] Y. Huang, V. Yang, Dynamics and stability of lean-premixed swirl-stabilized combustion, Prog. Energy Combust. Sci. 35 (2009) 293–364. https://doi.org/10.1016/j.pecs.2009.01.002.

[91] H. Soltanian, M.Z. Targhi, H. Pasdarshahri, Chemiluminescence usage in finding optimum operating range of multi-hole burners, Energy. 180 (2019) 398–404. https://doi.org/10.1016/j.energy.2019.05.104.

[92] H.H.W. Funke, S. Boerner, W. Krebs, E. Wolf, Experimental Characterization of Low Nox Micromix Prototype Combustors for Industrial Gas Turbine Applications, Proc. ASME Turbo Expo. 2 (2011) 343–353.

[93] B. Hollon, E. Steinthrorsson, A. Mansour, V. McDonell, H. Lee, Ultra-Low Emission Hydrogen/Syngas Combustion With a 1.3 MW Injector Using a Micro-Mixing Lean-Premix System, Proc. ASME Turbo Expo. 2 (2011) 827–834.

[94] D. Durox, T. Schuller, N. Noiray, S. Candel, Experimental analysis of nonlinear flame transfer functions for different flame geometries, Proc. Combust. Inst. 32 I (2009) 1391–1398. https://doi.org/10.1016/j.proci.2008.06.204.

[95] K.S. Kedia, A.F. Ghoniem, Mechanisms of stabilization and blowoff of a premixed flame downstream of a heat-conducting perforated plate, Combust. Flame. 159 (2012) 1055–1069. https://doi.org/10.1016/j.combustflame.2011.10.014.

[96] R.W. Schefer, Reduced Turbine Emissions Using Hydrogen-Enriched Fuels, Proc. 2002 DOE Hydrog. Progr. Rev. NREL/CP-61 (2002) 1–16.

[97] H.H. Funke, J. Dickhoff, J. Keinz, A.H. Ayed, A. Parente, P. Hendrick, Experimental and Numerical Study of the Micromix Combustion Principle Applied for Hydrogen and Hydrogen- Rich Syngas as Fuel with Increased Energy Density for Industrial Gas Turbine Applications, Energy Procedia. 61 (2014) 1736–1739. https://doi.org/10.1016/j.egypro.2014.12.201.

[98] S. Boerner, H.H. Funke, P. Hendrick, E. Recker, Development and Integration of a Scalable Low NOx Combustion Chamber for a Hydrogen-Fueled Aerogas Turbine, Prog. Propuls. Phys. 4. 4 (2013) 357–372. https://doi.org/10.1051/eucass/201304.

[99] A.M. Elkady, J. Herbon, D.M. Kalitan, G. Leonard, R. Akula, H. Karim, M. Hadley, Gas Turbine Emission Characteristics in Perfectly Premixed Combustion, J. Eng. Gas Turbines Power. 134 (2012) 1–7. https://doi.org/10.1115/1.4006058.

[100] M.H. Saberi Moghaddam, M. Saei Moghaddam, M. Khorramdel, Numerical study of geometric parameters effecting temperature and thermal efficiency in a premix multi-hole flat flame burner, Energy. 125 (2017) 654–662. https://doi.org/10.1016/j.energy.2017.02.116.

[101] A.S. AlAdawy, J.G. Lee, B. Abdelnabi, Effect of turbulence on NOxemission in a lean perfectly-premixed combustor, Fuel. 208 (2017) 160–167. https://doi.org/10.1016/j.fuel.2017.06.109.

[102] E. V. Jithin, V.R. Kishore, R.J. Varghese, Three-dimensional simulations of steady perforated-plate stabilized propane-air premixed flames, Energy and Fuels. 28 (2014) 5415–5425. https://doi.org/10.1021/ef401903y.

[103] J. Edacheri Veetil, C. V. Rajith, R.K. Velamati, Numerical simulations of steady perforated-plate stabilized Syngas air pre-mixed flames, Int. J. Hydrogen Energy. 41 (2016) 13747–13757. https://doi.org/10.1016/j.ijhydene.2016.06.120.

[104] A. Jatoliya, B. Pandian, V. Raghavan, Experimental Study of Pre-mixed Flames on a Multi-Hole Matrix Burner, Int. J. Integr. Eng. 4 (2012) 1–5.

[105] H.J. Kim, W. Choi, S.H. Bae, H.D. Shin, Characteristics of a Multi-jet Burner in Oxy-Liquefied Petroleum Gas (LPG) Flames, Energy & Fuels. 23 (2009) 1456–1463.

[106] K.S. Kedia, A.F. Ghoniem, An analytical model for the prediction of the dynamic response of premixed flames stabilized on a heat-conducting perforated plate, Proc. Combust. Inst. 34 (2013) 921–928.

[107] H. Biglarian, M. Khosravy-el-hosseini, Q. Dorostihassankiadeh, Optimization of Fluid Flow Pattern in a Perforated Porous Burner, 3 (2013) 166–177.

[108] H.M. Altay, K.S. Kedia, R.L. Speth, A.F. Ghoniem, Two-dimensional simulations of steady perforated-plate stabilized premixed flames, Combust. Theory Model. 14 (2010) 125–154. https://doi.org/10.1080/13647831003660859.

[109] S. Dodo, T. Asai, H. Koizumi, H. Takahashi, S. Yoshida, H. Inoue, Combustion characteristics of a multiple-injection combustor for a dry low-NOx combustion of hydrogen-rich fuels under medium pressure, Proc. ASME Turbo Expo. 2 (2011) 467–476.

[110] T. Asai, S. Dodo, H. Koizumi, H. Takahashi, S. Yoshida, H. Inoue, Effects of Multiple-Injection-Burner Configurations on Combustion Characteristics for Dry Low-NOx Combustion of Hydrogen-Rich Fuels, Proc. ASME Turbo Expo. 2 (2011) 311–320.

[111] J.M.N. Rodrigues, E.C. Fernandes, Stability Analysis and Flow Characterization of Multi-Perforated Plate Premixed Burners, in: 17th Int. Symp. Appl. Laser Tech. to Fluid Mech., 2014: pp. 7–10.

[112] L. Zhou, D. Gao, J. Zhao, H. Wei, X. Zhang, Z. Xu, R. Chen, Turbulent Flame Propagation with Pressure Oscillation in the End Gas Regionof Confined Combustion Chamber Equipped with Different Perforated Plates, Combust. Flame. 191 (2018) 453–467.

[113] S. Oh, Y. Shin, Y. Kim, Stabilization Effects of Perforated Plates on the Combustion Instability in a Lean-premixed Combustor, Appl. Therm. Eng. 107 (2016) 508–515.

[114] V. Raghvan, Experimental study of pre-mixed flames on a multi-hole matrix burner, Int. J Integr Eng. 4 (2012).

[115] S.S. Rashwan, M.A. Habib, Experimental study of atmospheric partially premixed oxy-combustion flames anchored over a perforated plate burner, Energy. 122 (2017) 159–167.

[116] A.H. Ibrahim, S.Y. Kamal, T.W. Abou-arab, M.A. Nemitallah, M.A. Habib, H. Kayed, Operability of Fuel / Oxidizer-Flexible Combustor Holding Hydrogen- Enriched Partially Premixed Oxy-Flames Stabilized over a Perforated Plate Burner, Energy & Fuels. 34 (2020) 8653–8665. https://doi.org/10.1021/acs.energyfuels.0c01407.

[117] M. Hussain, A. Abdelhafez, M.A. Nemitallah, A.A. Araoye, R. Ben-Mansour, M.A. Habib, A highly diluted oxy-fuel micromixer combustor with hydrogen enrichment for enhancing turndown in gas turbines, Appl. Energy. 279 (2020) 115818. https://doi.org/10.1016/j.apenergy.2020.115818.

[118] M. Aliyu, A. Abdelhafez, S.A.M. Said, M.A. Habib, M.A. Nemitallah, I.B. Mansir, Characteristics of Oxyfuel Combustion in Lean-Premixed Multihole Burners, Energy and Fuels. 33 (2019) 11948–11958. https://doi.org/10.1021/acs.energyfuels.9b02821.

[119] W. Ehrfeld, V. Hessel, H. Lowe, Microreactors: New Technology for Modern Chemistry, Wiley, Weinheim, 2000.

[120] Y.K. Lee, J. Deval, P. Tabeling, C.M. Ho, Chaotic Mixing in Electrokinetically and Pressure Driven Micro Flows, in: Proc. 14th IEEE Work. MEMS, Interlaken Switz., 2001: pp. 483–486.

[121] M. Yi, H.H. Bau, H. Hu, A Peristaltic Meso-Scale Mixer, in: Proc. of MEMS, ASME, IMECE Conf., 2000: pp. 367–374.

[122] W. Ehrfeld, K. Golbig, V. Hessel, H. Lo, T. Richter, Characterization of Mixing in Micromixers by a Test Reaction : Single Mixing Units and Mixer Arrays, (1999) 1075–1082. https://doi.org/10.1021/ie980128d.

[123] J. Branebjerg, P. Gravenson, J.P. Krog, R. Nielsen, Fast Mixing by Lamination, in: MEMS 96, San Diego, CA, 1996: pp. 441–446.

[124] M. Hoffmann, M. Schlüter, N. Räbiger, Experimental investigation of liquid-liquid mixing in T-shaped micro-mixers using μ-LIF and μ-PIV, Chem. Eng. Sci. 61 (2006) 2968–2976. https://doi.org/10.1016/j.ces.2005.11.029.

[125] S.H. Wong, M.C.L. Ward, C.W. Wharton, Micro T-mixer as a rapid mixing microimixer, Sensors Actuators B. (2004) 359–379.

[126] S.P. Vanka, G. Luo, C.M. Winkler, Numerical study of scalar mixing in curved channels at low Reynolds numbers, AIChE J. 50 (2004) 2359–2368. https://doi.org/10.1002/aic.10196.

[127] N. Docquier, S. Candel, Combustion control and sensors, Prog. Energy Combust. Sci. 28 (2002) 107–50.

[128] T.H. Zhang, F.G. Liu, X.Y. You, Optimization of gas mixing system of premixed burner based on CFD analysis, Energy Convers. Manag. 85 (2014) 131–139. https://doi.org/10.1016/j.enconman.2014.05.055.

[129] F. Liu, X. You, Q. Wang, R. Zhang, On optimal design and experimental validation of household appliance burner of low pollutant emission., Energy Convers. Manag. 76 (2013) 837–45.

[130] L. Li, Z. Yuan, Y. Xiang, A. Fan, Numerical investigation on mixing performance and diffusion combustion characteristics of H2 and air in planar micro-combustor, Int. J. Hydrogen Energy. 43 (2018) 12491–12498. https://doi.org/10.1016/j.ijhydene.2018.04.194.

[131] E. Roj, M. Dmoch, CFD study of gas mixing efficiency and comparisons with experimental data, Comput. Aided Chem. Eng. 24 (2007) 509–514. https://doi.org/10.1016/S1570-7946(07)80108-8.

[132] J.G. Lee, K. Kim, D.A. Santavicca, Effect of Injection Location on the Effectiveness of An Active Control System Using Secondary Fuel Injection, Proc. Combust. Inst. 28 (2000) 739–746.

[133] A.H. Ayed, K. Kusterer, H.H.-W. Funke, C. Striegan, D. Bohn, Experimental and numerical investigations of the DLN hydrogen micromix combustion chamber of an industrial gas turbine, Propuls. Power Res. 4 (2015) 123–140.

[134] A.H. Ayed, K. Kusterer, J. Dickhoff, H.H. Funke, J. Keinz, D. Bohn, Experimental and numerical investigations of the dry-low-NO x (DLN) syngas micromix combustion principle, Propuls. Power Res. (2017). https://doi.org/10.1016/j.jppr.2017.11.003.

[135] H. Lee, S. Hernandez, V. McDonell, E. Steinthorsson, A. Mansour, B. Hollon, Development of Flashback Resistant Low-Emission Micro-Mixing Fuel Injector for 100% Hydrogen and Syngas Fuels, ASME Turbo Expo. GT2009-595 (2009) 411–419.

[136] H.H.W. Funke, S. Boerner, J. Keinz, K. Kusterer, D. Kroniger, J. Kitajima, M. Kazari, A. Horikawa, Numerical and Experimental Characterization of Low NOx Micromix Combustion Principle for Industrial Hydrogen Gas Turbine Applications, ASME Turbo Expo. GT2012-694 (2012) 1069–1079.

[137] V. Raman, H. Pitsch, Large-Eddy Simulation of a bluff_body-stabilized non-premixed flame using a recursive filter_refinement procedure, Combust. Flame. 142 (2005) 329–347.

[138] A.L. Nichkoohi, A.M. Tousi, Numerical investigation of high pressure and high Reynolds diffusion flame using Large Eddy Simulation, J. Therm. Sci. 23 (2014) 412–421. https://doi.org/10.1007/s11630-014-0724-4.

[139] W. Malalasekera, S.S. Ibrahim, A.R. Masri, S.R. Gubba, S. Sadasivuni, Experience with the large eddy simulation (LES) technique for the modeling of premixed and non-premixed combustion, Heat Transf. Eng. 34 (2013) 1156–1170. https://doi.org/10.1080/01457632.2013.776876.

[140] A.Y. Snegirev, A.S. Frolov, The Large Eddy Simulation of a Turbulent Diffusion Flame, High Temp. 49 (2011) 690–703.

[141] A. Giusti, E. Mastorakos, Turbulent Combustion Modelling and Experiments: Recent Trends and Developments, Flow, Turbul. Combust. 103 (2019) 847–869. https://doi.org/10.1007/s10494-019-00072-6.

[142] J.R. Edwards, J.A. Boles, R.A. Baurle, Large-eddy/Reynolds-averaged Navier–Stokes simula_tion of a supersonic reacting wall jet, Combust. Flame. 159 (2012) 1127–1138.

[143] Gaurav Kewlani, Large Eddy Simulations of Premixed Turbulent Flame Dynamics: Combustion Modeling, Validation & Analysis, Massachusetts Institute of Technology, Cambridge, 2014.

[144] M.M. Salehi, W.K. Bushe, N. Shahbazian, C.P.T. Groth, Modified laminar flamelet presumed probability density function for LES of premixed turbulent combustion, Proc. Combust. Inst. 34 (2013) 1203–1211. https://doi.org/10.1016/j.proci.2012.06.177.

[145] U. Allauddin, M. Pfitzner, Development of a RANS Premixed Turbulent Combustion Model Based on the Algebraic Flame Surface Density Concept, J. Eng. Gas Turbines Power. 141 (2019). https://doi.org/10.1115/1.4041308.

[146] C.A. Velez, S.M. Martin, S.S. Vasu, Reacting Unsteady Reynolds-Averaged Navier – Stokes with the Tabulated Premixed Conditional Moment Closure Method, J. Press. Vessel Technol. 33 (n.d.). https://doi.org/10.2514/1.B35741.

[147] S.. Pope, PDF Methods for turbulent reacting flows, Prog. Energy Combust. Sci. 11 (1985) 119–192.

[148] A. Klimenko, R. Bilger, Conditional moment closure for turbulent combustion, Prog. Energy Combust. Sci. 25 (1999) 595–687.

[149] A. Parente, M.R. Malik, F. Contino, A. Cuoci, B.B. Dally, Extension of the Eddy Dissipation Concept for turbulence/chemistry interactions to MILD combustion, Fuel. 163 (2016) 98–111.

[150] D.B. Spalding, Mixing and chemical reaction in steady confined turbulent flames, Proc. Combust. Inst. 13 (1971) 649–657.

[151] F. Dupoirieux, A. Vincent, N. Bertier, A. Banh, Numerical simulation of a premixed CH4-air burner for comparison of RANS and LES methodologies, (2016).

[152] J. Bobren-diaz, S. Martin, B. Hitch, S. Vasu, E. Flight, R. Systems, C.F. Dynamics, S. Dissipation, T. Premixed, C. Moment, P.S. Reactor, R.P. Variable, S. Scientist, D. Beach, S. Member, S. Member, Assessment of Dodecane Turbulent-Chemistry Interactions Using Computational Fluid Dynamics II . Tabulated Premixed Conditional Moment Closure, in: 53rd AIA A/SAE/A SEE Jt. Propuls. Conf., 2017: pp. 1–13. https://doi.org/10.2514/6.2017-5081.

[153] A.Y. Klimenko, R.W. Bilger, Conditional Moment Closure for Turbulent Combustion, Prog. Eng. Combust. Sci. 25 (1999) 595–687.

[154] A.F. Sudarma, A. Al-Witry, M.H. Morsy, RANS Numerical Simulation of Lean Premixed Bluff body Stabilized Combustor : Comparison of Turbulence Models, J. Therm. Eng. 3 (2017) 1561–1573.

[155] W. Yang, J. Zhang, Simulation of swirl-stabilized turbulent partially premixed combustion, Numer. Heat Transf. Part A. 71 (2017) 189–201. https://doi.org/10.1080/10407782.2016.1257299.

[156] S. Brohez, C. Delvosalle, G. Marlair, A two-thermocouples probe for radiation corrections of measured temperatures in compartment fires, Fire Saf. J. 39 (2004) 399–411. https://doi.org/10.1016/j.firesaf.2004.03.002.

[157] A. Abdelhafez, S.S. Rashwan, M.A. Nemitallah, M.A. Habib, Stability map and shape of premixed CH 4 / O 2 / CO 2 fl ames in a model gas- turbine combustor, Appl. Energy. 215 (2018) 63–74. https://doi.org/10.1016/j.apenergy.2018.01.097.

[158] S. Taamallah, N.W. Chakroun, H. Watanabe, S.J. Shanbhogue, A.F. Ghoniem, On the characteristic flow and flame times for scaling oxy and air flame stabilization modes in premixed swirl combustion, Proc. Combust. Inst. 36 (2017) 3799–3807. https://doi.org/10.1016/j.proci.2016.07.022.

[159] H.S. Kwak, H.S. Uhm, Y.C. Hong, E.H. Choi, Disintegration of Carbon Dioxide Molecules in a Microwave Plasma Torch, Sci. Rep. 5 (2015) 1–13. https://doi.org/10.1038/srep18436.

[160] H.K. Kayadelen, Effect of natural gas components on its flame temperature, equilibrium combustion products and thermodynamic properties, J. Nat. Gas Sci. Eng. 45 (2017) 456–473. https://doi.org/10.1016/j.jngse.2017.05.023.

[161] R. Marsh, J. Runyon, A. Giles, S. Morris, D. Pugh, A. Valera-Medina, P. Bowen, Premixed methane oxycombustion in nitrogen and carbon dioxide atmospheres: Measurement of operating limits, flame location and emissions. Proceedings of the Combustion Institute, Proc. Combust. Inst. 36 (2017). https://doi.org/10.1016/j.proci.2016.06.057.

[162] M. Li, Y. Tong, M. Thern, J. Klingmann, Investigation of methane oxy-fuel combustion in a swirl-stabilised gas turbine model combustor, Energies. 10 (2017). https://doi.org/10.3390/en10050648.

[163] N.L. Carr, R. Kobayashi, D.B. Burrows, No Title, J. Pet. Technol. 6 (1954) 47–55.

[164] I. Zahmatkesh, H. Emdad, M.M. Alishahi, Two-fluid analysis of a gas mixing problem, Sci. Iran. 20 (2013) 162–171. https://doi.org/10.1016/j.scient.2012.12.017.

[165] H.A. McGee, Molecular Engineering, McGraw-Hill, New York, 1991.

[166] C.R. Wilke, No T, Chem. Eng. Prog. 46 (1950) 95–104.

[167] S. Chakraborty, N. Chakraborty, P. Kumar, P. Dutta, Studies on turbulent momentum, heat and species transport during binary alloy solidification in a top-cooled rectangular cavity, Int. J. Heat Mass Transf. 46 (2003) 1115–1137. https://doi.org/10.1016/S0017-9310(02)00402-7.

[168] S.S. Hsieh, J.W. Lin, J.H. Chen, Mixing efficiency of Y-type micromixers with different angles, Int. J. Heat Fluid Flow. 44 (2013) 130–139. https://doi.org/10.1016/j.ijheatfluidflow.2013.05.011.

[169] R. Johansson, B. Leckner, K. Andersson, F. Johnsson, Account for variations in the H 2 O to CO 2 molar ratio when modelling gaseous radiative heat transfer with the weighted-sum-of-grey-gases model, Combust. Flame. 158 (2011) 893–901. https://doi.org/10.1016/j.combustflame.2011.02.001.

[170] M.A. Rajhi, R. Ben-mansour, M.A. Habib, M.A. Nemitallah, K. Andersson, Evaluation of gas radiation models in CFD modeling of oxy-combustion, Energy Convers. Manag. 81 (2014) 83–97. https://doi.org/10.1016/j.enconman.2014.02.019.

[171] Ansys Fluent Theory Guide, in: Ansys® Acad. Res. Mech. Release 19.2, Help Syst., ANSYS, Inc., n.d.

[172] F. Yan, B. Farouk, Numerical simulation of gas flow and mixing in a microchannel using the direct simulation Monte Carlo method, Microscale Thermophys. Eng. 6 (2002) 235–251.

[173] M.S. Mansour, A.M. Elbaz, W.L. Roberts, M.S. Senosy, M.F. Zayed, M. Juddoo, A.R. Masri, Effect of the mixing fields on the stability and structure of turbulent partially premixed flames in a concentric flow conical nozzle burner, Combust. Flame. 175 (2017) 180–200. https://doi.org/10.1016/j.combustflame.2016.08.032.

[174] M. Le, I. Hassan, DSMC simulation of gas mixing in T-shape micromixer, Appl. Therm. Eng. 27 (2007) 2370–2377. https://doi.org/10.1016/j.applthermaleng.2007.03.012.

[175] D. Gobby, P. Angeli, A. Gavriilidis, Mixing characteristics of T-type microfluidic mixers, J. Micromechanics Microengineering. 11 (2001) 126–132.

[176] F. Zhang, A. Erriguible, S. Marre, Investigating laminar mixing in high pressure microfluidic systems, Chem. Eng. Sci. 205 (2019) 25–35. https://doi.org/10.1016/j.ces.2019.03.063.

[177] A. Amato, B. Hudak, D. Noble, P. D'Carlo, A. Amato, D. Scarborough, T. Lieuwen, J. Seitzman, Methane Oxycombustion for Low CO2 Cycles: Blowoff Measurements and Analysis, J. Eng. Gas Turbines Power. 133 (2011) 061503. https://doi.org/10.1115/1.4002296.

[178] E. Sullivan-Lewis, V. McDonell, Predicting Flameholding for Hydrogen and Natural Gas Flames at Gas Turbine Premixer Conditions, J. Eng. Gas Turbines Power. 138 (2016) 1–9. https://doi.org/10.1115/1.4034000.

[179] M.A. Nemitallah, M.A. Habib, Experimental and numerical investigations of an atmospheric diffusion oxy-combustion flame in a gas turbine model combustor, Appl. Energy. 111 (2013) 401–415. https://doi.org/10.1016/j.apenergy.2013.05.027.

[180] S. de Ferrières, A. El Bakali, B. Lefort, M. Montero, J.F. Pauwels, Experimental and numerical investigation of low-pressure laminar premixed synthetic natural gas/O2/N2 and natural gas/H2/O2/N2 flames, Combust. Flame. 154 (2008) 601–623. https://doi.org/10.1016/j.combustflame.2008.04.018.

[181] T.L.. Cong, P. Dagaut, Experimental and detailed kinetic modeling of the oxidation of methane and methane/syngas mixtures and effect of carbon dioxide addition, Combust. Sci. Technol. 180 (2008) 2046–2091.

[182] Y. Zhang, Z. Huang, L. Wei, J. Zhang, C.K. Law, Experimental and modeling study on ignition delays of lean mixtures of methane, hydrogen, oxygen and argon at elevated pressures, Combust. Flame. 159 (2012) 918–931.

[183] N.. Donohoe, A.. Heufer, W.K.. Metcalfe, H.J.. Curran, M.L.. Davis, O.. Mathieu, D.. Plichta, A.. Morones, E.L.. Petersen, F. Güthe, Ignition delay times, laminar flame speeds and mechanism validation for natural gas/hydrogen blends at elevated pressures, Combust. Flame. 161 (2014) 1432–1443.

[184] N. Stylianidis, U. Azimov, M. Birkett, Investigation of the effect of hydrogen and methane on combustion of multicomponent syngas mixtures using a constructed reduced chemical kinetics mechanism, Energies. 12 (2019) 1–23. https://doi.org/10.3390/en12122442.

[185] T.C. Williams, C.R. Shaddix, R.W. Schefer., Effect of syngas composition and CO2-diluted oxygen on performance of a premixed swirl-stabilized combustor, Combust. Sci. Technol. 180 (2008) 64–88.

[186] A.P. Shroll, Dynamic Stability, Blowoff, and Flame Characteristics of Oxy-Fuel Combustion, 2008.

[187] P. Glarborg, L.L.B. Bentzen., Chemical e ects of a high CO2 concentration in oxy-fuel combustion of methane, Energy and Fuels. 22 (2008) 291–296.

[188] F. Liu, H. Guo, G.J. Smallwood., The chemical effect of CO2 replacement of n2 in air on the burning velocity of CH4 and h2 premixed ames, Combust. Flame. 133 (2003) 495–497.

Vitae

Name :ARAOYE, ABDULRAZAQ ADENIYI

Nationality :NIGERIAN

Date of Birth :4/9/1986

Email :abdulrazaqaraoye@gmail.com, razaq026@gmail.com

Address :No 167a, off lemor hotel Agura, Sagamu Ogun, Nigeria

Zip code 121101

Academic Background

Ph.D. Mechanical Engineering

King Fahd University of Petroleum & Minerals, KFUPM May, 2021

MSc. Mechanical Engineering

King Fahd University of Petroleum & Minerals, KFUPM Jan, 2016

BSc. Mechanical Engineering

Obafemi Awolowo University, Ile-Ife, Nigeria Jan, 2011

RESEARCH

Thesis: Experimental and Numerical Investigation of Premixed Oxy-combustion in a gas turbine model combustor adapting multi-hole burner combustion technology

Thesis: Investigation of flow and erosion characteristics through a set of restricting orifices

PUBLICATIONS

- **Araoye, A.A.**; Abdelhafez, A.; Nemitallah, M.A.; Habib, M.A.; Ben-Mansour, R. Experimental and numerical investigation of stability and emissions of hydrogen-assisted oxy-methane flames in a multi-hole model gas-turbine burner. International Journal of Hydrogen Energy, Volume 46, Issue 38, 2021, pages 20093-20106, ISSN 0360-3199, https://doi.org/10.1016/j.ijhydene.2021.03.135.

- **Araoye, A.A.**; Abdelhafez, A.; Ben-Mansour, R.; Nemitallah, M.A.; Habib, M.A. On the quality of micromixing in an oxy-fuel micromixer burner for gas turbine applications: A numerical study. Chemical Engineering and Processing-Process Intensification, Volume 162, 2021, 108336, ISSN0255-2701, https://doi.org/10.1016/j.cep.2021.108336.

- Ben-Mansour R, Badr HM, **Araoye AA**, Toor IUH. Computational Analysis of Water-Submerged Jet Erosion. Energies 2021; 14:3074, https://doi.org/10.3390/en14113074.

- Ben-Mansour, R.; Hamdy, M.; Sanusi, Y.; **Araoye, A.A.**; Habib, M.A.; Mokheimer, E.; Numerical Investigation of Oxygen Permeation Through a Ba0. 5Sr0. 5Co0. 8Fe0. 2O3− δ Ion Transport Membrane with Impingement Flow, ASME. *J. Energy Resour. Technol*. June 2020; 142(6): 062101, https://doi.org/10.1115/1.4045550.

- **Araoye, A.A.**; Abdelhafez, A.; Nemitallah, M.A.; Habib, M.A.; Ben-Mansour, R., Hussain M. "Shape and stability characteristics of hydrogen-enriched natural-gas oxy-flames in a micromixer burner" (revised manuscript in review in CST)

- Hussain, M.; Abdelhafez, A.; Nemitallah, M.A.; **Araoye, A.A.**; Ben-Mansour, R.; Habib, M.A. A highly diluted oxy-fuel micromixer combustor with hydrogen enrichment for enhancing turndown in gas turbines, Applied Energy, Volume 279, 2020, 115818, ISSN 0306-2619, https://doi.org/10.1016/j.apenergy.2020.115818.

- **Araoye, A.A.**; Badr, H.M.; Ahmed, W.H.; Habib, M.A.; Alsarkhi, A. Erosion of a multistage orifice due to liquid-solid flow, Wear, Volumes 390-391, 2017, pages 270-282, ISSN 0043-1648, https://doi.org/10.1016/j.wear.2017.07.010.

- **Araoye, A.A.**; Badr, H.M.; Ahmed, W.H.; Investigation of flow through multi-stage restricting orifices. Annals of Nuclear Energy, 104, 2017, pages 75-90, ISSN 0306-4549, https://doi.org/10.1016/j.anucene.2017.02.002.

- **Araoye, A.A.**; Badr, H.M.; Ahmed, W.H. Dynamic Behaviour of Flow through Multi-Stage Restricting Orifices, Proceedings of the 3rd International Conference on Fluid Flow, Heat and Mass Transfer (FFHMT'16). Ottawa, Canada.161, 2016, https://doi.org/10.1159/FFHMT16.161.

- **Araoye, A.A.**; Ahmed, W.H.; Al Sarkhi, A.; Bamidele, O.; Badr, H.M.; Alsurakji, I.H. Characterizing drift velocity for two-phase flow using particle image velocimetry. WIT Transactions on Engineering Sciences, 105, 2016, pages 87-97, WIT Press, https://doi.org/10.2495/AFM160091.